The Role of the Indian Ocean in the Global Climate System: Recommendations Regarding the Global Ocean Observing System

OOSDP Background Report Number 6

Prepared by

J. S. Godfrey, A. Alexiou, A. G. Ilahude,
D. M. Legler, M. E. Luther, J. P. McCreary, Jr.,
G. A. Meyers, K. Mizumo, R. R. Rao,
S. R. Shetye, J. H. Toole, S. Wacongne

Ocean Observing System Development Panel

February 1995

Ocean Observing System Development Panel

Dr. Michael McPhaden (NOAA/PMEL)
Dr. Lilliane Merlivat (Université Pierre et Marie Curie)
Dr. George Needler (Bedford Institute of Oceanography)
Dr. Worth Nowlin, Jr. (Texas A&M University), Chairman
Dr. Raymond W. Schmitt (Woods Hole Oceanographic Institution)
Dr. Neville Smith (Bureau of Meteorology Research Centre)
Dr. Peter K. Taylor (James Rennell Centre for Ocean Circulation)
Dr. Alain F. Vézina (Universite du Quebec a Rimouski)
Dr. Masaaki Wakatsuchi (Hokkaido University)
Dr. Robert Weller (Woods Hole Oceanographic Institution)
Mr. Arthur Alexiou (Staff Scientist to the Panel from IOC)

This report may be cited as:
Godfrey, J. S., A. Alexiou, A. G. Ilahude, D. M. Legler, M. E. Luther, J. P. McCreary, Jr., G. A. Meyers, K. Mizuno, R. R. Rao, S. R. Shetye, J. H. Toole, and S. Wacongne. 1995. The Role of the Indian Ocean in the Global Climate System: Recommendations Regarding the Global Ocean Observing System. Report of the Ocean Observing System Development Panel, Texas A&M University, College Station, TX, U.S.A. 89 pp.

Additional copies of this report may be obtained from: Dr. Worth D. Nowlin, Jr., Department of Oceanography, Texas A&M University, College Station, Texas 77843-3146, U.S.A. Fax: (409) 845-0888.

The Role of the Indian Ocean in the Global Climate System: Recommendations Regarding the Global Ocean Observing System

OOSDP Background Report Number 6

J. S. Godfrey, A. Alexiou, A. G. Ilahude,
D. M. Legler, M. E. Luther, J. P. McCreary, Jr.,
G. A. Meyers, K. Mizumo, R. R. Rao,
S. R. Shetye, J. H. Toole, S. Wacongne

A background paper prepared on behalf of the Ocean Observing System Development Panel

Foreword

Building a permanent global ocean observing system is now an accepted international goal. It is generally recognized that all marine activities stand to benefit from a comprehensive multi-purpose ocean observing system. The observational elements associated with climate form a set, or module, of such measurements with high priority.

With the need for systematic global observations in mind, the Committee on Climate Change and the Oceans of the Scientific Committee on Oceanic Research–Intergovernmental Oceanographic Commission and the Joint Scientific Committee of the International Council of Scientific Unions–World Meteorological Organization jointly established the Ocean Observing System Development Panel (OOSDP). The OOSDP was charged with formulating the conceptual design of a long-term systematic observing system to monitor, describe, and understand the physical and biogeochemical processes that determine ocean circulation and the effects of the ocean on seasonal to decadal climate changes, and to provide the observations needed for climate prediction.

Pursuing that change, the OOSDP has prepared an initial scientific design for the climate module of the Global Ocean Observing System. That module is intended to be also the ocean component of the Global Climate Observing System.

As part of its work, the OOSDP commissioned a series of background papers to help identify system design considerations. It is the hope that these informal background papers will help: (1) design the climate-related module of the Global Ocean Observing System, which is to be essentially the same as the ocean component of the Global Climate Observing System; (2) identify existing capabilities available to meet these needs; and (3) identify new types of systems that should be encouraged to meet these needs more economically and efficiently in the future.

This is one background report. It represents the opinions of the authors, most of whom are members of the WCRP Indian Ocean Panel, which considered this document at its August 1992 and May 1994 meetings. It is being distributed widely within the community. Your comments, criticisms and suggestions may be sent to the primary author, Dr. J. Stuart Godfrey (CSIRO Division of Oceanography, GPO Box 1538, Hobart, Tasmania 7001, AUSTRALIA) or Prof. Worth D. Nowlin, Jr. (Department of Oceanography, Texas A&M University, College Station, TX 77843-3146, USA).

Clearly the ultimate success of implementing an ocean observing system hinges on broad acceptance of its plan by the ocean science community and by the national agencies and intergovernmental organizations that will have to implement it. That, in turn, depends on broad informed participation in its planning. We thank the WCRP Indian Ocean Panel for this report which should inform and challenge its readers and future planners of the common module of the Global Ocean Observing System and the Global Climate Observing System.

Ocean Observing System Development Panel

Table of Contents

1. Introduction

There has been considerable activity over the last three years, directed towards building a Global Ocean Observing System (GOOS). GOOS is designed to have five modules, of which one—the climate module—will be a major component of the Global Climate Observing System (GCOS) as well. The GOOS climate module is intended to provide (among other things) an ocean data set collected regularly over decades, of sufficient quantity to document at least the major large-scale changes in ocean circulation over that time. In this paper we will focus only on the climate module of GOOS. The Ocean Observing System Development Panel (OOSDP) has met ten times, and several reports discussing specific issues have been prepared by or for that Panel as discussion documents (e.g., Smith, 1991; Weller and Taylor, 1993). These have dealt with such issues as the role of ocean modeling in the climate module; carbon monitoring strategies; the global freshwater balance; and requirements for surface fields and air-sea fluxes. The Joint Scientific and Technical Committee for GCOS has also met, and made some recommendations regarding the general nature of required ocean observations. Implementation of the Indian Ocean component of WOCE is now imminent, and results from this can be expected to influence the design of the ocean observing system for climate. Various proposals (CLIVAR, GOALS) for designing a new program to carry on the momentum developed by TOGA and WOCE will also have a bearing on the design of the ocean observing system for climate. The report of the first meeting of the TOGA/WOCE XBT/XCTD Programme Planning Committee held October 1991 (WOCE, 1992) gives an up-to-date picture of the status of the Indian Ocean XBT network. A draft version of the present document was circulated in 1992; the Chairman of OOSDP requested that a modified version of the document be prepared as a Background Paper for OOSDP.

As stressed in other OOSDP reports, the ocean observing system for climate is likely to evolve over a number of years, through an interplay between practical and logistic considerations (e.g., where the commercial shipping lanes run) and scientific needs. Within each ocean basin it is likely that a few countries will choose to take responsibility for implementing the observing system, and the design will therefore naturally reflect their national priorities. For example, a common concern of all countries bordering the Indian Ocean is to improve the prediction of the monsoon rains, and to obtain better forecasting of the typhoons which create great damage in all countries of the region. Evidently, if an Indian Ocean component of the ocean observing system for climate is to be given long-term support by Indian Ocean countries and also by countries outside the region, it should be designed to achieve both the local needs of countries bordering on that ocean, and the global needs of GOOS and GCOS. This document, by the WCRP Indian Ocean Panel, naturally stresses the needs of Indian Ocean countries. Thus much of the emphasis in this document is on the behavior of the upper ocean, which controls SST anomalies within the Indian Ocean. Emphasis is also placed on recent numerical model results, since models will have to play major roles in an observing system.

A large part of the motivation for developing the ocean observing system for climate is that the ocean and atmosphere are tightly coupled. This is especially true in the tropics, where the water vapor fluxes from the ocean supply the rainfall; the latent heat released by this rain (and radiation effects of the associated clouds) energizes the Trade and Monsoon wind systems; and these winds drive the ocean currents and modify SST in several ways. Finally, SST changes in turn feed back on the water vapor fluxes, completing the feedback loop. Spontaneous fluctuations can occur

within this coupled ocean-atmosphere system—the El Niño-Southern Oscillation (ENSO) phenomenon, which brings drought to Indonesia and Australia and frequently also to India, is a famous example. The design of the observing system must be undertaken with as sophisticated an understanding as possible of the coupled ocean-atmosphere system, because the data to be collected by the observing system will ultimately be used to initialize the ocean component of coupled ocean-atmosphere models.

There are still many problems to be solved before coupled models reach maturity, but they are already generating climate forecasts a season or more in advance with demonstrable skill (e.g., Philander, 1990; Cane, 1992). It should be noted, however, that nearly all the skill demonstrated so far is due to improvements in modeling the atmosphere, and the Pacific Ocean: so far coupled models that include the Indian Ocean are much less advanced. Atmospheric numerical models find that the huge observed variations in the Pacific Ocean SST field are considerably more important than those in the Indian Ocean for controlling the ENSO phenomenon, at least for controlling the global-scale atmospheric circulation (Palmer et al., 1992). However, now that the role of the equatorial Pacific Ocean in ENSO is getting to be fairly well understood it may be that further progress depends on understanding the more subtle variations that occur in the Indian and Atlantic Oceans (e.g., Webster, 1994)—and on obtaining the data to document their year-to-year changes.

The oceans affect climate on long time scales because heat absorbed by the ocean in one place can be returned to the atmosphere in another place, many thousands of kilometers away, and years, decades or even centuries later. But ocean heat storage and transport properties are much more dependent on topographic detail than their atmospheric counterparts; in particular, the Indian Ocean behaves very differently as a component of the global climate system than the other two oceans. In this review we summarize our present knowledge of the role of the Indian Ocean in the global climate system. We also summarize our knowledge of SST variations in the Indian Ocean, and their effect on climate. We emphasize particularly the horizontal transport of heat, and heat storage. These only partially control the SST, but they typically change on time scales of months or years or longer, and are therefore a predictable element of the climate system.

Part of the uniqueness of the Indian Ocean is due to the fact that it is bounded to the north at quite low latitude (unlike any other ocean), so all heat absorbed in the northern Indian Ocean must escape southwards. It is also well known that the seasonal reversal of the winds over most of the Indian Ocean north of 15°S gives rise to complex, seasonally-reversing flows in much of this region. However, the ocean's role in absorbing and transporting heat and freshwater is not so well known—indeed, in the Indian Ocean, research on this subject is still at a fairly early stage. A major objective of the ocean observing system for climate will be to document changes in heat (and freshwater) content of the ocean, for initializing and validating numerical ocean models—either on their own, or as part of a coupled climate model. Such observations are expensive: what are the most important measurements to make? Such a question can only be answered when the major processes are at least qualitatively understood.

A fairly non-technical approach has been used in this review, since some of those interested in the ocean observing system for climate may have little or no background in physical oceanography. Furthermore, since the aspects of oceanography of greatest concern to Indian Ocean countries are the upper-ocean phenomena, we concentrate on those—though we do include some discussion of

the deeper aspects of flow. For those not familiar with them, a brief description of the present status of the TOGA network of ocean monitoring that has been operating in the Indian Ocean since 1985 and WOCE Indian Ocean plans for 1994-1996 can be found in the U.S. Contribution to WOCE Core Project 1 The Program Design for the Indian Ocean (U.S. WOCE, 1993; updated information available from the U.S. WOCE Office, 305 Arguello, College Station, TX, USA 77840; fax: (409) 845-0888; internet: uswoce@astra.tamu.edu or from the U.S. WOCE Home Page on the World Wide Web: http://www-ocean.tamu.edu/WOCE/uswoce.html).

We begin our discussion of the Indian Ocean's role in global heat transport by describing the dynamics of the annual-mean circulation and heat transport patterns in the Indian Ocean, in relation to the rest of the world ocean (Section 2). A brief discussion of the freshwater transport, and freshwater effects on heat transport, is also included. Despite the massive seasonal cycle that occurs in the Indian Ocean, this annual mean picture is quite useful for understanding many aspects of the circulation and the transport of heat and fresh water in the Indian Ocean. The annual mean is much simpler to understand, and it provides a useful starting point for explaining events that occur over the seasonal cycle. Nevertheless seasonal aspects of the forcing are almost certainly important, even for the annual mean. Section 3 considers the dynamics and thermodynamics underlying the mean seasonal cycle of SST in the Indian Ocean; for a more detailed treatment, the reader is referred to the very thorough coverage of the subject by McCreary et al. (1993).

In Section 4 we consider the observed interannual SST variations in the Indian Ocean and their effects on the atmosphere. These effects have often been found empirically by correlating SST anomalies with certain types of meteorological anomalies (e.g., ENSO events, strong and weak Indian monsoons, Australian or African rainfall, etc.). "Composites" of years in which these effects are particularly marked are often taken, as a device for seeing the signal in the associated SST above the background noise. Atmospheric General Circulation Models (AGCMs) also provide much useful information. While discussing these SST anomalies, we discuss what is known so far about the role of ocean dynamics in maintaining them. Section 5 considers what we know of interannual variability in other ocean fields (surface meteorological variables, subsurface temperatures and sea levels, and surface currents).

The "composite" approach used in studying the relationships of SST with rainfall tends to average out data errors. The data errors are much more important when trying to forecast climate anomalies, starting from the climate state of a particular date (e.g., the present time). Issues of data quality and—especially—data paucity then become crucial (particularly for any plans for developing the observing system). The issue of observational inadequacies is addressed in Section 6, where the present observational network is considered. The subject of fluxes has been exhaustively dealt with in OOSDP Background Report 3 (Weller and Taylor, 1993) but some remarks on fluxes in the Indian Ocean will be given in Section 6 (particularly of momentum); there are some rather striking examples of discrepancies between available climatologies of wind stresses and surface heat fluxes. Also, the available hydrographic data set (including the XBT network) is particularly sparse in the Indian Ocean. Recent studies of the adequacy of XBT coverage are also reviewed.

In Section 7 we summarize this material, in the context of the design of an Indian Ocean component of the ocean observing system for climate. One conclusion is that we do not yet know

enough about how the Indian Ocean works as a component of the global climate system to confidently design *permanent* Indian Ocean components of the observing system, apart from those components that are set by existing shipping lanes. A period of exploratory monitoring is needed, such as that which occurred in the Pacific during the 1980s and early 1990s with the development of the TAO array. It is also concluded that studies of air-sea exchange and of mixed layer dynamics are probably of about equal importance to traditional studies of ocean dynamics, for purposes of predicting SST anomalies—particularly on seasonal timescales. Also, the southern Indian Ocean near 10°-20°S stands out as being particularly important, both for the relationship of SST anomalies there with rainfall and for the potential of wind anomalies there to drive SST anomalies in the northern Indian Ocean.

2. The Annual Mean Transport of Properties in the Indian Ocean.

This section describes the annual mean circulation of the Indian Ocean, and the annual mean transport of heat and freshwater. Parts of the present section are adapted from Chapters 11 and 12, and the Indian Ocean sections of Chapter 18, of Tomczak and Godfrey (1994); this text provides a more detailed review of the (seasonally varying) current system than is provided here. This review may also be considered an update of Wyrtki's (1973a) and Knox's (1987) reviews of the physical oceanography of the Indian Ocean.

2.1. Annual Mean Circulation of the Indian Ocean

It is convenient to begin by describing the annual mean depth-integrated circulation of the Indian Ocean, relative to that found in the rest of the World Ocean. Many aspects of it are described surprisingly well by the simple Sverdrup (1947) theory that assumes water below a "depth of no motion" (typically 1500 m or so) to be at rest, and flow above that level to be slow, and frictionless except in the surface wind-driven layers. The theory predicts that *annual mean* northwards mass transport V at a given part of the upper ocean is simply proportional to the "curl" of the *annual mean* wind stress (though these relationships definitely do not hold on a season-by-season basis). The wind stress curl may be roughly estimated by eye from Figure 1. For example, it is clear that the Westerlies (centered near 40°S in the Indian Ocean) and the Trades (centered near 15°S) are particularly strong in the South Indian Ocean compared to other oceans, and so the "curl" between them is strong and one expects strong northwards transport V between these latitudes. Eastward mass transport U may be found from V by mass continuity, with the assumption that there is no flow through the eastern boundary. According to the theory, all resulting mass imbalances must be taken up in the intense western boundary currents, where Sverdrup's assumptions fail. Figure 2 shows the world Sverdrup streamfunction evaluated from the annual mean wind stresses of Figure 1. Figure 2 differs surprisingly little in the interior of the Indian Ocean from the pattern obtained in much more sophisticated models, for example figure 10 of Semtner and Chervin (1992). The Agulhas Current along the southeast African coast is predicted by the Sverdrup relation to have one of the strongest mass transports of any western boundary current in the world—67 Sverdrups near the southern tip of Africa (1 Sverdrup $=10^6 m^3 s^{-1}$). Its large size comes about mainly because of the great intensity of the wind stress curl between the Trades and the Westerlies just mentioned. 51 Sv flow north across 32°S in the open Indian Ocean in Figure 2, which must return south in the Agulhas Current. This is augmented by the Indonesian Throughflow, which is predicted from the

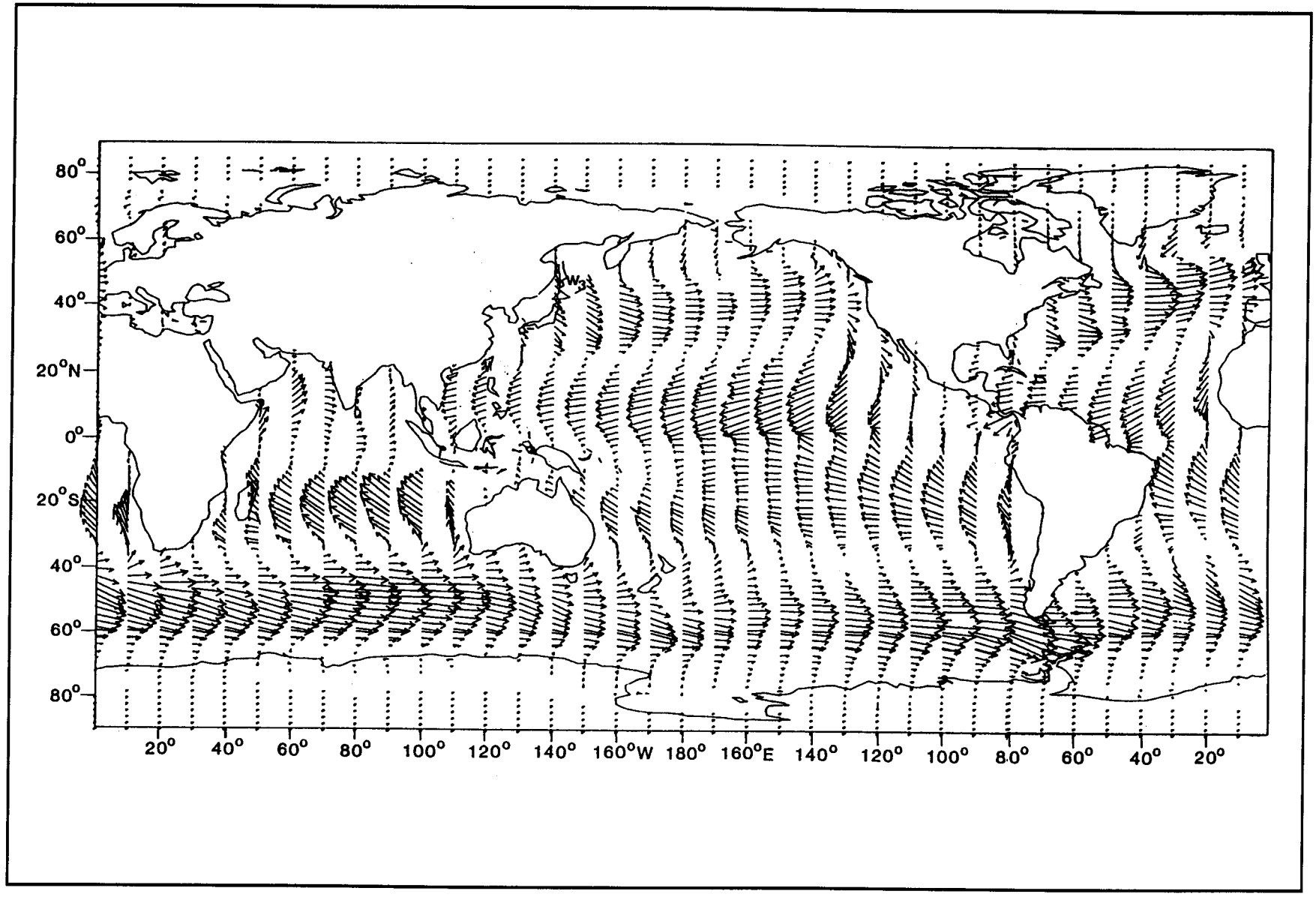

Figure 1. Global annual mean wind stress pattern (from Hellerman and Rosenstein, 1983). Largest vector = 0.2 newtons/m^2.

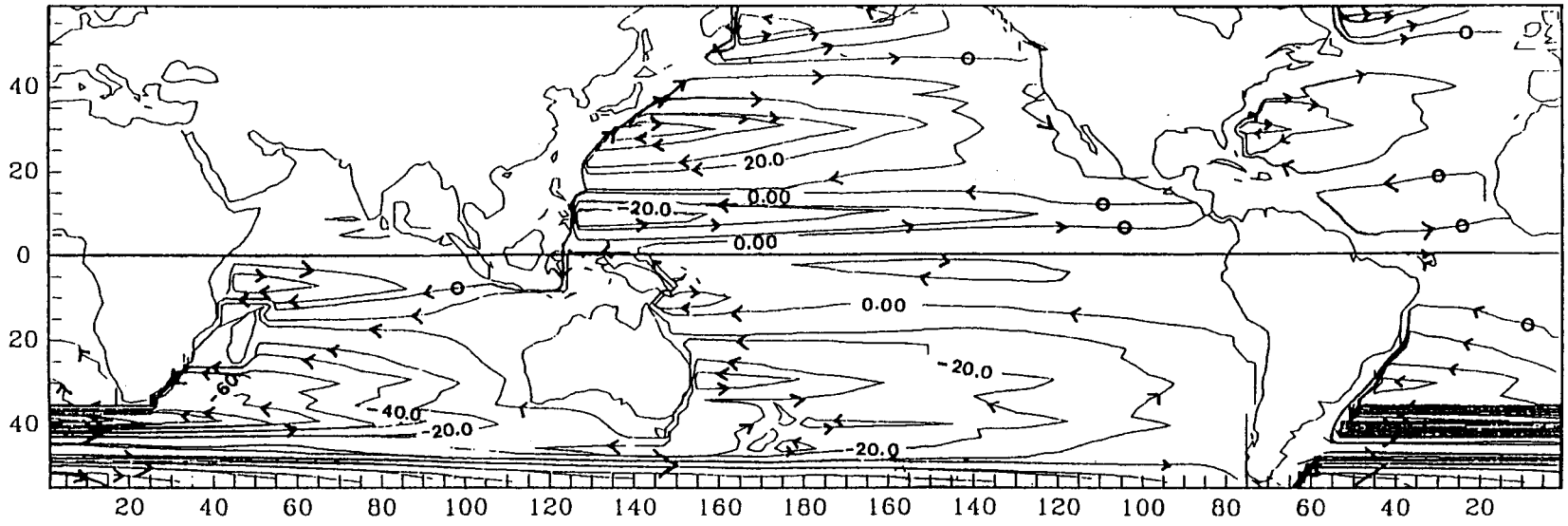

Figure 2. Sverdrup stream function for annual mean depth-integrated flow, calculated from the winds of Figure 1. Contour interval 10 Sv (1 Sv = 10^6 m^3s^{-1}) (from Godfrey, 1989).

Sverdrup model to be 16 Sverdrups, due to wind circulation around Australasia in the Pacific Ocean (Godfrey, 1989). Hence the predicted strength of the Agulhas Current at 32°S is 67 Sv.

By contrast, Toole and Warren (1993) find an even stronger southward transport of 85 Sv for the Agulhas Current near 32°S, above 2000 m. The difference between Toole and Warren's measured value and the Sverdrup estimate may be largely due to upwelling through 2000 m, which is not accounted for in the Sverdrup calculation. Toole and Warren find that this upwelling has a magnitude of about 27 Sv in the Indian Ocean; this is of considerable interest for the heat budget of the global ocean (see further discussion in Section 2.5). The sum of this upwelling and the Sverdrup estimate is 94 Sv—reasonably close to Toole and Warren's value of 85 Sv. Uncertainty in the magnitude of the Indonesian Throughflow is greater in relative terms, but it now seems probable that it contributes an annual mean flow of order 10 Sv to the Agulhas Current (e.g., Fieux et al., 1994; Godfrey et al., 1993).

The Agulhas Current is much the strongest western boundary current in the Southern Hemisphere, and it is the primary source of heat for the Southern Ocean. Much of its outflow flows east-south-east to join the South Indian Current (Stramma, 1992); it loses heat along the way to form deep mixed layers known as Sub-Antarctic Mode Water (McCartney, 1977). This water then moves slowly north to supply the Sverdrup flow in the interior of the South Indian Ocean. The Agulhas Outflow continues east-southeast, ultimately supplying heat to Antarctica. Some Agulhas water also flows westward into the Atlantic: Gordon (1986) suggested that this may be the major source of the warm water needed to supply the formation of North Atlantic Deep Water. Other sources may also be important (e.g., Rintoul, 1991). The ultimate fate of the Agulhas waters is a very complex question, because the Agulhas Current breaks up into intense eddies. Figures 3a and 3b provide a qualitative indication of the behavior. The properties of these eddies—in the presence of complex bottom topography—are crucial to the larger-scale questions. This is a very active area of research, both observationally (e.g., Olson et al., 1988; Gordon et al., 1992) and in numerical models (e.g., Ou and de Ruijter, 1986; Semtner and Chervin, 1992). However, these questions lie at the edge of the region considered in this review, so we will not discuss them further.

Another major feature of Figure 2 in the Indian Ocean is the South Equatorial Countercurrent (flowing east between the equator and 10°S). According to the Sverdrup relation, the South Equatorial Countercurrent should be stronger than its counterparts in the other oceans, except for the North Pacific, because (as can be seen from Figure 1) the wind stress curl near 10°S is stronger in magnitude in the Indian Ocean than in any other part of the equatorial oceans. This curl drives *southward* flow across 10°S, while the curl is weak nearer the equator. The South Equatorial Countercurrent is therefore required by mass continuity, to supply the mass divergence. Hydrographic observations (see, for example, Chapter 8 of the excellent and much-used atlas of Wyrtki, 1971) show that the observed South Equatorial Countercurrent does indeed strengthen towards the west of the Indian Ocean at about the rate seen in Figure 2. The predicted bifurcation of the western boundary current off Madagascar at about 20°S also seems quite realistic (Swallow et al., 1988; Schott et al., 1988). According to Figure 2, the (annual mean) circulation north of the equator is predicted to be quite weak. The observations are rather ambiguous on this point, because the seasonal flow in this region is by comparison so strong and complex (e.g., see the review by Tomczak and Godfrey, 1994). Similar remarks apply to the flow through the Mozambique Channel (Donguy and Piton, 1991).

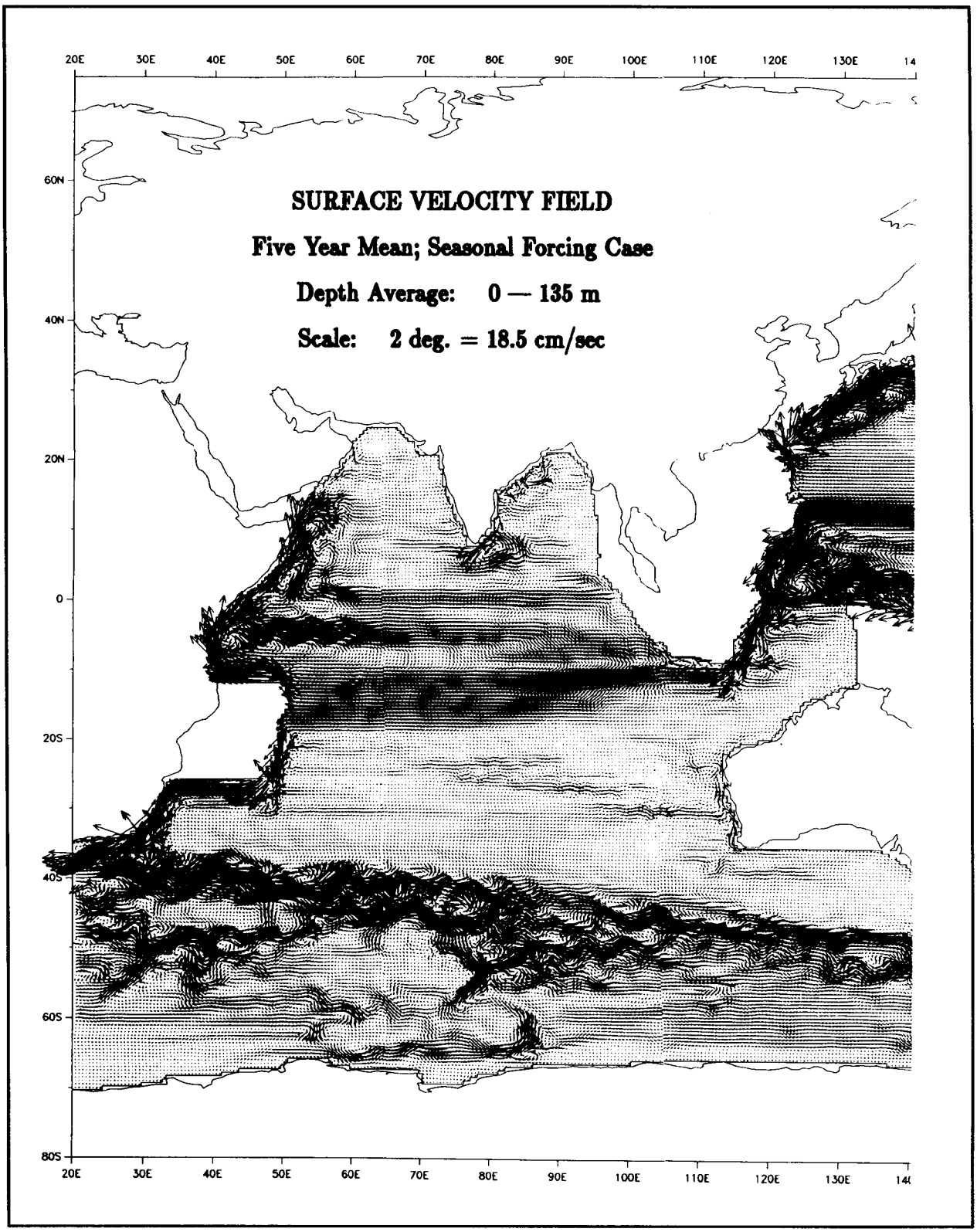

Figure 3a. Five-year-mean velocity field, averaged over the top 135 m, from a seasonally-forced 0.5° x 0.5° resolution model (Semtner and Chervin, 1992).

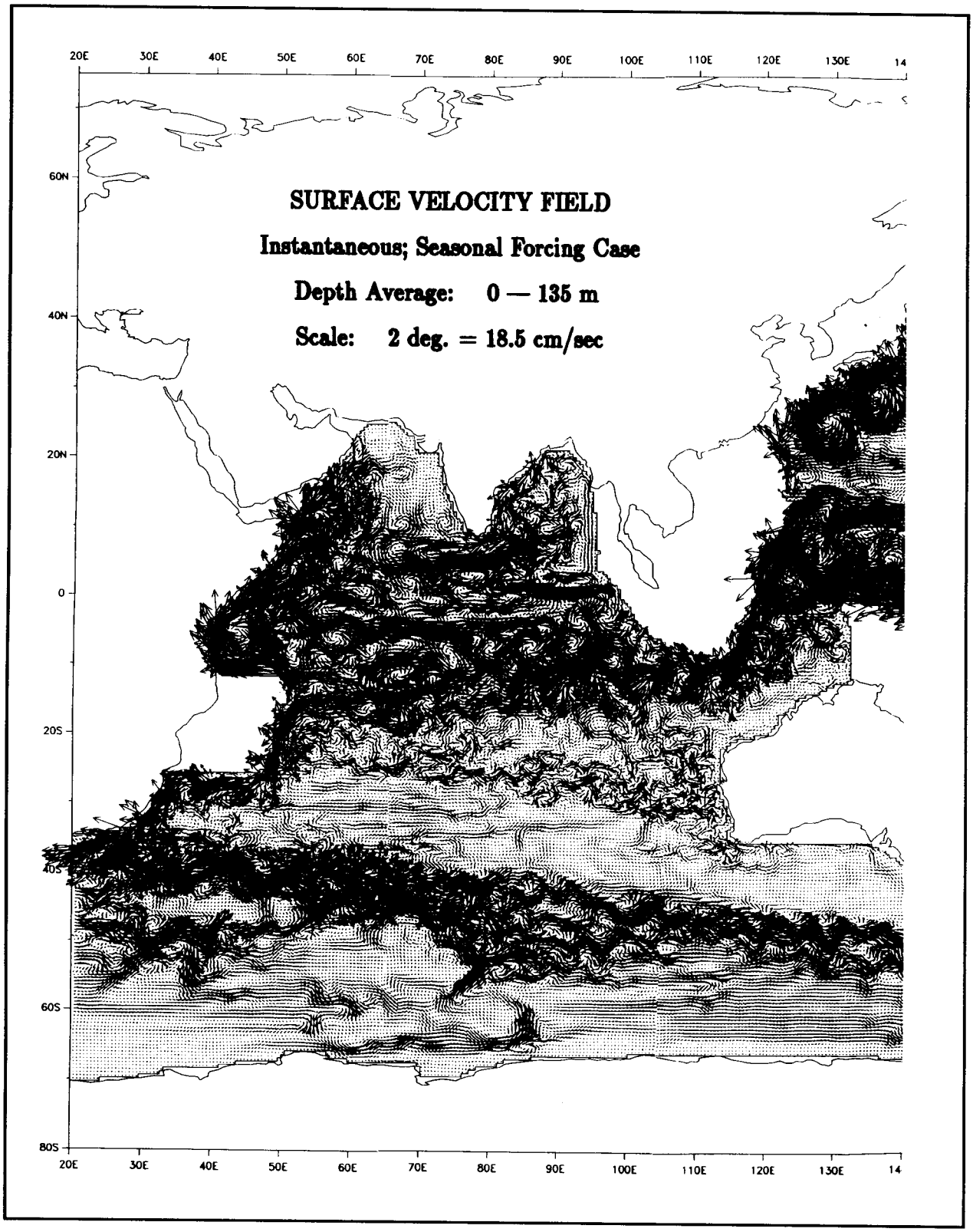

Figure 3b. Instantaneous (October) velocity field, averaged over the top 135 m, from a seasonally-forced 0.5° x 0.5° resolution model (Semtner and Chervin, 1992).

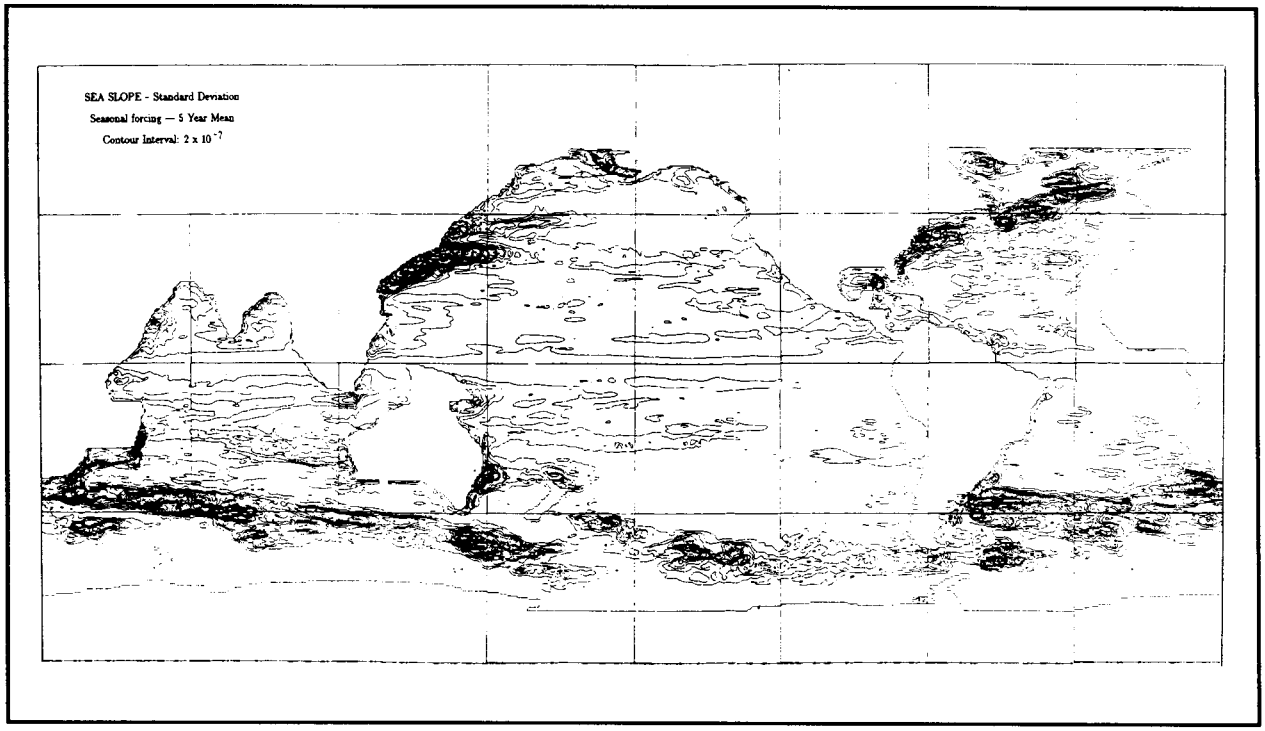

Figure 3c. Mean variance of sea level slope in the Semtner-Chervin (1992) model.

However, this depth-integrated picture evidently can give no indication of how these currents are distributed with depth, and this information is crucial to understanding how heat and other properties are transported in the ocean. The various currents of Figure 2 (and other currents) have very different depth distributions. For example, the South Indian subtropical gyre and the Agulhas Current extend extremely deep, being clearly apparent in temperature maxima offshore from the Agulhas Current down to 2000 m (Wyrtki, 1971; Levitus, 1982). By contrast, the Leeuwin Current system of surface currents, consisting of zonal flow towards Western Australia and southward flow along the Western Australian coast, has a corresponding northward undercurrent and offshore flow centered near 500 m (e.g., Godfrey and Ridgway, 1985). These are nearly equal and opposite in mass transport, so there is no discernible contribution of the Leeuwin Current to the depth-integrated flow. This is apparent in Figure 4 which shows the surface steric height relative to 2000 db (from Levitus, 1982) and the depth-integrated steric height of all levels above 1500 db, relative to 1500 db (from the data of Levitus, 1982); the Sverdrup estimate of depth-integrated steric height is also shown, Figure 4c. In the Indian Ocean, Figures 4b and 4c are quite similar, confirming the effectiveness of the Sverdrup relation for predicting broad-scale *depth-integrated* flows; but both are very different from the surface geostrophic flow of Figure 4a, because of the strong eastward geostrophic flow feeding the Leeuwin Current (referred to hereafter as the "Leeuwin Current Extension"). In between the extremes of the Agulhas and Leeuwin Current Extension (in terms of depth distribution) are the currents of the tropical Indian Ocean, with typical mean depths of about 200-400 m. These sometimes show reversals with depth, but not as marked as in the Leeuwin Current system.

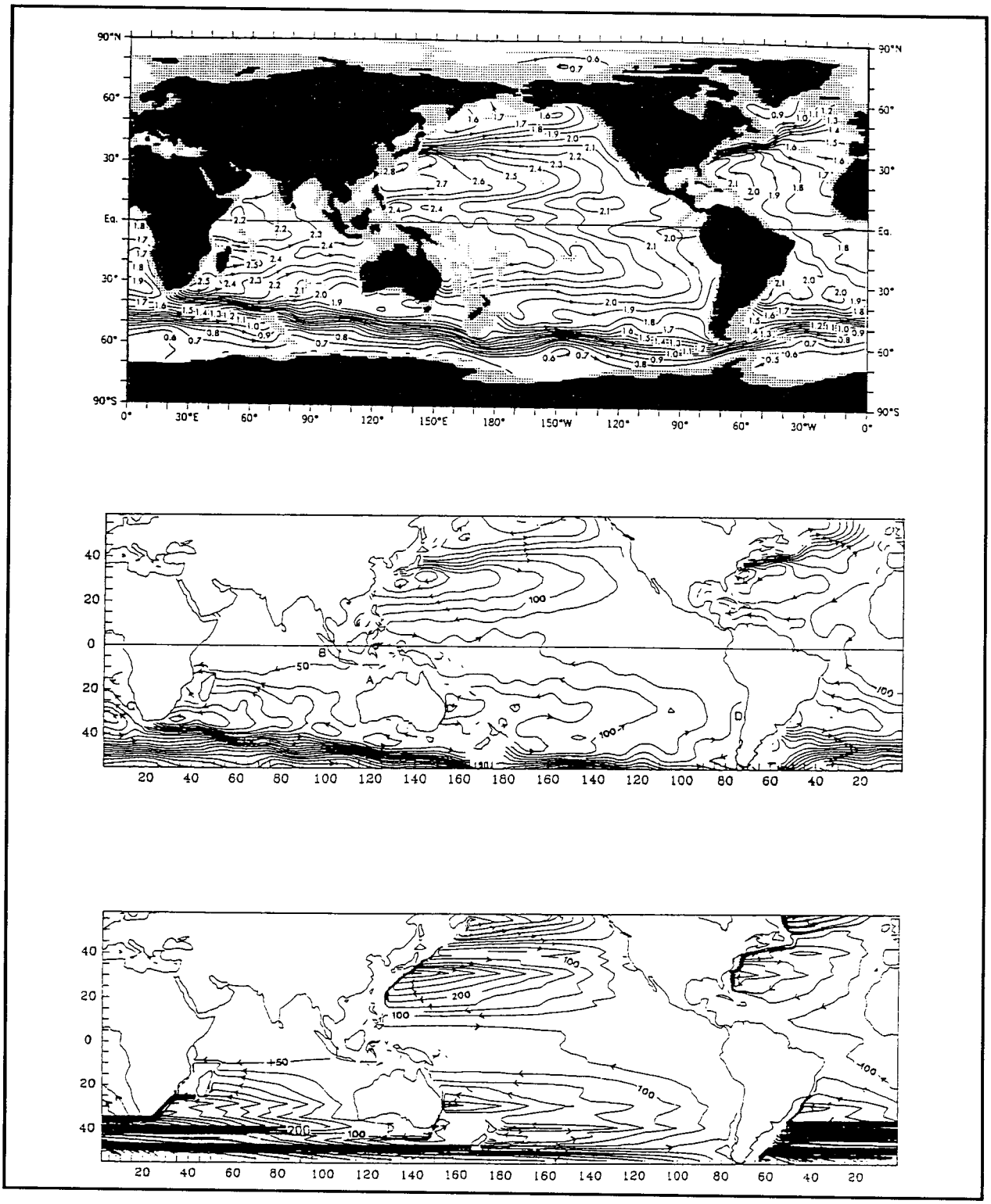

Figure 4. (a) Surface steric height (m) relative to 2000 db (from Levitus, 1982). Contour interval 0.1 m. (b) Depth-integrated steric height of the top 1500 db relative to 1500 db (from the data of Levitus, 1982). (c) Depth-integrated steric height calculated from the Sverdrup relation (from Godfrey, 1989). Contour interval 50 m^2.

Such currents are typically accompanied by vigorous eddies, with length scales of order 100 km. Figures 3a and 3b provide a schematic illustration of their amplitude, relative to the annual mean, from a recent, rather high-resolution (0.5° x 0.5°) numerical model (Semtner and Chervin, 1992). Figure 3a shows the annual mean currents in the top 135 m. The Indonesian Throughflow, South Equatorial Current and Countercurrent, Agulhas Current and the South Indian Current are all visible, along with the upper arm of the Leeuwin Current Extension (flowing east between Madagascar and Western Australia). Strong annual mean northward flows are seen in this model along the Somali coast, with a roughly similar southward counterflow a few hundred kilometers offshore, feeding an eastward equatorial jet; and a mean eastward flow occurs southeast of India. However, the major interest lies in an instantaneous picture of the velocity field (Figure 3b). In the model at least, eddies are a major feature of the circulation. Semtner and Chervin note that globally, observed variability of sea surface slope from the Geosat altimeter data of 1986-1988 (Sandwell and Zhang, 1989) is very similar to their model's variability (Figure 3c), though the model underestimates typical eddy slope variance by a factor of 2 or so.

Ocean eddies can sometimes play an important role in the horizontal transport of heat and freshwater, and may need to be considered in the design of the ocean observing system for climate for this reason. Of equal importance is the fact that they add noise, complicating the task of diagnosing interannual variations in ocean currents and thermal structure from limited data sets. The properties of eddies have generally received little attention in the Indian Ocean. An exception occurs in the tropical Indian Ocean, where Luther and O'Brien (1989) found that—when their model was driven with mean seasonal winds—the vigorous eddies associated with the Somali Current developed in a very regular way each year. When observed, annually-varying winds were applied, the eddies became much more variable from year to year (and thus more in accord with observations). Kindle and Thompson (1989) found that eddies with a very well-defined periodicity of 26-28 days occurred near the equator, in their model; they were also found by Woodberry et al. (1989). They are associated with a type of wave motion (mixed Rossby-gravity waves), and are manifested in the meridional velocity. This periodicity is observed in Indian Ocean equatorial current meter records (O'Neill, 1984; Luyten and Roemmich, 1982). Tsai et al. (1992) showed from satellite SST data that these waves are also clearly evident in the observed SST.

2.2. How Does the Indian Ocean Transport Heat?

The subtler aspects of the ocean's role in climate—its ability to take heat from one region, and release it in another many thousands of kilometers away and many years later—are controlled by the horizontal advection of heat. A large part of the rest of this paper concerns the advection of heat, and the related heat fluxes through the ocean surface. In particular, Figures 5a and 5b show two climatologies for the annual mean net heat flux into the world ocean. They differ fairly strongly from one another, because they are estimated as a relatively small sum of four quite large terms from empirical rules, and some of these rules are not very accurate (e.g., Isemer et al., 1989). However, these and other climatologies agree that on annual average there is positive heat flux into the Indian Ocean, nearly everywhere north of 15°S. The integral of the net heat influx into the Indian Ocean over the area north of 15°S ranges between about 0.5-1.0 x 10^{15} watts, depending on choice of climatology. Thus on annual mean, there must be a net inflow of cold water, and a corresponding removal of warmed water, to carry this heat influx southward, out of the tropical Indian Ocean.

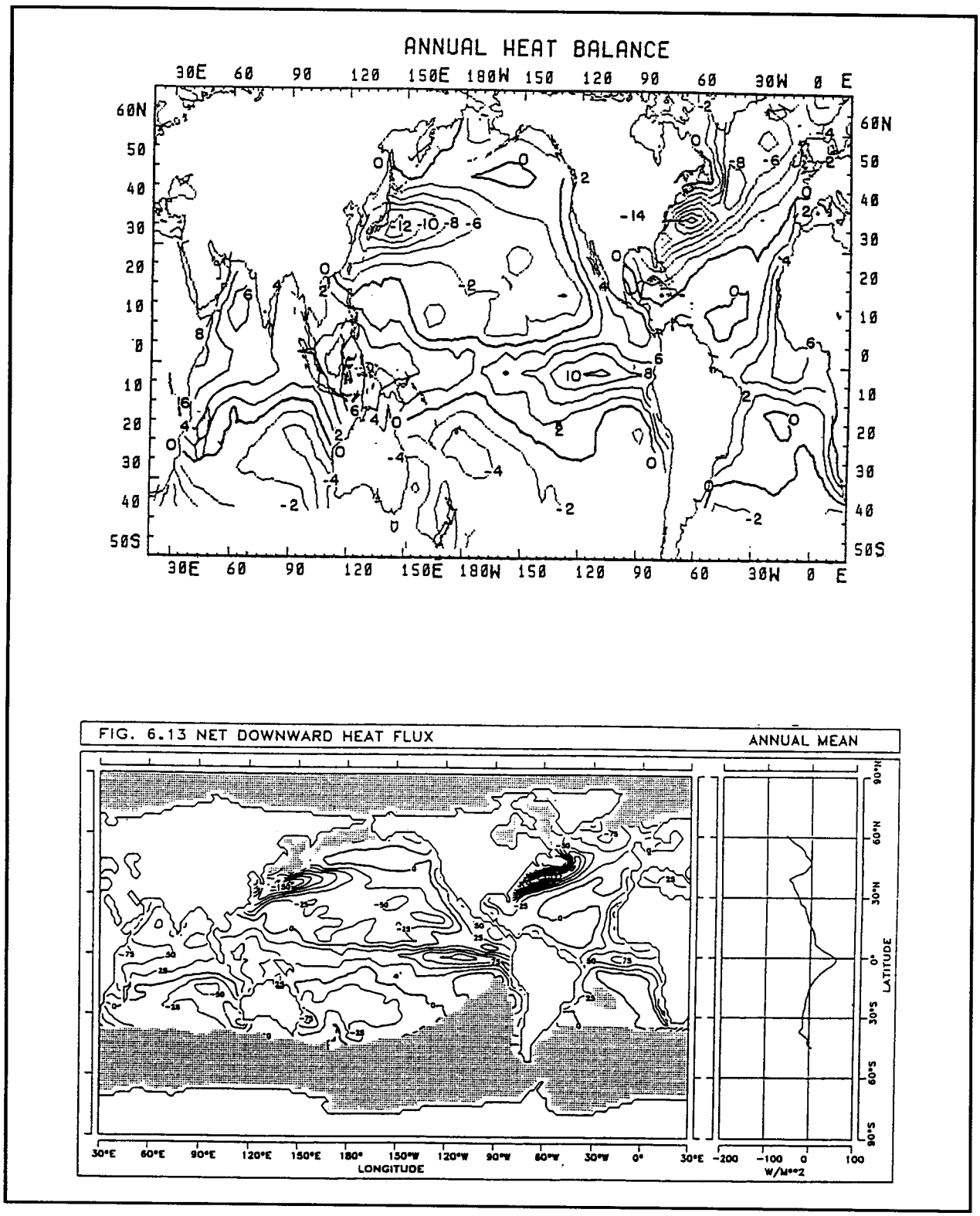

Figure 5. Annual mean net heat flux into the ocean, according to (a) Hsiung (1985) (unit 10 watts/m^2; contour interval 20 watts/m^2) and (b) Oberhuber (1988) (contour interval 25 watts/m^2).

How are Indian Ocean flows organized to achieve this removal? What are the main driving forces for these flows—wind forcing, or buoyancy forcing? Are there major interannual variations in these heat transports, and if so, are their causes to be found primarily in the wind driving or the buoyancy forcing? These are questions for which we should have at least a qualitative idea of the answer before we attempt to design an Indian Ocean component of GOOS, because they may determine what quantities should be measured, and where the observational effort should be concentrated.

To get a feel for such questions—and to become aware of the paucity of relevant data—it is useful to begin the discussion by carrying out an order-of-magnitude analysis, to find out what flow patterns are likely to make important contributions to the northwards advective heat flux $Q_v(\theta,t)$ at time t across latitude θ, in the Indian Ocean. An accurate expression for Q_v is

$$Q_v(\theta,t) = \rho C_p \int v(\theta,x,z,t)T(\theta,x,z,t)\, dx\, dz, \qquad (1)$$

where $v(\theta,x,z,t)$ is the northwards velocity and $T(\theta,x,z,t)$ the potential temperature; ρ is water density and C_p the heat capacity of water. The integral is taken over the full range of the cross-section in zonal distance (x) and depth (z). (1) is only well-defined for sections across closed basins, for which

$$\int v(\theta,x,z,t)\, dx\, dz = 0. \qquad (2)$$

Basically, (2) must follow by mass continuity if *all* water movements contributing to heat supply or removal are accounted for. In practice (2) means that for the Indian Ocean, at latitudes south of the Indonesian Throughflow, (1) must be supplemented by a similar term to account for the temperature transport through the Indonesian Archipelago.

ρC_p is close to 4×10^6 joules/m^3/°C, so to remove the $0.5\text{-}1.0 \times 10^{15}$ watts mentioned earlier, the integral in (1) should have a value in the range $125 - 250 \times 10^6$ (m^3s^{-1})°C. This could be met (for example) by a 20 Sverdrup inflow being warmed by 6-12°C, or by a 4 Sverdrup inflow being warmed by 30°-60°C. Since the latter temperature range exceeds the top-to-bottom temperature difference in the Indian Ocean, we can be sure that meridional water flows of more than 4 Sv are needed to remove the observed heat out of the northern Indian Ocean.

$Q_v(\theta,t)$ can be split into two parts, by writing $v(\theta,x,z,t)$ and $T(\theta,x,z,t)$ each as the sum of zonal averages ($\mathbf{v}(\theta,z,t)$, $\mathbf{T}(\theta,z,t)$) and remainders ($v'(\theta,x,z,t)$, $T'(\theta,x,z,t)$). On substituting into (1) the cross terms are zero, so the result is

$$Q_v(\theta,t)/\rho C_p = \int W(\theta,z)\mathbf{v}(\theta,z,t)\mathbf{T}(\theta,z,t)\, dz + \int v'(\theta,x,z,t)T'(\theta,x,z,t)\, dx\, dz \qquad (3)$$

where $W(\theta,z)$ is the width of the basin. The first term may be called the "overturning term", because a net meridional inflow to the basin at one depth must rise or fall vertically within the enclosed region to flow at some other depth—with another temperature.

Define V'_N to be the integral of all positive values of v' over the cross section, and V'_S to be the integral of all negative values. By definition of v', $V'_S = - V'_N$. Roughly speaking (north of the Indonesian Throughflow), one of these will be the western boundary current flow whose annual mean is estimated in Figure 2, while the other will be the interior flow. (3) can then be rewritten

$$Q_v(\theta,t) = \rho C_p \int W(q,z)v(\theta,z,t)\mathbf{T}(\theta,z,t)\, dz + \rho C_p\, V'_N(T'_N-T'_S) \qquad (4)$$

$$= \mathbf{Q}(\theta,t) + \rho C_p V'_N(T'_N-T'_S)$$

where T'_N,T'_S are transport-weighted *horizontal* temperature differences between the northgoing (V'_N) and southgoing (V'_S) water. Inspection of Figure 2 suggests that on annual mean, V'_N has a maximum of about 30 Sverdrups near 10°S; V'_N has strong seasonal variations due to the monsoon wind reversal, but 50 Sverdrups is definitely a reasonable upper limit to its magnitude, in the tropical Indian Ocean. Inspection of maps of temperature on horizontal surfaces (e.g., Wyrtki 1971) suggests that at least in the tropics, $(T'_N-T'_S)$ is unlikely to be as large as 2°C. While it is possible with these figures for the second ("lateral") term of (4) to have a magnitude of order ρC_p x 100 x 10^6 (m^3s^{-1})°C or 0.4 x 10^{15} watts, this seems unlikely on annual mean; and model results, described in Section 3.1 below, suggest that this term is in fact quite small, at least in the tropical Indian Ocean.

Thus the "overturning" term on the right of (3) must at least be important, and it may be the dominant term in the meridional advection of heat. In the integrand of this term, $\mathbf{T}(\theta,z,t)$ is quite well-defined, at least on annual average (Figure 6a). Unfortunately, however, the zonally-integrated mass flow, $W(\theta,z)v(\theta,z,t)$ is far from being well-defined. Fu (1986) gave pictures of $W(\theta,z)v(\theta,z)$ at 18°S and 32°S, but these pictures seem somewhat inconsistent: for example, they imply massive, deep upwelling within the Mozambique Channel, which is not supported by observations. Only at 32°S do we have a clear picture of this quantity, from direct observations across the entire Indian Ocean basin (Toole and Warren, 1993) (Figure 6b). These observations show that 27 Sv flow north rather uniformly with depth between 5000 and 2000 m, and these (with 7 Sv of Indonesian Throughflow) exit mainly in the top 1000 m. Without performing a careful calculation, it is apparent from inspection of Figure 6a and 6b that the inflow across 32°S will have a mean temperature of about 2°C, while the outflow will have a transport-weighted temperature of order 12°C. Thus the integral in the first term on the right of (3) is of order 27 x 10^6 (m^3s^{-1}) x 10°C, at 32°S. While no attempt has been made here to account for the temperature integral for Indonesia, this example confirms that the "overturning term" $\mathbf{Q}(\theta,t)$ can indeed be quite large enough to account for net heat fluxes of order 0.5-1 x 10^{15} watts at this latitude.

However, in the tropics it seems likely that the shape of $W(\theta,z)v(\theta,z)$ is qualitatively different from Figure 6b: there seem to be *two* cells in the vertical, not one. The solid line in Figure 6c shows a qualitative sketch of the shape of the zonally-integrated flow across 10°S. In the top few tens of meters is a thin layer of southward-flowing water, known as the Ekman layer. Its mass

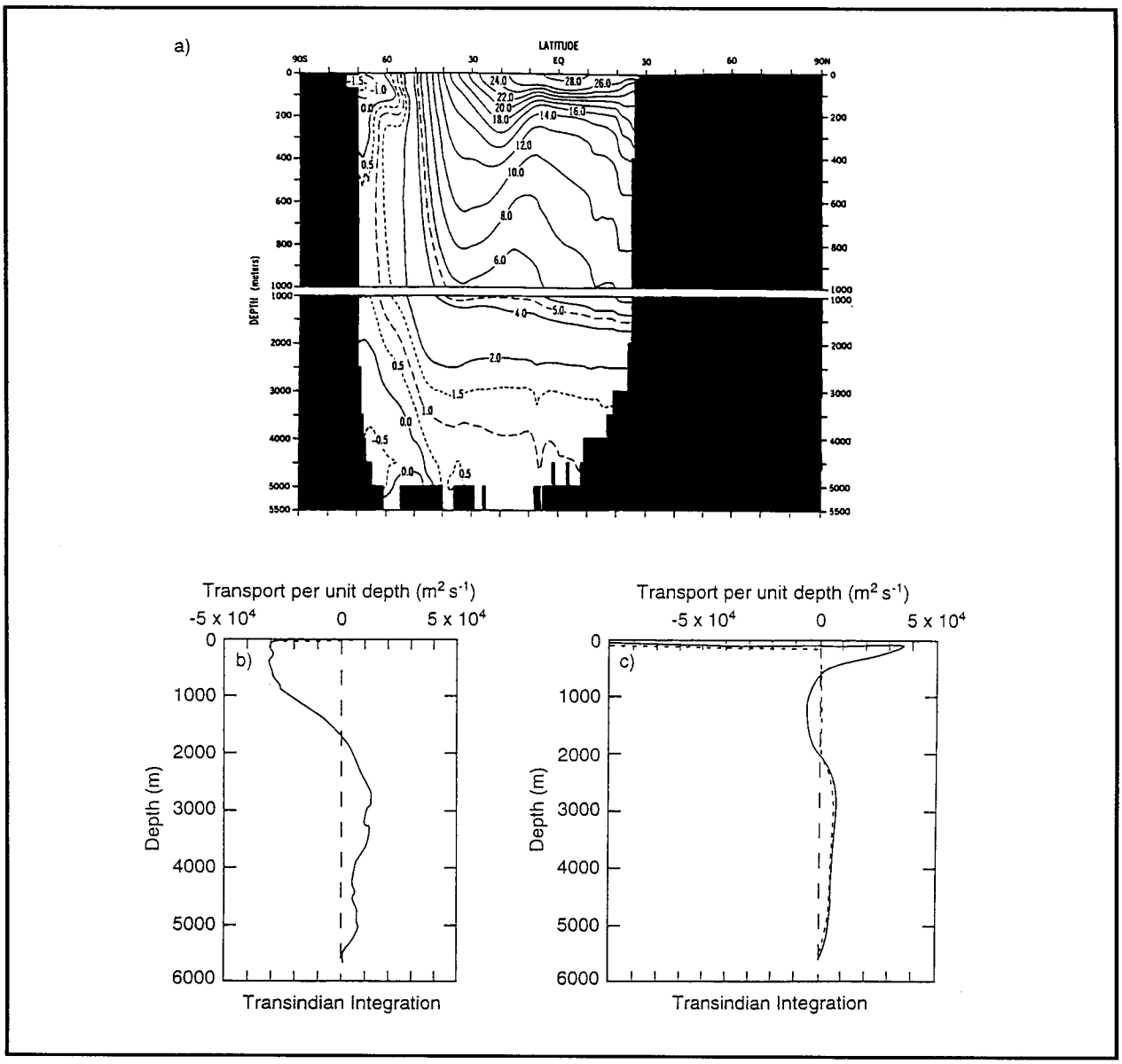

Figure 6. (a) Zonally-averaged temperature in the Indian Ocean, from Levitus (1982). (b) Meridional mass transport across 32°S as a function of depth (from Toole and Warren, 1993). Solid line: geostrophic flow; dashed line: total (Ekman plus geostrophic) flow, with Ekman flow distributed over the top 50 m. (c) Qualitative sketch of two possible forms for the net meridional mass transport across 10°S, as a function of depth. In both, 10 Sv of Ekman flow are distributed over top 100 m. For the solid line, the deep inflow is assumed all to leave at the depth of the oxygen minimum (about 800 - 1000 m). The Ekman transport is all replaced by flow within the thermocline, i.e., above 800 m. For the dashed line, the deep inflow rises to the surface to become part of the Ekman outflow. The real flow pattern is probably more like the solid line than like the dashed line. Because of the very strong near-surface tropical stratification (a), the upper cell (above 600 m, in the solid line) transports more heat southward than the deep cell.

transport is set by the pattern of wind stress*; although they are hard to measure directly, oceanographers are confident that the formula for Ekman transport is quite accurate except within a few degrees of the equator, because (for example) the convergence of Ekman transports is the forcing function giving rise to the Sverdrup flow patterns of Figure 2. The Indian Ocean is unique in that, because the mean wind stresses change from easterly to westerly across the equator (Figure 1), the annual Ekman transports are southward on *both* sides of the equator. Evidently this surface southward flow must be supplied by upwelling from below. As seen in Figure 6c, near 10°S this southward Ekman transport is large—quite comparable to the known deep components of flow. The question arises: Is all of the Ekman transport supplied from the south by flow within the thermocline, as in the solid line? Or is some of it supplied from deeper levels by the northward abyssal flows seen by Warren (1981) and Toole and Warren (1993)?

Discussion relating to this topic date back at least to 1973, when Wyrtki (1973a) noted that along surfaces of constant water density (isopycnals), dissolved oxygen concentrations decrease steadily from saturated values in the Southern Ocean to very low values in the Arabian Sea (e.g., Figure 7). One interpretation of these data is that water flows slowly towards the Arabian Sea along isopycnal surfaces, losing dissolved oxygen as it goes through oxidation of organic matter. Another is that the flow is not along isopycnal surfaces, but wells up within the Indian Ocean from deep inflows. However, Wyrtki (1973a) concluded that "without being able to substantiate this conclusion, it appears that most of the water ascending from the bottom and the deep water returns south in the layer near the oxygen minimum, especially along the western side of the oceans". If so, the deep inflows return south at typical temperatures of 6°-7°C (Wyrtki, 1971); and the large annual mean southward Ekman transports in the tropical Indian Ocean are presumably supplied by inflow *above* the level of the oxygen minimum. The solid line in Figure 6c has been drawn to be consistent with this hypothesis.

More recently, Olson et al. (1993) used observed concentrations of freon-11—an anthropogenically-produced gas whose concentration was near zero before 1964—to deduce that in the depth range of 200 m to 1000 m or so, there was a net *northwards* flow across the southern border of the Arabian Sea at 12°N of about 4 x 10^6 m^3s^{-1}—very similar to the annual mean southward Ekman transport out of this region. Swallow(1984) had arrived at a similar conclusion earlier, from salinity considerations. Their results suggest that this inflow may balance the Ekman-induced outflow (though it probably still does not rule out the possibility that some of it upwells though 1000 m, rather than entering from the south within the thermocline).

At the equator, current meter data are available within about 200 km of the Somali coast for a 2-year period in 1984-1986 (Schott et al., 1989, 1990 and references therein). Schott et al. show that

---

* On time scales of more than a few days, wind stresses induce "Ekman transports" in the top few tens of meters of the ocean, which flow at 90° to the left (right) of the wind in the southern (northern) hemisphere, relative to the unstressed water just beneath. Ekman transports have a magnitude of $(\tau/\rho f)$, where τ is the wind stress vector; ρ is the average water density, and $f = 4\pi \sin\theta/T_d$ is the Coriolis parameter. In the expression for f, T_d is one day and θ is latitude. Note that unless τ changes sign across the equator, $(\tau/\rho f)$ becomes large in magnitude near the equator (θ=0), and changes sign across it; in practice, wind stresses induce downwind rather than crosswind surface flows within about two or three degrees of the equator. Applying these rules either to the annual mean wind stress field (Figure 1) or to the strong boreal summer winds (Figure 8) shows that the Ekman transport is southward throughout the northern Indian Ocean, except perhaps within a few degrees of the equator.

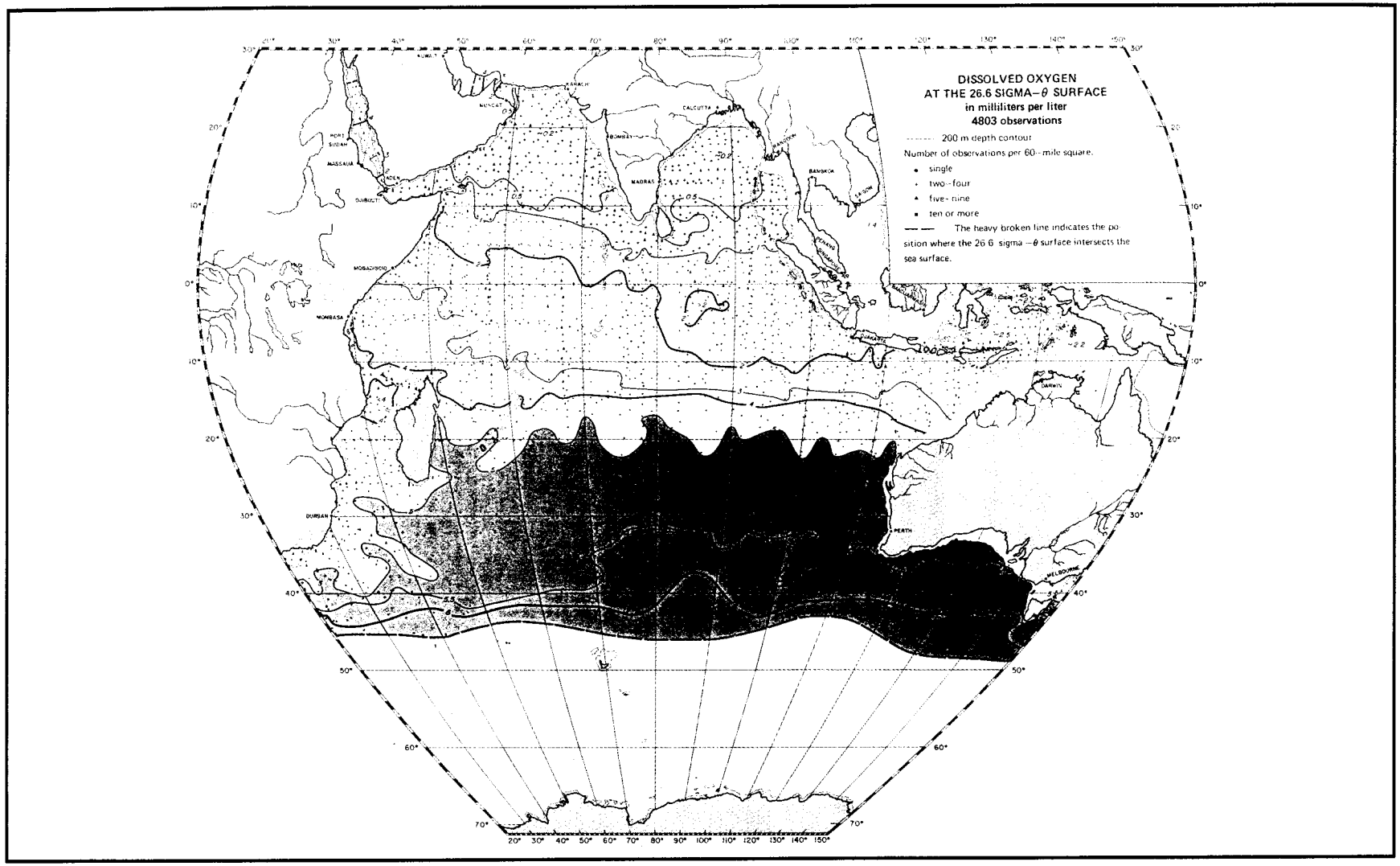

Figure 7. Dissolved oxygen concentration along the surface of constant density σ_0 = 26.6, which occurs at about 270 m in the equatorial Indian Ocean. If water flow primarily follows isopycnals at such depths, the figure suggests a slow flow from the sources of oxygen, at the surface in the Southern Ocean, toward the northern Indian Ocean, with slow deoxygenation en route (from Wyrtki, 1971).

there is a rather steady northward flow between about 120 and 400 m depth, with a seasonally-reversing (downwind) flow above 150 m. On annual mean, there is about 10 Sv of northward flow in the top 500 m, with weak flow between 500 and 1000 m. These data in themselves cannot be used to check the validity of a picture like that of Figure 6c, since there may be large flows across the equator within the interior. However, recently Wacongne and Pacanowski (1995) analyzed the output of a numerical model of the Indian Ocean, in which (at least on annual mean) the southward Ekman transports north and south of the equator flow across the equator in the interior of the ocean, and are supplied by northward flow within the thermocline, at the western boundary. The model reproduced the currents observed by Schott et al. (1990) at the western boundary quite well, which tends to give credence to the model flow patterns in the interior. More detailed discussion of this model is given in Section 3.

The flow in the upper cell (solid line, Figure 6c) has been drawn to have zero net mass flow, so its contribution to the heat transport can be estimated independently of what occurs beneath it. For this flow distribution the transport-averaged temperature between 100 and 1000 m is about 12°C, while the surface Ekman drift has a temperature of about 25°C.This contribution, at 10°S, is of order ρC_p x 10 Sverdrups x 13°C, or 0.5 x 10^{15} watts—a major contribution to the observed surface heat flux of 0.5-1.0 x 10^{15} watts.

Beneath this upper cell, a second cell has been sketched in the solid line of Figure 6c. This contains the northward-flowing water below 2000 m discussed by Toole and Warren (1993) and Warren (1981), and its southward return flow at intermediate depths as suggested by Wyrtki (1973a). Since there is northwards flow in the thermocline, this return flow must be confined below some depth, probably in the range 800-1500 m. Flow within this cell at least is probably driven by thermohaline processes (Warren, 1994), rather than by the Ekman flows thought to be of importance in the upper cell . The deep inflow has a transport-averaged temperature of near 2°C; the estimated temperature of the return flow depends strongly on the details of the velocity distribution, sketched in Figure 6c, but is here assumed to be that of the oxygen minimum water, which is at about 7°C near the equator. The magnitudes of these two flows is probably less than Warren (1981) obtained at 18°S, namely 18 x 10^6 m^3s^{-1}, so the contribution to the heat budget from these terms in tropical latitudes is perhaps of order 0.3 x 10^{15} watts. If the flow were as sketched in the solid line of Figure 6c, the upper cell would thus transport rather more heat than the lower cell. If it were as sketched in the dashed line, there is only one cell, whose heat transport would be about 1.0 x 10^{15} watts—rather large compared to climatology, though not impossible. WOCE data will be needed to find out which of the two alternatives is closer to the truth.

Returning to (1), we note that the breakdown into "overturning" and "lateral" cells is artificial. In reality, all the northward flow in the thermocline across 10°S in fact occurs in the western boundary current—the flow further offshore is in fact southwards, so that the net northward flow through 10°S is probably accomplished only after several passes around the South Equatorial Countercurrent and South Equatorial Current of Figure 2. We saw above that the "lateral" term in (3) was probably less than 0.4 x 10^{15} watts; model results reported below suggest that it is substantially smaller than this. If this is true, it is very convenient for purposes of analyzing the data, because it implies that the horizontal details of the flows in the northern Indian Ocean—which vary in a very complex way through the seasons—are not very important for understanding the net meridional heat flux out of the region. The important quantities (for the upper cell of Figure 6c) are

the magnitude and temperature of the southward Ekman flux (both well-known quantities), and the transport-weighted mean temperature of the *net* geostrophic influx within the thermocline, whose magnitude equals the Ekman transport.

2.3. Annual Mean Heat Flux, Wind Stress, and Heat Transports

On seasonal timescales, the view that Ekman transports and their subsurface replacements play a major role in controlling heat flows in the northern Indian Ocean is strongly supported by two recent numerical model studies of the heat budget of this region (McCreary et al., 1993, referred to below as MKM; and Wacongne and Pacanowski, 1995, referred to below as WP). Neither of these models, nor any other known to the authors, has yet succeeded in reproducing the large northward flow of deep water into the Indian Ocean observed by Toole and Warren (1993). Despite this defect, the MKM and WP models generally do quite well in predicting observed features of the near-surface circulation (top 500 m, say); they produce spatial patterns of surface heat flux which agree reasonably well with observed climatologies; and in the case of WP, the modeled seasonal variation of the net meridional heat transport matches observations surprisingly well. Magnitudes of predicted annual mean meridional heat transports are somewhat small compared to climatology, due at least in part to failure to reproduce the deep cell. Since these models do well on seasonal timescales, they can probably also account for interannual variability of SSTs within the Indian Ocean, on timescales of a few years. Here we discuss the annual mean heat flux patterns within these models.

In these models, Ekman transports induce upwelling of cold subsurface waters in a number of places. Near the Somali and Arabian coasts, the intense longshore winds seen in boreal summer in Figure 8 (and on the annual mean, Figure 1) induce offshore Ekman transports, so intense upwelling occurs in both places—though the details may be rather different in the two places due to the intense boundary currents along the Somali coast compared to the Arabian coast (e.g., Swallow, 1984). Inspection of the longshore winds of Figure 8 suggests that offshore Ekman transport and upwelling must also occur to a lesser extent along both coasts of India, in boreal summer. This is also true on annual mean, though Figure 1 does not have sufficient resolution to show this. Upwelling will be particularly marked near the southern tips of India and Sri Lanka, where quite strong winds blow parallel to the coast and the Coriolis parameter is small. Winds favor upwelling along the south coast of Java during the Asian summer monsoon. Finally, broader-scale but weaker wind-driven upwelling might also be expected in the western Indian Ocean between about 5° and 10°S, because the southward Ekman flows increase in strength from 5°S to 10°S. Some upwelling might be expected south of the equator on the African coast, in northern winter. One striking anomaly of the Indian Ocean is that upwelling does *not* occur along the Western Australian coast, despite strong upwelling-favorable winds. This is a special feature associated with the fact that the onshore Leeuwin Current Extension overwhelms to offshore Ekman transport (Godfrey and Weaver, 1991).

Numerical model results suggest that most of these upwelling regions are indeed major contributors to the heat flux into the northern Indian Ocean. The numerical model of MKM generates an annual mean surface heat flux pattern in the Indian Ocean (Figure 9a) rather like that of Figure 5. For more detailed comparison, Figure 9b shows another climatology, specific to the

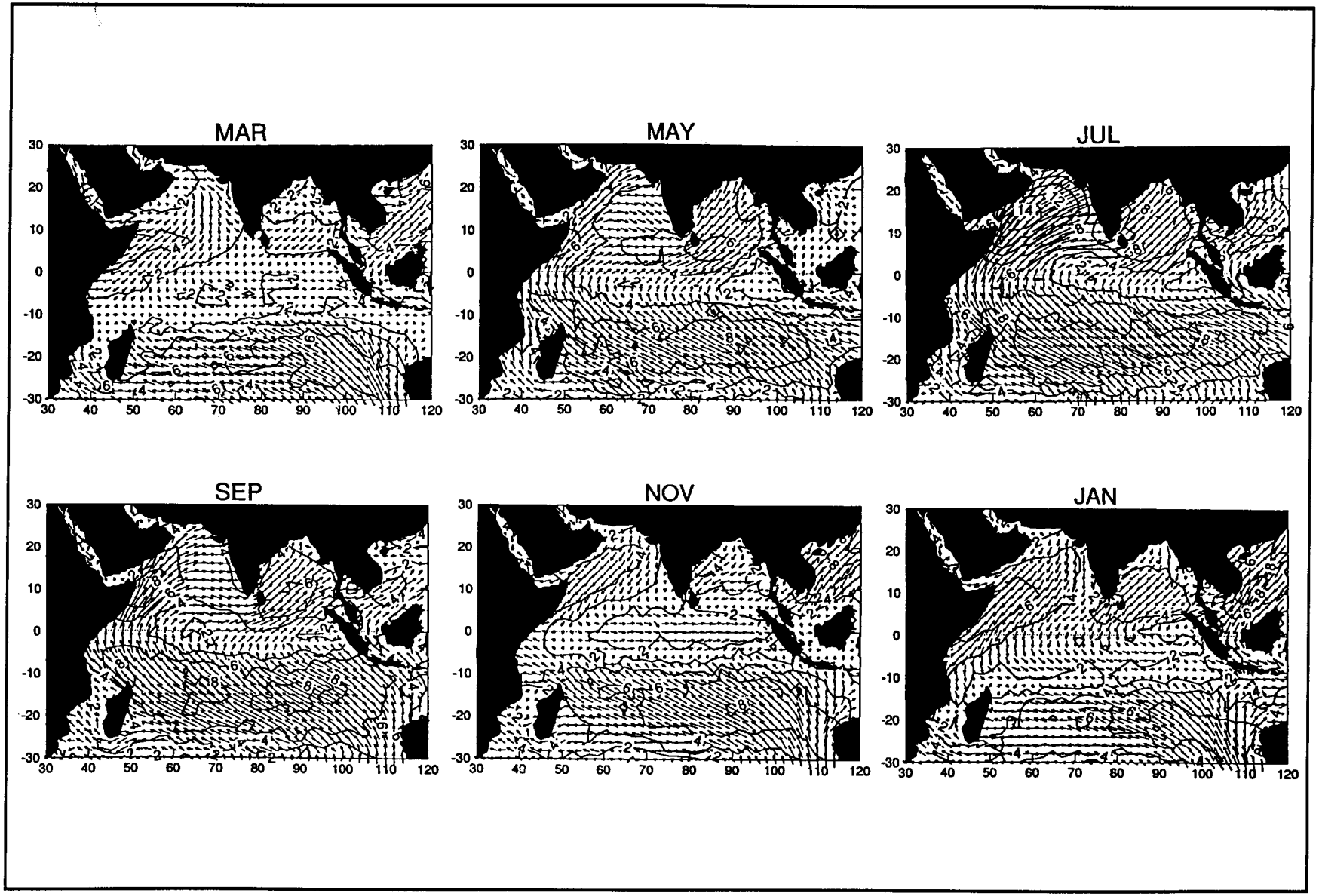

Figure 8. Seasonal mean resultant wind vectors at two-month intervals (from Rao et al., 1991). Contours show wind speed (in m/s).

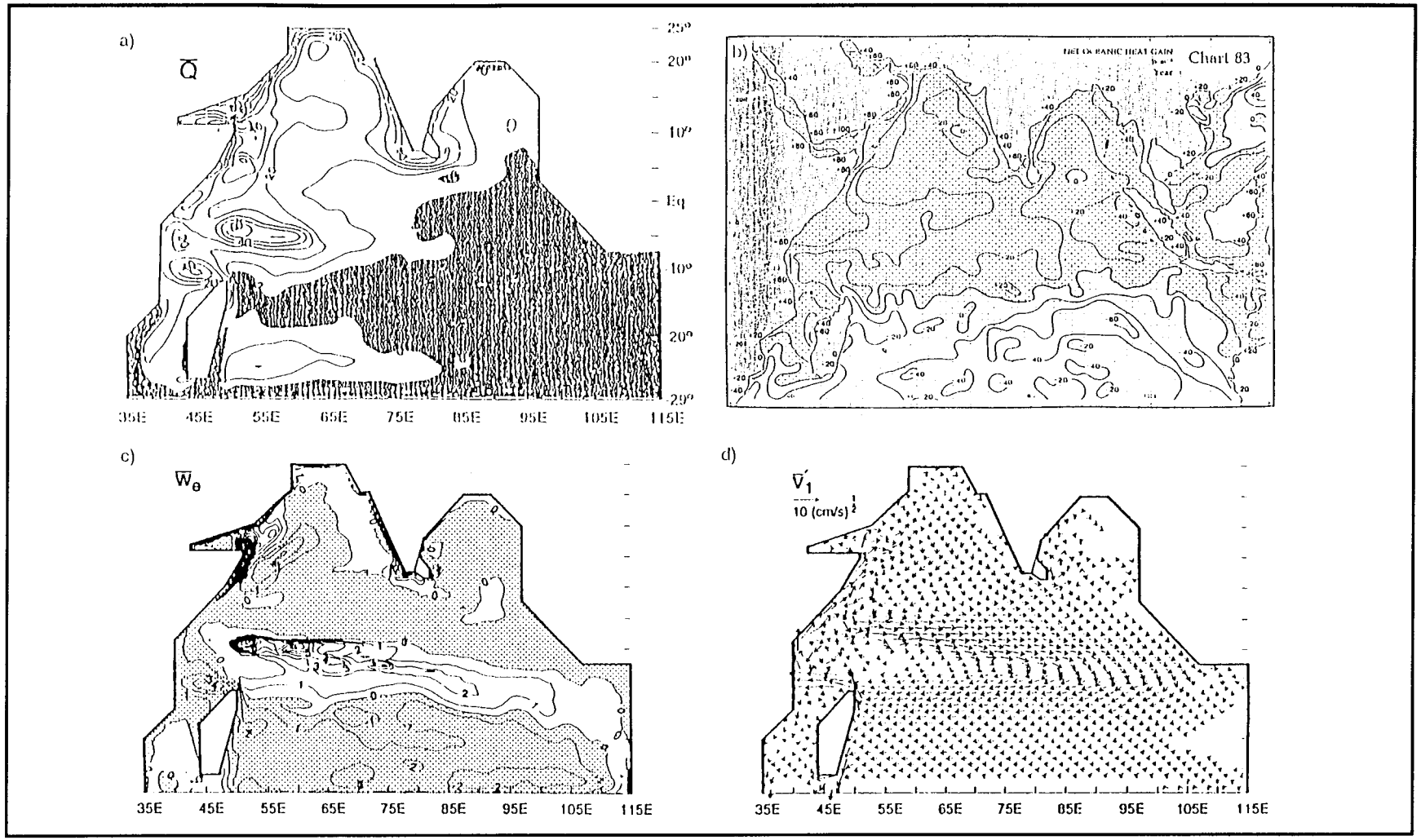

Figure 9. (a) Annual mean net heat flux into the Indian Ocean from the model of McCreary et al. (1993). Contour interval 20 watts/m^2. (b) Annual mean heat flux into the Indian Ocean according to Hastenrath and Lamb (1979). Contour interval 20 watts/m^2. (c) Annual mean entrainment velocity into the surface mixed layer from McCreary et al. (1993). Unshaded regions imply upward entrainment velocity (upwelling). (d) Annual mean surface-layer velocity from McCreary et al. (1992). Magnitudes of the vectors are proportional to the square root of current speed.

Indian Ocean and with somewhat higher horizontal resolution than those of Figure 5. Several other models also produce annual mean surface heat flux patterns with qualitatively similar distributions (e.g., Semtner and Chervin, 1992, figure 26)—though the results depend to some extent on the detailed choice of surface temperature boundary condition. MKM provide a useful season-by-season interpretation of how their pattern (and the associated ocean currents) come about in their model. More recently WP also analyze the heat budget of an Indian Ocean GCM. MKM and WP complement one another, since they come from very different ocean models.

To keep interpretation simple MKM chose a model with only two dynamically active layers and a superposed mixed layer; hence some of the differences of Figures 5 and 9b from Figure 9a may be due to model deficiencies. However, there are several points of qualitative agreement. In particular, in Figures 9a and 6b there is a broad band of maximum heat gain by the ocean along the entire coastline from equatorial east Africa around the Arabian Sea and India to the northern Bay of Bengal. The strongest heating in both occurs near Arabia, and near the southern tip of India. In addition (in MKM) there is another band of heat gain in the western Indian Ocean centered near (5°S, 50°E); a somewhat similar band in the observations is seen in Figures 5a, 5b, and 9b, though it seems to be weaker and more diffuse, and centered on the equator rather than south of it. These regions of maximum heat gain are due, in the MKM model, to "entrainment" (basically, wind-driven upwelling) near these places (Figure 9c). In other words they are due to the detailed features of the wind stress field noted above. The region of the ocean where heat is absorbed in Figure 9a (unshaded region) is broader than the region of upwelling (unshaded region of Figure 9c), because upwelled water typically continues to absorb heat for several months after upwelling (e.g., Seager et al., 1988), and it can be advected through distances of order 1000 kilometers or more in this time. It can be seen that in the model, the annual mean advection velocities (Figure 9d) are offshore and southward in the Arabian Sea, due to mean Ekman transports. Surface flows south of the heating patch at 5-10°S have a strong westward component in addition to the southward Ekman drift, so the heated water is brought into the Madagascar-Africa western boundary current system before it has traveled far south. The patch of ocean heat gain west of Madagascar's northern tip, in Figure 9a, is associated with warming of water that passes equatorward (i.e. into a warmer climate) in the Madagascar western boundary current and then flows to Africa in a zonal jet. There is no clear sign of this heating patch in the observations. The region of heat loss in the eastern Indian Ocean in Figure 9a is associated with the model representation of the Indonesian Throughflow, discussed earlier. Observations actually show strong heat *gain* in the Indonesian Archipelago and for a short distance into the Indian Ocean (Figures 5, 9b). This is thought to be due to strong tidal mixing in this region (Ffield and Gordon, 1992), which is not accounted for in MKM—or in any other model known to the authors; see also Qu et al.,1994, for an analysis of the heat budget in this region in the Semtner and Chervin (1992) model.

Returning to the main body of the tropical Indian Ocean: as already noted, the northwards mass transport in the thermocline which supplies the water upwelled in the tropical Indian Ocean must equal the southward Ekman mass fluxes—thus its mass transport is basically a function of the wind stress field alone. However, the heat flux into the Indian Ocean is proportional to the product of this mass flux with the temperature difference between surface (Ekman) transports and the compensating inflow. What sets the temperature of the inflowing water? Is it likely to be subject to marked interannual variability? If so, it could be a major cause of SST variability in the Indian Ocean. (For example, during ENSO events the *volume flux* of upwelled water changes little in the

East Pacific—what changes is the *temperature* of the upwelled water, e.g., Zebiak and Cane, 1987).

MKM's model specified the temperature of the upwelled water in the Indian Ocean rather than predicting it, because it contained only 2 dynamically active layers (though MKM provide a useful discussion of the horizontal pathways followed by their deep inflow, towards the upwelling regions). WP have supplied a more detailed picture of the vertical structure of flow in the Indian Ocean, by analyzing the output of the Philander and Pacanowski 27-level numerical model. They find (like MKM) that zonally-averaged meridional overturning plays a dominant role in transporting heat, with meridional mass transports basically determined by the Ekman transports. However, the temperature difference between northward and southward flows is a function of their choices of some model details (eddy diffusivity and southern boundary conditions), rather than being specified as in MKM. Figures 10a and 10b show two views of the annual mean, zonally-averaged meridional stream function in the Wacongne and Pacanowski model. A shallow cell, confined to the top 600 m, carries (relatively) cold water north. At most latitudes it is returned by the surface Ekman flow. An exception occurs near the equator, where Ekman dynamics break down and surface water flows downwind. Generally speaking, this means that surface flow on the equator is northward at times of year that Ekman flows are southward, and vice versa (see Figure 8). In the WP model, the ocean responds to this by developing a shallow cross-equatorial "roll" (Figure 10a): the annual mean Ekman transport in effect "dives below" the surface in the northern hemisphere and reemerges at the surface just south of the equator. The northward flow across the equator in Figure 10, between 100 m and 500 m, all occurs near the western boundary; the near-surface cross-equatorial "roll" mainly occurs in the ocean interior.

Figure 10c shows another view of this cell. To generate it, the meridional velocity at each latitude was binned into temperature classes, and then integrated zonally at constant temperature; the average of the result was taken over a year. By integrating this field as a function of temperature, an annual mean streamfunction is created which shows meridional flow as a function of temperature. At 15°S, the inflow (above the zero contour of the stream function at about 10°C—or about 500 m at 15°S, see Figure 10b), is found from the data of Figure 10c to have temperatures between 11° and 22°C* while the outflow has a temperature between 22°C and 27°C. The annual mean mass transport Q in each flow is about 15 Sv; the net resulting estimate of southward heat flux is $\rho C_p Q \Delta T$, where C_p is the heat capacity of water and ΔT is the transport-weighted temperature difference (about 10°C) between the two flows. This is 0.6×10^{15} watts, which is the annual mean heat flux across 15°S in the model (Figure 11).

The annual mean meridional heat transport deduced from the WP model is somewhat small compared to estimates from two climatologies (Figure 11), suggesting either that the model may be missing some other important heat flux mechanism, or that the real temperature difference ΔT is even larger than 10°C. An obvious candidate for a "missing mechanism" is the deep cell of Figure 6c, which is not captured in the WP model. As discussed earlier this deep cell would be expected to remove an additional 0.3×10^{15} watts from the northern Indian Ocean.

---

* It is interesting in this context to note that Warren et al. (1966) observed surface temperatures as low as 13°C, in small regions near Somalia during the Southwest Monsoon. However, it is thought that such waters commonly sink back below the surface, some distance offshore (e.g., Swallow, 1984).

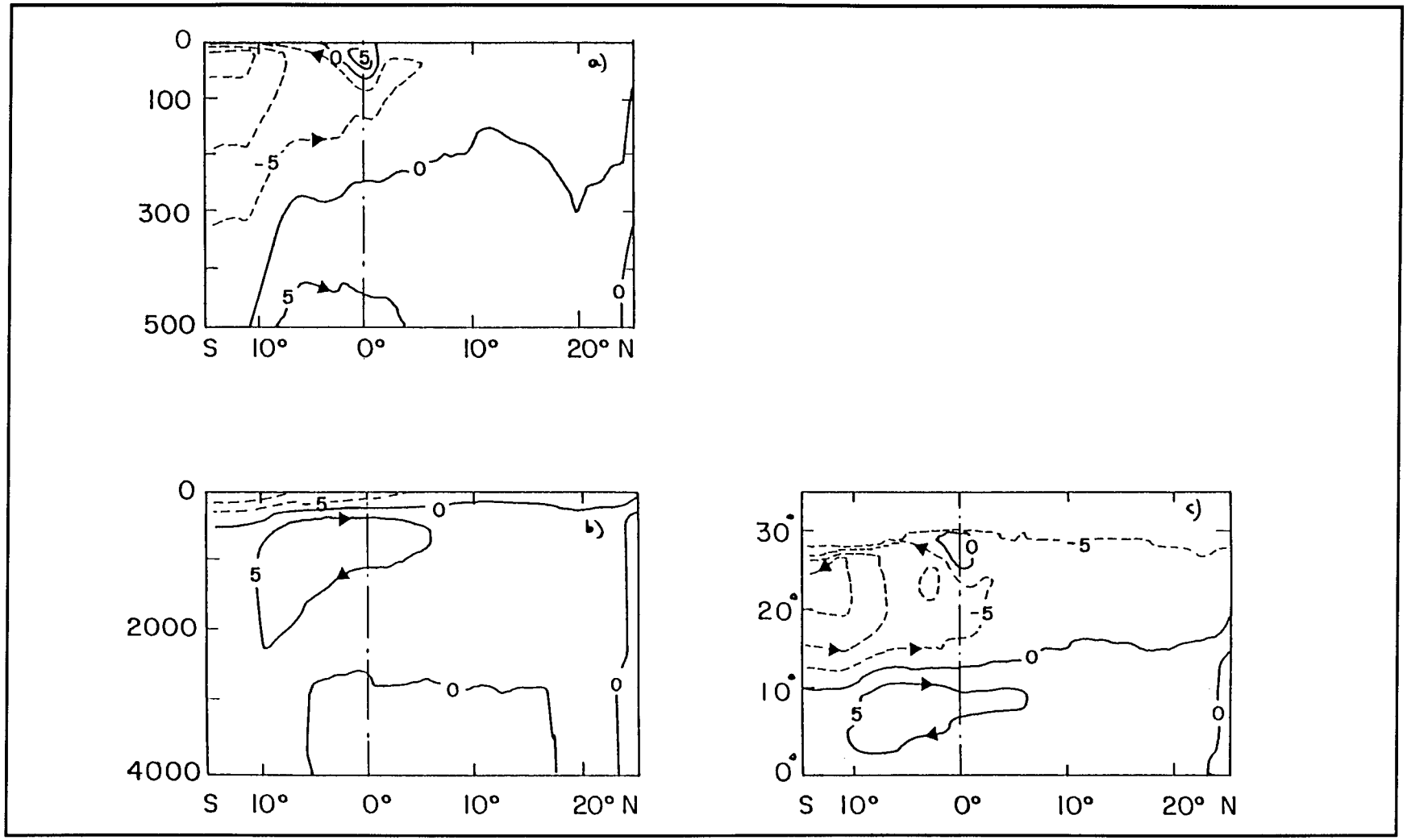

Figure 10. (a) Annual mean meridional stream function for the top 500 m of the Wacongne and Pacanowski model. Contour interval 5 Sv. Note the shallow equatorial "roll". (b) Expanded version of (a) for the entire water column. Ekman transports are too shallow to be seen explicitly. The deep circulation is unrealistic. (c) Meridional stream function from the Wacongne and Pacanowski model, showing meridional and vertical flow as a function of temperature class. (All from Wacongne and Pacanowski, 1994.)

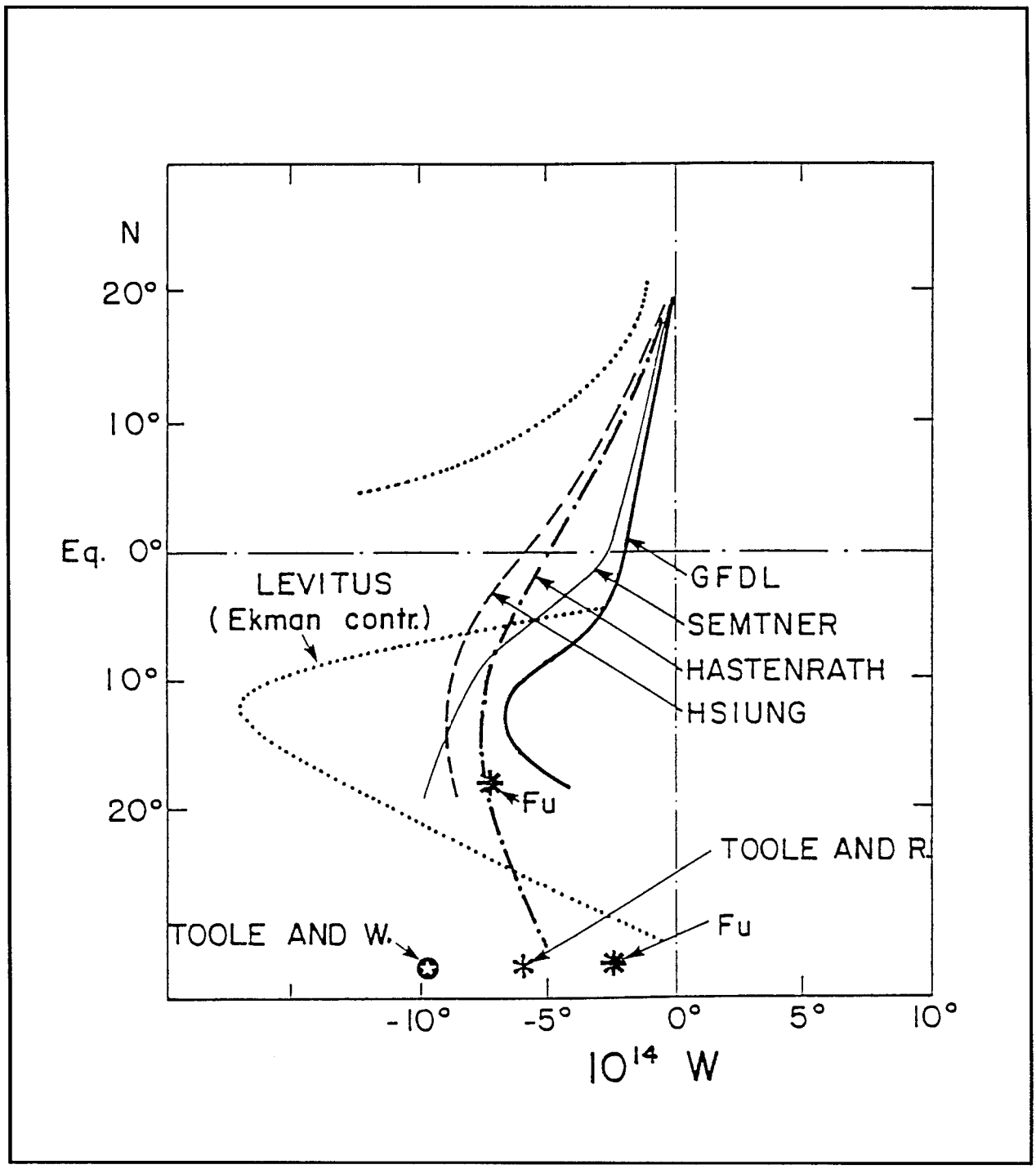

Figure 11. Annual mean southward heat transport in the Indian Ocean, estimated from two climatologies (Hastenrath and Lamb, 1979b; Hsiung, 1985) and from two ocean models (Semtner and Chervin, 1992; Wacongne and Pacanowski, 1995). Estimates from the hydrographic sections of Toole and Warren (1993) and Fu (1986) are also shown (asterisks). The dashed line shows Levitus' (1987) estimates from Ekman fluxes, times the difference between the surface and the depth-mean temperatures. (From Wacongne and Pacanowski, 1995.)

2.4. The Indonesian Throughflow and the Southern Indian Ocean

In most parts of the ocean, mean horizontal circulation (e.g., Figure 2) plays a rather secondary role in the oceanic heat transport compared to the overturning circulation (e.g., Figure 10), because the various circulation cells in Figure 2 (known as "gyres") are quite narrow in latitudinal extent, so the transport-weighted mean temperatures of the northgoing and southgoing parts of the gyres generally differ by only a few degrees Centigrade. The Indonesian Throughflow provides an important exception. The inflow to the Indian Ocean occurs from the equatorial west Pacific where thermocline depths are about the greatest in the world, so transport-averaged temperatures through Indonesia are of order 18°C. Topographic constraints imply that this water must return to the Pacific south of Tasmania, where the transport-averaged temperature is probably of order 6-8°C. A mean throughflow of 10 Sv would therefore export about 0.5 petawatt (1 petawatt = 10^{15} watts) from the Pacific to the Indian Ocean—a substantial fraction of the total heat absorbed by the equatorial Pacific Ocean! Gordon (1986) suggested that this may be a major contributor to the heat supply feeding North Atlantic Deep Water formation (which in its turn is thought to be a major determinant of long-term climate variations, e.g., Manabe and Stouffer, 1988). In this section we outline what is known so far about the effect of the Indonesian Throughflow on the Indian Ocean.

This topic has been studied primarily by several "thought experiments", in which the Indonesian Throughflow has been blocked or otherwise modified in a numerical model, to test the effect on the Indian Ocean circulation and particularly on its surface heat flux field (Godfrey and Weaver 1991; Hughes et al., 1992; Hirst and Godfrey, 1993, 1995). Such "thought experiments" should provide some guidance to the effects that are likely to occur as a result of natural, seasonal and interannual fluctuations of the Indonesian Throughflow—which are now known to be quite substantial (Meyers, personal communication). It is interesting that in models at least (e.g., Pariwono et al., 1986; Godfrey, 1989; Wajsowicz, 1993) these variations are primarily controlled by winds in the *Pacific* rather than the Indian Ocean, especially at the latitudes of the tips of Australasian continent—i.e. the equator and 44°S.

It is concluded from these "thought experiments" that the opening of the Indonesian passages affects the Indian Ocean in four main ways:

i) In a Sverdrup model, the Indonesian Throughflow passes as a zonal jet across the Indian Ocean at its latitude of entry (12°S), thereby increasing the strength of the South Equatorial Current (Figure 12a). It then flows rapidly down the African coast to contribute to the Agulhas Current. Sverdrup models predict an unrealistic zonal jet across the Atlantic at the southern tip of South Africa, returning eastward across both the Atlantic and Indian Oceans at the latitude of southern Tasmania (44°S). A coarse-grid numerical model (Hirst and Godfrey, 1993, 1995; Figure 12b) suggests that the difference between runs with the Indonesian Throughflow open and closed is roughly as predicted by the Sverdrup model, except that the equal and opposite jets across the Atlantic are at least partly "short-circuited" by the Agulhas Retroflection. In this model a large part of the heat loss from the Indonesian Throughflow waters occurs in a band centered at about 40°S, as they move relatively slowly across the South Indian Ocean, exposed to Antarctic winds and cooling (Figure 13). This cooling takes place over a few years, owing to the very deep mixed

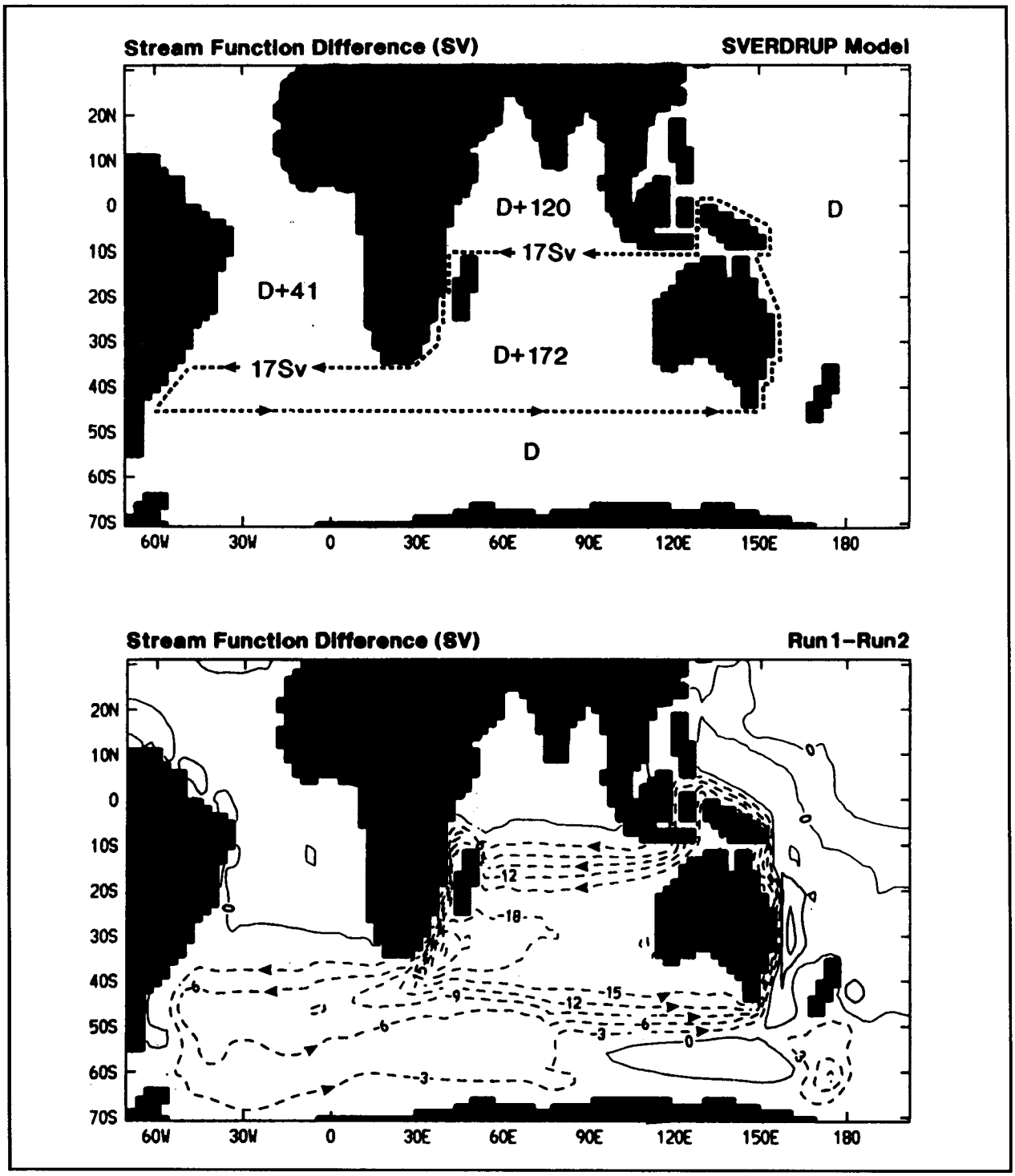

Figure 12. Difference in depth-integrated flow between runs with the Indonesian Throughflow open and closed, according to (a) a Sverdrup model and (b) a coarse-grid primitive equation numerical model (Hirst and Godfrey, 1993). The numbers in Figure 12a represent the changes in depth-integrated steric height, in m^2 (i.e., the double depth-integrated density anomaly) needed to keep the flow differences in geostrophic balance.

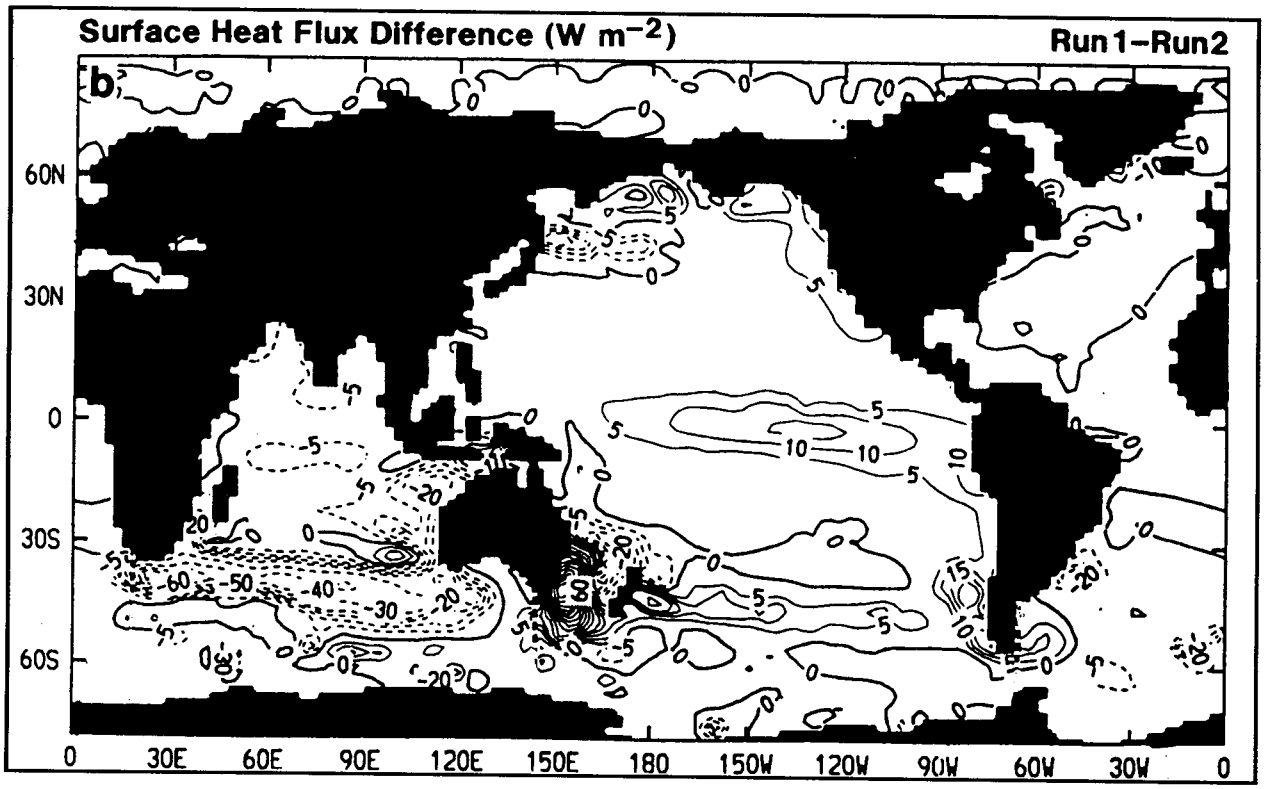

Figure 13. Difference in surface heat flux between runs of a coarse-grid primitive equation numerical model with the Indonesian passages open and closed. (Hirst and Godfrey, 1993).

layers that are formed. Studies of transient runs (Hirst and Godfrey, 1995) suggest that following an increase in the Throughflow, the increase in SST in the Agulhas Outflow will mostly occur 1-4 years afterwards.

ii) More heat loss occurs in Figure 13 in the eastern Indian Ocean, at lower latitudes—nearer the entry of Indonesian Throughflow waters. In the models this is associated with the generation of the Leeuwin Current Extension, discussed in Section 2.1 above. When the Indonesian passages are open, coastal-trapped waves can propagate rapidly from the equatorial Pacific to the northwest Australian coast. These waves act strongly to bring temperatures at each depth along the northwest Australian coast towards the very high values found in the western equatorial Pacific. Consequently mean steric heights off northwestern Australia are also quite similar to those found in the western equatorial Pacific, making them higher than off any other eastern boundary in the world, by some 0.3-0.6 m (Figure 4a). Water temperatures at 50 m off northwestern Australia are about 7°-10°C warmer than at similar latitudes off western America or Africa (Levitus, 1982).

South of 20°S, such high temperatures must result in heat loss to the atmosphere. This reduces the temperatures progressively with distance southwards, in the top 100-200 m near the coast. A "density current" system develops throughout the southern Indian Ocean to maintain geostrophic balance—the Leeuwin Current Extension. That such heat losses do occur is evident from Figures

5a and 5b. In the observed heat flux patterns of Figure 5 (and Figure 9b) heat loss occurs in the eastern Indian Ocean nearly everywhere south of a line that extends NW from 20°S off Western Australia, and then along 10°S to Madagascar. This behavior is markedly different from the Pacific and Atlantic Oceans, in both of which the contour of zero heat flux in Figures 5a and 5b meets the eastern boundary at 45° or 50°N or S—i.e., nearly 3000 km further poleward (except, of course, off South Africa, where the coast stops at 34°S).

According to the ocean modeling experiments mentioned above, these large heat losses (unique to the eastern Indian Ocean) are intimately linked with the existence of the Leeuwin Current Extension (also unique to the Indian Ocean). These flows represent a convection current system, superimposed on the more energetic Sverdrup flow. Basically, what appears to happen is the following:

a) Over the bulk of the Indian Ocean, the warm near-surface waters of the Indonesian Throughflow are carried southward from the South Equatorial Current, by the Ekman transports associated with the strong Trades. The Ekman flows lose heat as they reach higher latitude. The loss of heat also leads to the southward decrease of surface steric height seen in Figure 4a, in the eastern Indian Ocean; an eastward geostrophic flow develops, to keep the steric height gradient in geostrophic balance. The associated geostrophic volume flux towards Western Australia is about 5 times larger than the opposing Ekman flux, associated with the equatorward winds along the Western Australian coast (Figure 1).
b) When this cooled water reaches the coast, it results in nearshore steric heights that are substantially lower than those off Northwest Australia. This longshore steric height gradient cannot be balanced geostrophically, so flow accelerates southwards (into the prevailing wind). This is the Leeuwin Current (Cresswell and Golding, 1980).
c) The onshore flow cools and sinks (i.e., there is downwelling at the Western Australian coast, instead of the Ekman-induced upwelling more common at eastern boundaries). Since momentum fluxes do not play an important role in the formation mechanism of the Leeuwin Current system, the depth-integrated flow associated with the Leeuwin Current system must be nearly zero in order to preserve the Sverdrup depth-integral; hence the deep return flow is basically equal and opposite in transport to the surface flow.

The Leeuwin Current system obtained by the models—particularly those of Hughes et al. (1992) and Hirst and Godfrey (1993, 1995)—are in reasonable agreement with observations (e.g., Godfrey and Ridgway, 1985), apart from the fact that the longshore Leeuwin Current is much too broad and weak. This may be a limitation set by the coarse grid resolution used in all these models (e.g., Batteen and Rutherford, 1990; Weaver and Middleton, 1989). Alternatively, onshore flow may be strong enough to counteract the offshore propagation of Rossby waves (McCreary et al., 1992). The mechanism just described thus seems to provide a useful qualitative picture of the observed distribution of the Leeuwin Current and its associated flows. McCreary and Kundu (1986) provided the first successful model of the Leeuwin Current; in their model the width of the Leeuwin Current is controlled by the decay of westward-propagating Rossby waves, under the action of a surprisingly large vertical diffusion. In the later models, the strong vertical diffusion is supplied naturally by convective overturn. Northward advection by the background Sverdrup flow probably also plays a role (Hirst and Godfrey, 1995). In any case, the patch of net heat loss difference from the ocean, extending for some thousands of kilometers northwest from western

Australia in Figure 13, may be thought of as the heat loss needed to drive the Leeuwin Current in the Hirst-Godfrey model. As discussed earlier, the band of eddies that occurs between southwestern Australia and Madagascar in the Semtner-Chervin model seems to be associated with the Leeuwin Current Extension, and its location in the SC model matches Geosat observations well (Figures 3b and 3c). A very similar band occurred in the Hirst-Godfrey model; they concluded that it represented a front, separating waters that were directly affected by the Indonesian Throughflow from those that are not.

It is interesting that a coastal flow against prevailing winds that is similar, though weaker, than the Leeuwin Current is observed off the west coast of India (Shetye et al., 1991a). Both the Leeuwin Current and west Indian Current are strongest in local winter.

iii) The third way that the opening of the Indonesian passages affects Indian Ocean circulation and heat flux distribution is that it results in marked increases in the depth-integrated steric height throughout the Indian Ocean. According to a Sverdrup model, the changes needed are 172 m^2 between 44°S and 15°S in the Indian Ocean, and by 120 m^2 everywhere north of there (numbers shown on Figure 12a). These are simply the changes needed to preserve geostrophic balance, when the predicted 16 Sv of the throughflow is moved from 44°S (Throughflow blocked) to 16°S (Throughflow open). Since depth-integrated steric height is a double depth integral of density (or roughly, of temperature), the upper ocean must warm as a result: though the amount of warming at a given depth depends sensitively on the depth distribution of the two zonal jets. This warming is reflected (if weakly) in the modeled distribution of heat flux difference in the northern Indian Ocean, as a result of opening the throughflow (Figure 13). Patches of heat loss difference (i.e. reduced heat gain) are seen in each of the major regions of net heat gain in the northern Indian Ocean, namely off the Arabian coast; off southern India; and in a band in the western Indian Ocean, near 5-10°S. It seems likely that the temperature of upwelled water in these regions has increased because of the opening of the Throughflow, resulting in reduced heat gain by the ocean. The magnitude of this effect is small in the Hirst-Godfrey model, but this magnitude is probably model-dependent.

iv) More recent work suggests a fourth way the Indonesian Throughflow affects the heat budget of the Indian Ocean. In southern winter, upwelling-favorable Trade Winds blow along the south coast of Java and Sumatra (Figure 8): it might be expected that these will result in reduced surface temperature and strong heat gain by the ocean. However, (again, in a numerical model—Qu et al., 1994), the cooling from this source is essentially counterbalanced by warming from another—the reduced steric heights along the Java south coast cause the Indonesian Throughflow to increase, and this brings more warm water into the Indian Ocean. A further factor of potential importance for understanding the heat budget of this region is that there appears to be vigorous tidal mixing throughout the Indonesian archipelago (e.g., Ffield and Gordon, 1992, and references therein). This may be the reason that according to most climatologies (e.g., Figure 5) a large amount of heat is absorbed within the Indonesian Archipelago, and for some distance downstream along the path of the Throughflow.

2.5. Freshwater Transport and Freshwater Effects on Heat Transport

Figure 14a shows an estimate of the net freshwater flux into the ocean, from Oberhuber (1988). Such estimates are subject to even greater uncertainty than the net heat flux; however the qualitative nature of the pattern—e.g., that the southeast Indian Ocean and Arabian Sea are regions of strong net evaporation, while the Bay of Bengal and the waters west of Indonesia are regions of strong net rainfall—are too close to common experience to be doubted. The pattern is roughly mirrored by the salinity distribution at 100 m (Figure 14b, from Wyrtki, 1971), except that the Indonesian Throughflow introduces a tongue of fresh water along 15°S that reaches the African continent. The pattern is still evident, though increasingly distorted by intrusions of fresher water from the Southern Ocean, down to 600 m depth; and the saline nature of the Arabian Sea persists down to 3000 m (e.g., Wyrtki, 1971), apparently due to the mixing of dense, salty inflows from the Red Sea and Gulf down to these depths.

To the authors' knowledge, no attempt has yet been made to understand the pattern of freshwater transports in the Indian Ocean needed to maintain this salinity distribution, in the face of freshwater transports. However, since such strong east-west gradients of net freshwater input are evident in Figure 14a, the simple meridional picture of Section 2.2 will not be adequate. Presumably the strong, seasonally-varying zonal currents of this region must play a major role in this process.

The subject is of interest because freshwater inputs can modify the surface heat budget—whose interannual variations are of primary interest to the ocean observing system for climate. The Bay of Bengal provides one of the clearest known examples of this effect. Boreal summer winds are strongly favorable to upwelling along the east coast of India (Figure 8). They must draw denser water into the surface Ekman layer. However, the Bay of Bengal is very strongly salt-stratified at this time; hence the dense water that is upwelled may be saltier, rather than colder, than the ambient surface water. This may alter the surface heat budget considerably compared to the Somali Current region (Shetye et al., 1991a, b).

2.6. Deep Circulation and Heat Exchange

Theoretical understanding of the abyssal ocean circulation dates back to the seminal work of Stommel and Arons (1960). As opposed to the wind-driven currents discussed earlier, this analysis focused attention on flows driven by buoyancy. The canonical overturning circulation [so-called the thermohaline circulation for the flow driven by air-sea exchange of temperature and salinity (fresh water)] consists of formation of dense water by air-sea interaction (typically at high latitude), the export of these waters from the cooling regions and gradual warming in the ocean interior, and finally a compensating return flow to the deep water formation sites of warmer waters from shallower depths. Owing to its northern termination at low latitude, no water is made sufficiently dense by air-sea exchange in the North Indian Ocean to sink to the bottom. Thus all the abyssal waters found in the Indian Ocean must be imported. They are, in fact, traceable to dense water formation sites in the northern North Atlantic Ocean and around Antarctica.

Within the Stommel-Arons framework, the deep upwelling supported by the introduction of newly formed bottom waters drives interior circulations that are closed by deep western boundary

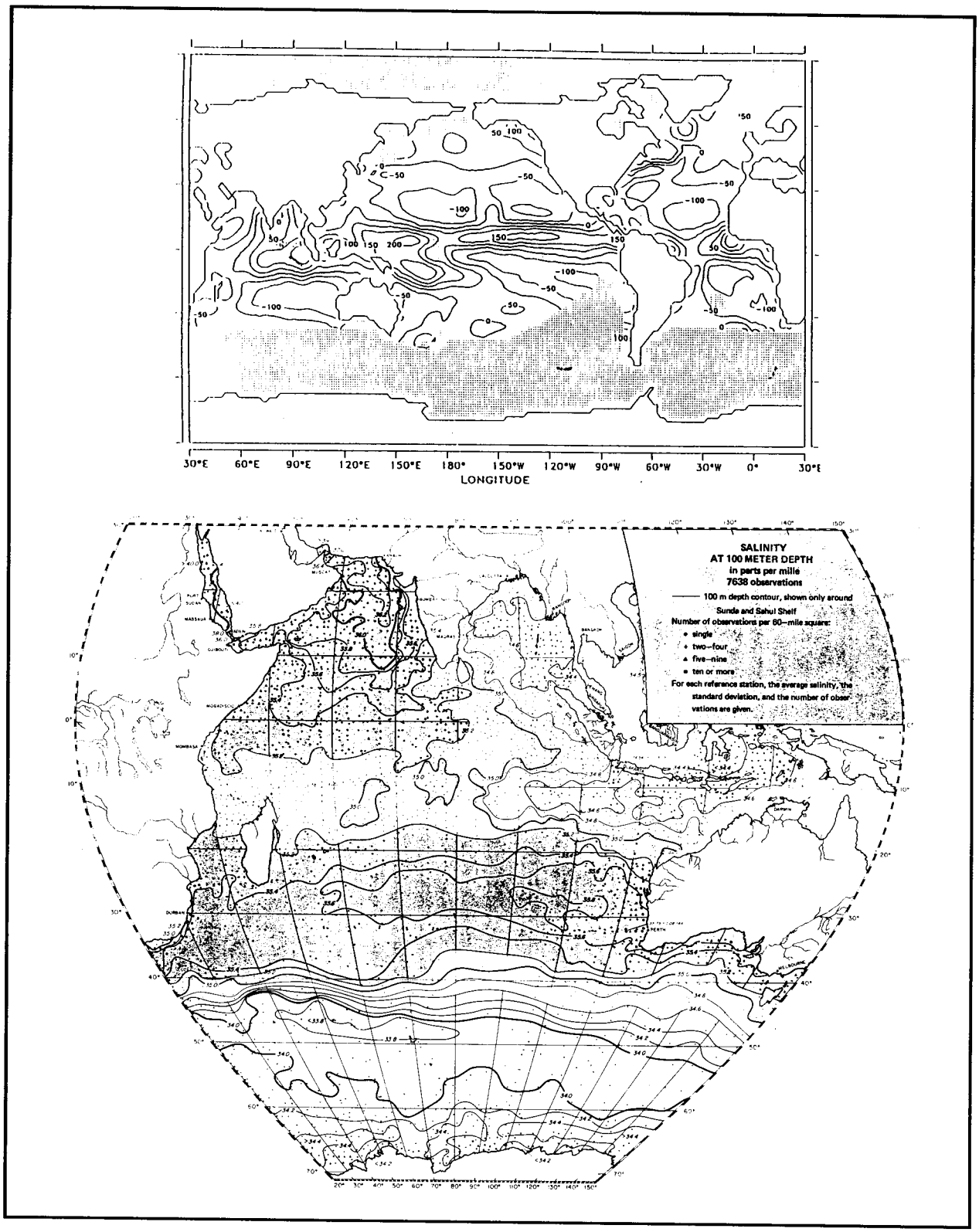

Figure 14. (a) Annual mean net freshwater flux (precipitation-evaporation) (from Oberhuber, 1988). Contour interval 50 mm/month. (b) Mean salinity at 100 m (from Wyrtki, 1971). Contour interval 0.2.

currents. The Indian Ocean is notable for its rich, complex bathymetry that subdivides the Ocean into multiple basins. Within the majority of these, deep boundary currents have been identified carrying newly formed and recirculating bottom waters northward.

The eventual fate of these northward flowing bottom waters remains unclear, but increasing evidence suggests that significant conversion of cold, dense bottom waters to warmer, less dense waters occurs within the Indian Ocean. Thus, the Indian Ocean circulation may represent a significant part of the return limb of the global thermohaline circulation (Schmitz, manuscript in preparation). The evidence includes estimates of horizontal flow convergence through hydrographic sections implying balancing vertical, cross-isothermal motions (i.e., Johnson and Warren, 1979; Toole and Warren, 1993), inference of enhanced upwelling strength from the transport of deep western boundary currents via the Stommel-Arons formalism (Warren, 1981), and chemical tracer measurements (Sjoberg and Stigebrandt, 1992).

Equally uncertain are the mechanisms responsible for modifying the cold, dense bottom waters. North of 30°S, ocean surface temperatures fall no lower than about 10°C. Thus, while air-sea exchange processes might be invoked to explain ocean temperature change at temperatures greater than 10°C, alternate explanations must be found for conversion of colder waters. For example, Toole and Warren (1993) estimated that some 25 Sv of deep water moves vertically across the 2000 m level within the Indian Ocean north of 30°S in a process that must involve water property modification. (They deduced that cold water moving north through their section below 2000 m, was converted within the Indian Ocean interior, and returned southward as warmer thermocline water.) Internal mixing appears capable of supporting such a conversion. (Indeed, there are few alternative explanations possible. Geothermal heating, for example, is not nearly strong enough to support so large a conversion.)

In recent years, a series of ocean microstructure measurements have been made to diagnose the intensity of mixing in the ocean and to document its causes. Instability of the ubiquitous ocean internal wave field appears to support only minimal mixing (Gregg, 1987; Polzin et al., 1995). However, stronger mixing appears possible when the intensity of the internal wave field is elevated. Model results of Sjoberg and Stigebrandt (1992) suggest that due to its rugged bathymetry, the Indian Ocean might be a region of enhanced internal wave generation and, in turn, mixing. Significantly enhanced mixing has been observed adjacent to sloping bathymetry (Toole et al., 1994a, b) presumably due to the kinematics of internal wave reflection from the bottom. If this is a universal result, hypsographic considerations would suggest enhanced mixing in the deep Indian Ocean versus, say, the North Pacific as a larger fraction of the deep Indian's volume is in close proximity to the bottom than the Pacific's.

The overturning circulation diagnosed for the Indian Ocean in which cold, dense waters move north to be converted to warmer thermocline waters that return south has associated with it a significant meridional heat flux. For balance, this heat transport must be balanced by fluxes across the surfaces of the Indian Ocean. As geothermal heating is quite small, that leaves heat exchange between the atmosphere and ocean. The Toole and Warren (1993) circulation had an associated heat flux divergence figure of order 1 pW. This is somewhat larger than, but comparable to estimates of air-sea exchange based on meteorological calculations (e.g., Figure 11). Recent consideration of the dissolved silica budget for the Indian Ocean suggests a somewhat smaller

overturning circulation than found by Toole and Warren (J. Toole, personal communication), but nevertheless sizable. Extensive observations during the WOCE Indian Ocean Expedition in 1995-1996 will significantly refine the estimate of overturning in this ocean and its role in the global thermohaline circulation.

3. Seasonal Variations in SST, Heat Fluxes, and Mixed Layer Depth

3.1. Zonally-integrated Heat Transports

As for the annual mean heat budget, it is useful in examining the seasonal heat budget to consider zonal averages first. Hastenrath and Lamb (1980) performed the first such analysis: they began by analyzing the two broad regions (0-30°N) and (0-30°S) They found that the behavior of the southern hemisphere, on this average picture, is reasonably simple. The area-mean SST in the southern hemisphere follows a "traditional" seasonal cycle, with highest SST in southern autumn (March) and lowest in southern spring (September). They also showed that the seasonal pattern of the net surface heat flux into the water is a near-sinusoid, that is nearly in quadrature with the seasonal cycle of SST. Furthermore, the annual average of this net heat flux is small compared to the amplitude of the sinusoid. At any time, the net heat flux into the ocean must be balanced by the sum of the rate of change of heat storage (Q_t) and the meridional advection of heat Q_v—and Q_t must be zero on annual average, so Q_v must be small, at least on annual average. Hastenrath and Lamb concluded that the simplest hypothesis to explain their results was that in the southern hemisphere—at least on area average—the Indian Ocean heat budget is dominated by local heat storage (Q_t), which varies sinusoidally through the year in a readily understandable way.

A similar treatment of the northern hemisphere revealed a much more complex behavior, due to the monsoons. It showed that Q_v and Q_t must be of similar magnitude, and that both must have strong and complex seasonal variations. However, Hastenrath and Lamb (1980) found that hydrographic data available at that time were inadequate to test this hypothesis.

A little later, Hsiung et al. (1989) were able to perform a detailed analysis of meridional average heat budgets, latitude by latitude. They used Levitus' (1982) global data set of seasonal-mean hydrographic data to obtain the heat content $Q(\theta,t)$ of the top 300 m of the Indian Ocean north of a given latitude θ, as a function of season. Its time derivative $Q_t(\theta,t)$ gives an estimate of the rate of change of heat storage north of θ. They then subtracted $Q_t(\theta,t)$ from the area-integrated net surface heat flux north of the given latitude θ, in season t. In most parts of the world ocean these two terms would largely cancel one another, but in the northern Indian Ocean they do not, so the difference is well-defined and large. This difference must be the net meridional heat transport $Q_v(\theta,t)$ across the latitude θ, in the Indian Ocean. Figure 15a shows their result, as a function of latitude and season. More recently, Hastenrath and Greischar (1993) obtained a similar pattern, using a more extensive hydrographic data set (Figure 15b).

It is apparent from Figure 15a that the net northward heat transport into the Indian Ocean displays a strong seasonal cycle, whose amplitude is large compared to its annual mean. It is strongly southward (negative) in northern summer, when zonal mean Ekman drifts (Figure 15c) are southward on both sides of the equator; and it is northward—though less strongly so—in northern

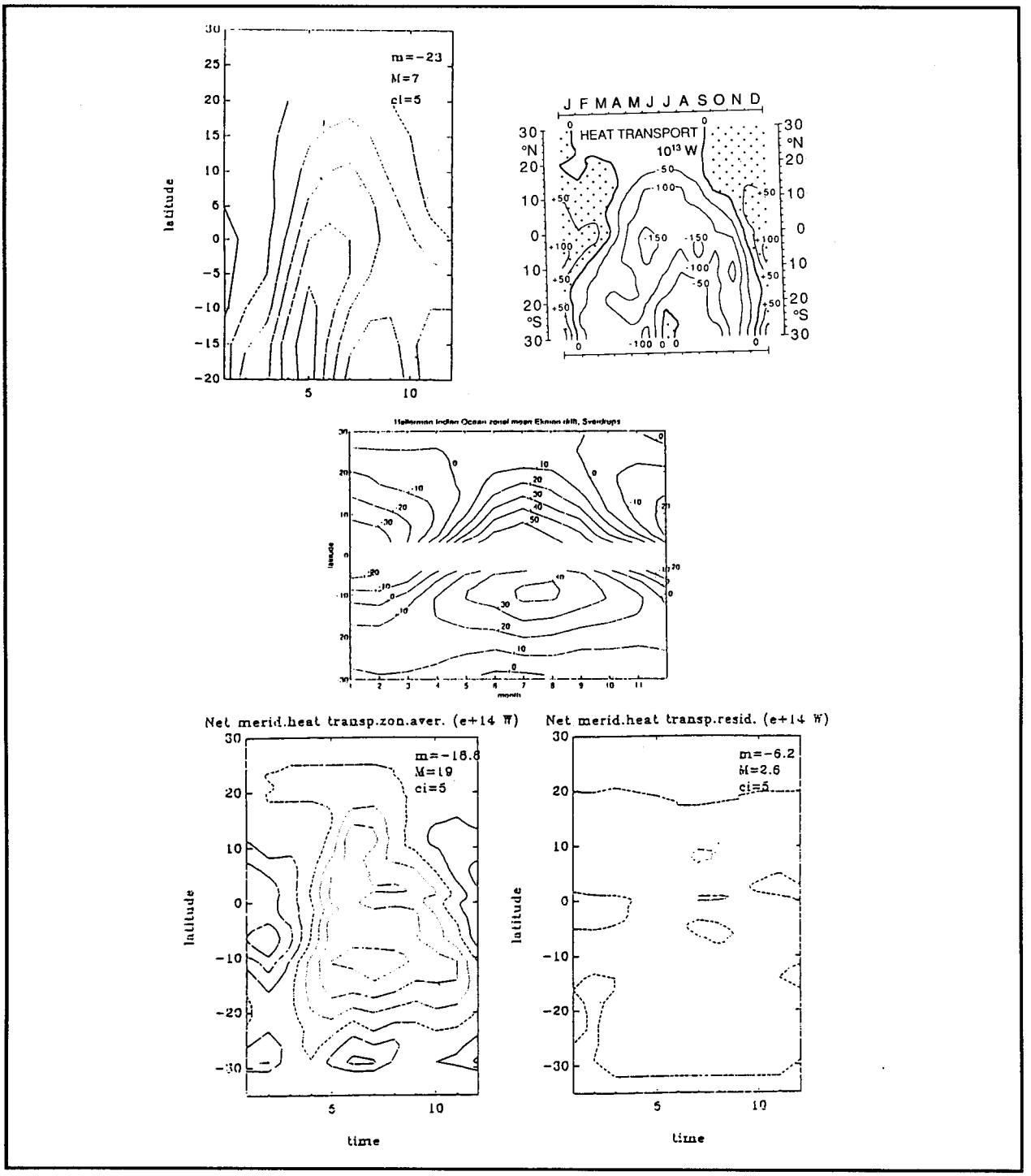

Figure 15. (a) Seasonal mean northward heat transport in the Indian Ocean as a function of latitude and season. Drawn from the data of Table 1, Hsiung et al., 1989. Contour interval 5 x 10^{14} watts. (b) As for (a), from Hastenrath and Greischar, 1993. (c) Zonally-integrated northward Ekman transport as a function of latitude and season from Hellerman and Rosenstein (1983) winds. Contour interval 10 Sv. (d) As for (a), from the model result of Wacongne and Pacanowski, 1995. (e) Lateral heat transport term from the model result of Wacongne and Pacanowski, 1995.

winter, when Ekman drifts are northward on both sides of the equator. This result suggests that, as proposed by Levitus (1987) and Wacongne and Pacanowski (1995), Ekman transports (and their cooler subsurface replacements) may play a dominant role in carrying the net surface heat flux out of the northern Indian Ocean—not just on annual mean, but seasonally. This is seen specifically by noting that if the transport-weighted temperature difference between the Ekman flow and its subsurface replacement were *constant* seasonally then Figure 15c would simply be proportional to the Ekman-forced component of meridional heat transport. Best agreement of Figures 15c with Figures 15a and 15b occurs for a temperature difference of about 10°C.

There are clear differences between Figures 15a and 15b and Figure 15c. For example, the strongest July Ekman transports north of the equator (at 4°N) are larger than the strongest Ekman transports south of the equator (at 13°S); by contrast, the seasonal-maximum heat transports get steadily stronger with distance southwards, at least to 10°S (Figures 15a and 15b). Another difference is that the strongest heat transports occur in May to July, one to two months earlier than the strongest Ekman transports. However, the results suggest that the Ekman transport and its subsurface replacement play a major role in removing heat from the northern Indian Ocean.

Figure 15d shows the net meridional heat transport from the GFDL model discussed in the previous section (Wacongne and Pacanowski, 1995). North of the model's "sponge layers" (i.e., north of about 20°S), Figure 15d agrees quite well quantitatively with Figures 15a and 15b, within the uncertainties of the latter—including the region near the equator, where Ekman transports are ill-defined. Wacongne and Pacanowski find that, in their model, the shallow "overturning cell" discussed earlier plays a dominant role in northern summer. In northern winter the Ekman convergence into the northern hemisphere is not removed by outflow within the thermocline; i.e., it is not simply the reverse of the summer pattern. Instead the whole thermocline is displaced downwards, and abyssal flows move southwards along the eastern sides of topographic features such as the mid-ocean ridge at 90°E. Nevertheless, the agreement suggests also that their model is generating a fairly accurate value of the transport-weighted temperature difference between the Ekman flow and its subsurface replacement, at least for the seasonally-varying component (it is likely to be different from the annual mean component).

The agreement of Figure 15d with Figures 15a and 15b raises an important question: how important is the "lateral" heat flux term (second term of (4))? WP explicitly calculated it in their model; it is shown in Figure 15e, as a function of latitude and season. Evidently, it is almost negligible in their model, independent of season.

If this is true in reality, it is a very important result. It means that the massive (and very complex) horizontal variations of current that occur seasonally in the upper tropical Indian Ocean play little role in the net meridional transport of heat. This would greatly simplify the task of keeping track of interannual variations. The result is also surprising (it is definitely not true at 32°S, e.g., Toole and Warren, 1993). As noted earlier, the size of the horizontal variations in transport are up to 40 Sv , so the WP result must mean that the horizontal variations in temperature $\Delta T'$ defined earlier must be very small in their model—definitely less than 1°C. Unfortunately, this is a difficult result to test observationally. The WOCE Indian Ocean campaign should provide a few snapshots that will allow observational testing of the magnitude of the lateral heat transport term, relative to the overturning term.

3.2. Geography of the Heat Budget in the Northern Indian Ocean

As for the annual mean, it is necessary to supplement this zonally-averaged picture with a detailed geographic look at where and when heat is absorbed. One extremely important role for an Indian Ocean the ocean observing system for climate would be the provision of the data needed to initialize a model of the Indian Ocean each April-May, before the Asian monsoon onset. The evolution of SST predicted by a coupled model over the following summer monsoon season will depend on this choice of initial state, because the mixed layer typically deepens during this time, exposing layers of water to the atmosphere that were covered by warmer water in May. Upwelling will also bring deeper, colder water to the surface, and the resulting SSTs are strongly dependent on pre-monsoon conditions (e.g., Anderson et al., 1991). Thus anomalies in subsurface temperatures in April-May should translate into SST anomalies a few months later.

To understand interannual anomalies of SST, it is at least necessary to begin from a thorough understanding of what causes SST to change in a typical year, not just on area average but locally. MKM provide a detailed analysis of this process, emphasizing particularly the development of the monsoon ocean currents. The following remarks are based on MKM; but in the interests of brevity we include only minimal discussion of monsoon-reversing ocean currents. These can now be quite accurately modeled, including major nonlinear features such as the "Great Whirl" off Somalia (e.g., McCreary and Kundu, 1988; Luther and O'Brien, 1989). However, as discussed above, these do not seem to play a major role in *zonally-averaged* heat transport. While they must certainly be important for local effects on the heat budget, and will modify the simple interpretation given below, they will not be discussed here; the reader is referred to MKM for details.

In "quiet" ocean locations far from land, SST is usually warmest at the end of local summer, and coldest at the end of winter. This is valid in the southern Indian Ocean, south of 15°S, which cools by 3°-5°C from March to September (Figure 16). By contrast, Figure 16 shows that in an average year SST *also* cools by 2°-3°C from May to September throughout most of the northern Indian Ocean. This is partly due to the fact that much of the northern Indian Ocean becomes cloudy and windy with the onset of the Asian summer monsoon. According to Hastenrath and Lamb (1979b), between April and July solar radiation actually falls by 40-80 w/m^2 in most of the northern Indian Ocean; and latent heat loss, which is nearly uniform at 80 w/m^2 throughout the northern Indian Ocean in April, increases to 120-160 w/m^2 in July. An important exception occurs in the western Arabian Sea, which remains cloudfree so solar radiation input remains roughly constant; and latent heat loss remains near 80 w/m^2. However, the seasonal upwelling is strongest at this time of year. Generally speaking, detailed inspection of Figures 8, 16, and 17 shows that the cause of the general cooling from May to September can be traced to enhanced surface heat loss away from the western and northern boundaries, and to the effects of upwelling near them. Another factor contributing to the SST decrease from May to September is wind mixing. Away from the coastal upwelling regions, the mixed layer deepens from about 30 m in May to 50 m or more in September (Figure 18; see below).

It is instructive to follow the sequence of net surface heat flux (Figure 17) every two months through the year, using the winds (Figure 8) and SSTs (Figure 16) for guidance. In March the Northeast Monsoon winds are weakening (Figure 8). The heat flux into the ocean (Figure 17) is

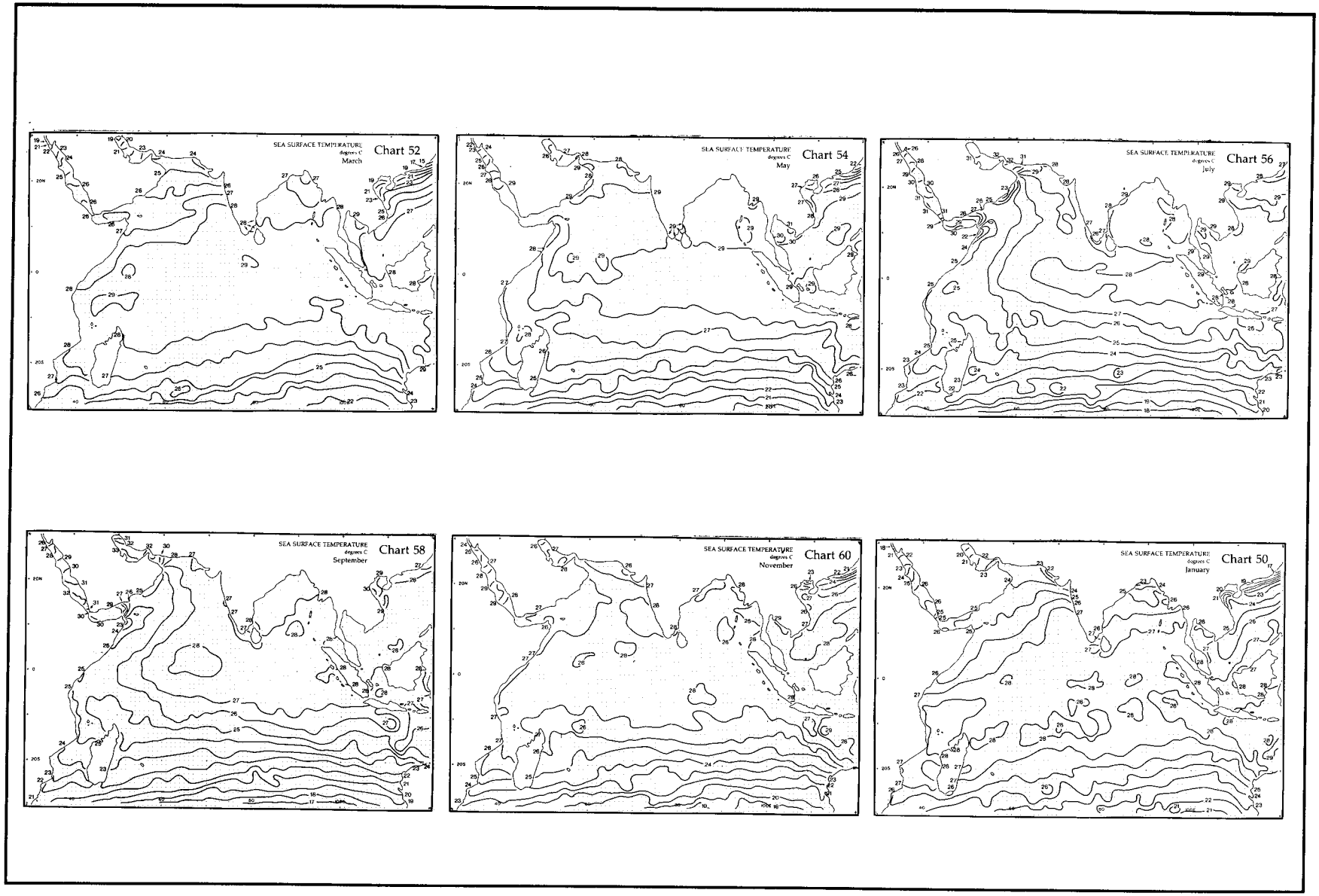

Figure 16. Seasonal mean SST in the Indian Ocean at two-month intervals (from Hastenrath and Lamb, 1979a).

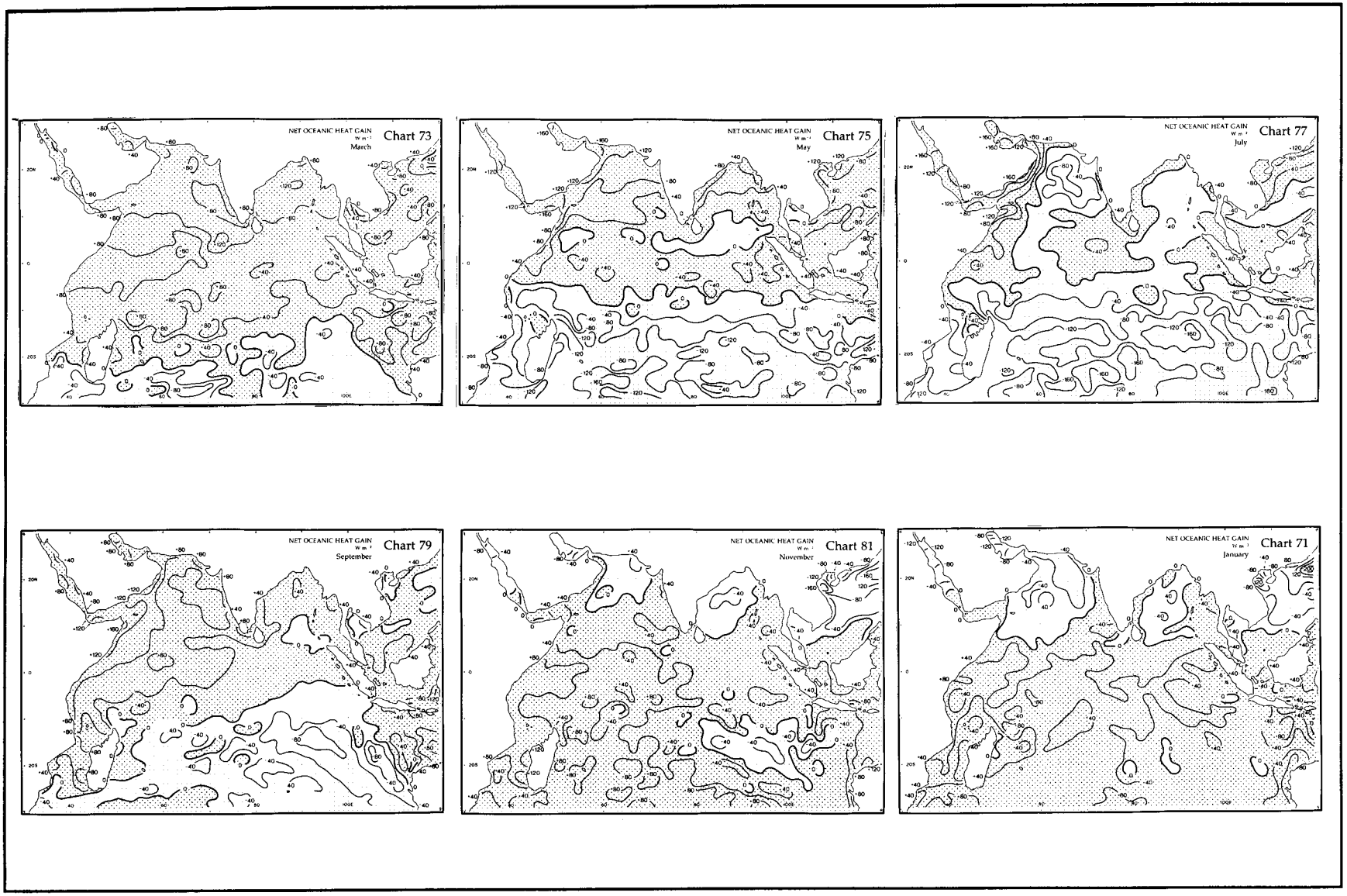

Figure 17. Seasonal mean net heat flux into the ocean at two-month intervals. Contour interval is 40 watts/m^2 (from Hastenrath and Lamb, 1979).

rather uniform zonally at this time, but with a strong bias towards the northern hemisphere due to the relative lack of clouds there. By May, the Southwest Monsoon winds have begun, and maxima in net heat flux have developed near the Somali, Arabian and eastern Indian coasts. At this stage quite strong westerlies blow along the equator, particularly southeast of Sri Lanka (Figure 8): the resulting patch of high latent heat loss causes the region of net heat loss from the ocean there in May, in Figure 17. Similarly, the net heat loss in the Bay of Bengal and the central and western Arabian Sea in July (Figure 17) reflect high winds and latent heat loss (and enhanced cloudiness) in these regions in July. The region of heat gain near the Somali and Arabian coasts is intense in July; heat gain is greater at the coast than just offshore, and SSTs are cooler, along almost the entire coast from equatorial Africa to Bangladesh. This suggests that upwelling is significant along all these coasts. By September the monsoon winds are still present, but they have slackened, and the region of heat gain has broadened away from the coast (presumably due to offshore advection of cool upwelled water). From then right through into the following March, the ocean gains heat throughout most of the northern Indian Ocean; the only exceptions occur at the northern ends of the Arabian Sea and Bay of Bengal, where cold, dry Northeast Monsoon winds cause strong latent heat loss in November and January.

The general impression from Figures 16 and 17 is that cold water is upwelled during the Asian summer monsoon over several months, at a number of locations along the coastline from equatorial Africa to Bangladesh. Strongest upwelling occurs near Somalia, Arabia and the southern tip of India (minima in SST, maxima in net heat flux). The upwelled water absorbs heat over several months as it moves away from the upwelling zones. This is at least qualitatively consistent with the picture formed from the discussion of the annual mean heat flux pattern.

Curiously, however, in Figure 17 there is no indication of the patch of heat gain by the ocean near 10°S, in the western equatorial Indian Ocean, predicted in Figure 6a; nor is there any clear sign of it in the annual mean of Figure 17 (Figure 9b). Furthermore, the observed SSTs show no minimum near this location. On the other hand, the observed seasonal pattern of mixed layer depth (MLD) (Figure 18, from Rao et al., 1989. A similar climatology has been prepared by Hastenrath and Greischar, 1989) shows a band of minimum MLD along 10°S, near where it would be expected from Ekman divergence, throughout the year; it is a persistent feature of the regular XBT sections through this region (Meyers, personal communication). It remains to be seen whether the discrepancy in the surface heat fluxes between Figures 6a and 6d is due to some inadequacy of the model (note that other models show a similar feature, e.g., Semtner and Chervin, 1992; Hirst and Godfrey, 1993) or to a problem with the observations (Bauer et al., 1991).

We start the discussion of the MLD seasonal cycle in May. MLD is shallowest throughout the northern Indian Ocean at this time, except for a region of deep MLD in the eastern equatorial Indian Ocean. The latter reflects the accumulation of water in this region by the May Wyrtki jet. These are strong eastward surface jets along the equator, driven by the equatorial westerly winds of May and November (Wyrtki, 1973b). The May minimum in MLD throughout the northern Indian Ocean (and annual maximum in SST, see Figure 16) is to be expected, since it follows a period of strong net heat flux into the ocean and weak winds; mixed layer models predict shallowing MLDs and rapid SST rise under these circumstances. By July—after 2 months of strong monsoon winds—the MLD pattern has changed drastically. Deep maxima in MLD occur in the central Arabian Sea and Bay of Bengal. Coastal MLDs do not deepen nearly so much, from the Somali coast to

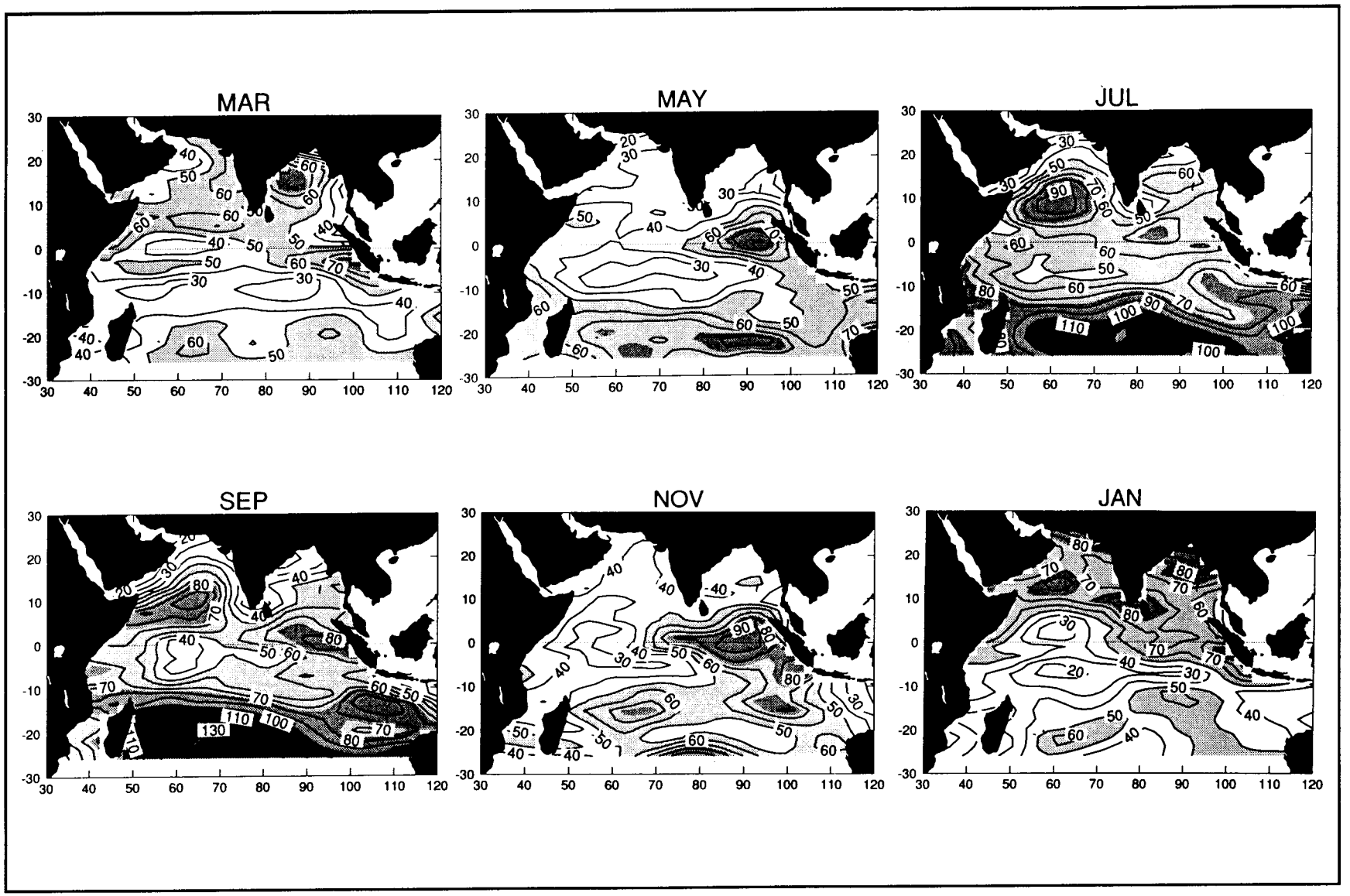

Figure 18. Seasonal mean mixed layer depth (defined by the depth at which temperature is 1°C less than at the surface) at two month intervals. Contour interval is 10 m (from Rao et al., 1989).

Bangladesh. The maximum mixed layer depths in July occur near (10°N, 60°E), to the southeast of the strongest SW Monsoon winds (Figure 8), where Ekman surface fluxes converge. Very deep mixed layers have developed south of 15°S, under the influence of strong net surface heat loss (Figure 17), and strong wind mixing and Ekman convergence (Figure 8). Details of these processes in the Arabian Sea have been studied by Rao (1986) and Rao and Mathew (1990).

These conditions persist through September. By November the SSTs have warmed somewhat under the light winds of October, except in the northern Bay of Bengal and Arabian Sea where cold, dry Northeast Monsoon winds start to cool them (Figure 8); and MLD shallows in most of the northern Indian Ocean. By January the Northeast Monsoon winds have apparently caused substantial cooling and MLD deepening in the northernmost Indian Ocean. South of 15°S net heat flux into the ocean and reduced wind speeds have resulted in a shallowing of the mixed layer and surface warming.

The MLD patterns of Figure 18, which are estimated by taking MLD as the depth at which temperature is 1°C colder than at the surface, has a maximum throughout the year in the eastern equatorial Indian Ocean. However, this is a region of heavy rainfall, and a strong salinity-stratified "barrier layer" is found in this region (Sprintall and Tomczak, 1992); so the true MLD (which should reflect an increase in water density, rather than a decrease in temperature) is probably less than shown in Figure 18. This may also apply to the January deepening of MLD in the northernmost Indian Ocean.

The Indian Ocean equatorial currents differ from the other two oceans in that they are much more variable. Models (and data) indicate that their dynamics are dominated by wave radiation. (A flow structure similar to the "classical" Equatorial Undercurrent only exists in the western Indian Ocean during the spring.) Zonal advection of temperature is not likely to be an important thermodynamic process because the horizontal gradients of temperature are small.

In the Pacific during ENSO downwelling Kelvin waves radiate from the western Pacific, deepen the pycnocline on the eastern Pacific, and hence weaken the upwelling of cold water. A similar process, but less direct, may occur in the Indian Ocean: downwelling equatorial Kelvin waves radiate around the Bay of Bengal into the Arabian Sea, eventually deepening the pycnocline in the upwelling regions and weakening the cooling there (e.g., Potemra et al., 1991).

3.3. Geography of the Heat Budget in the Southern Indian Ocean

It has already been noted that on area average, the seasonal behavior of SST in the southern Indian Ocean is quite like that expected from the "classical" picture of mixed layer development (e.g., Kraus and Turner, 1967). However, two major seasonal features are worth discussing. One is the existence of an extremely vigorous annual Rossby wave, near 12°S: the phase of these waves propagates west-southwestwards, basically along the axis of the South Equatorial Current, at a speed of about 0.10-0.18 m/s. (The group velocity is west-northwestwards). At this speed the waves take about 2 years to cross the Indian Ocean. Perigaud and Delecluse (1992) obtain good agreement between the observations of these waves—from Geosat altimeter data—and a model driven by observed winds. The maximum amplitude of the wave is about 0.12 m. This implies

large seasonal variations in thermocline depth, and probably also in mixed layer depth: it is not yet known if these variations have an appreciable effect on the net surface heat flux and SST.

The second strongly seasonal feature of the South Indian Ocean is the Leeuwin Current. This flows most strongly southward along the Western Australian coast in May. As a result, the highest SSTs occur on the Western Australian continental shelf in May, rather than March (Cresswell and Golding, 1980; Godfrey and Ridgway, 1985; Smith et al., 1991). This May maximum in current largely reflects the fact that the southerly winds along this coast are weakest around May, though seasonal variations in the longshore pressure gradients may also contribute. If so, they must be confined to a nearshore region—in the open ocean the meridional pressure gradients show little seasonal variation.

4. Interannual Variability of Indian Ocean SST and its Effect on Climate

4.1. Indian Ocean SST Anomalies and the El Niño-Southern Oscillation (ENSO) Phenomenon

Not surprisingly, the largest known pattern of SST anomalies in the Indian Ocean is associated with the largest known interannual climate signal, namely ENSO. Cadet (1985) and Wright et al. (1985) both provide an analysis of this topic. Many of the conclusions below are drawn from Cadet (1985), but we illustrate them with results from Wright et al. (1985). The latter authors undertook a comprehensive analysis of relationships between surface variables and ENSO, using the global COADS (Comprehensive Ocean-Atmosphere Data Set) data set (Fletcher et al., 1983). They were able to combine the useful illustrative nature of the "composite" approach to studies of the Southern Oscillation Index (e.g., Rasmusson and Carpenter, 1982) with the mathematical advantages of a study of correlation and regression. Noting that sea level pressure at Darwin makes a useful index of the Southern Oscillation by itself, and that changes in Darwin pressure anomaly tend to occur around April of each year, they defined an annual mean Southern Oscillation Index (SOI) as the average Darwin pressure anomaly for May of the given year to April of the following year. They correlated this Index with three-month means of anomalies of SST, wind, air temperature and cloudiness throughout the global ocean, over the period 1950-1979, starting from December-February preceding the "Darwin pressure year" and continuing to March-May at the end of that year. High Darwin pressures imply ENSO-like conditions, so the regression coefficient maps of Figures 19-21 in effect provide a composite history of events in an ENSO year.

Figure 19 shows the regression coefficients of surface winds on annual mean Darwin pressure, for the Indian and Pacific Oceans, starting in March-May of the "Darwin pressure year" (Figure 19a). (The preceding December-February regressions are very weak everywhere). The most striking feature of Figures 19a-e is the development of "westerly wind bursts" in the western equatorial Pacific Ocean, with easterlies in the eastern Indian Ocean developing about 3 months later. Notice that these pictures show no noticeable changes in the Southwestern Monsoon winds along the Somali coast in June-August (Figure 19b). This is somewhat surprising, since monsoon rainfall is definitely weaker over India during ENSO events on average, and winds and rainfall are usually closely related. A minor strengthening of the NE Monsoon winds can be seen in Figure 19c. The band of easterlies along 10°S in December-February (Figure 19d) indicate a weakening of the Australasian Monsoon winds during an ENSO year.

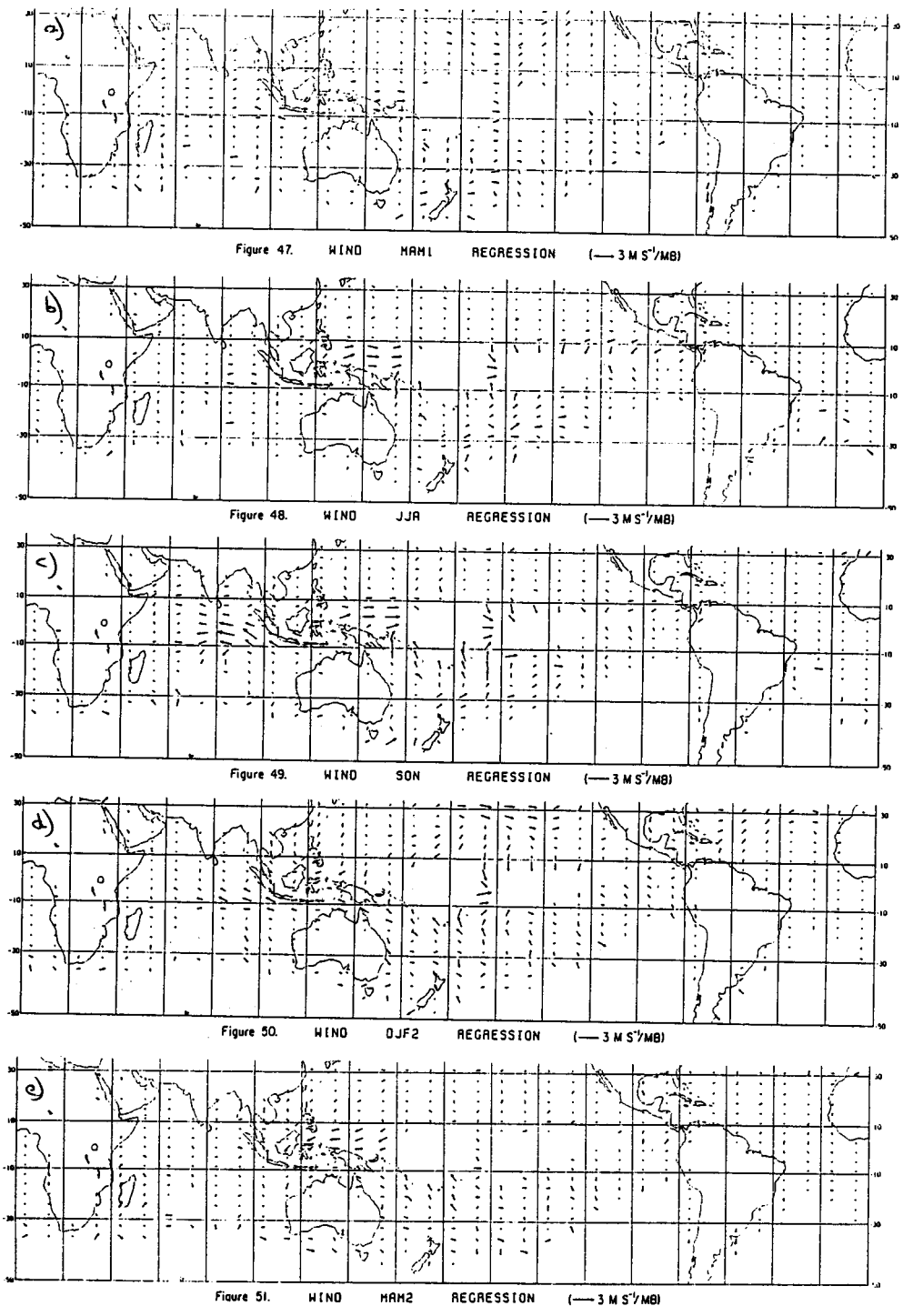

Figure 19. Regression of COADS wind anomalies in the Indian and Pacific Oceans with sea level pressure at Darwin, averaged annually from May through the following April. Adapted from Wright et al. (1985). (a) Regression of December-February anomalies with the following May-April mean Darwin pressure; (b) - (e) As in (a) for subsequent three-month periods.

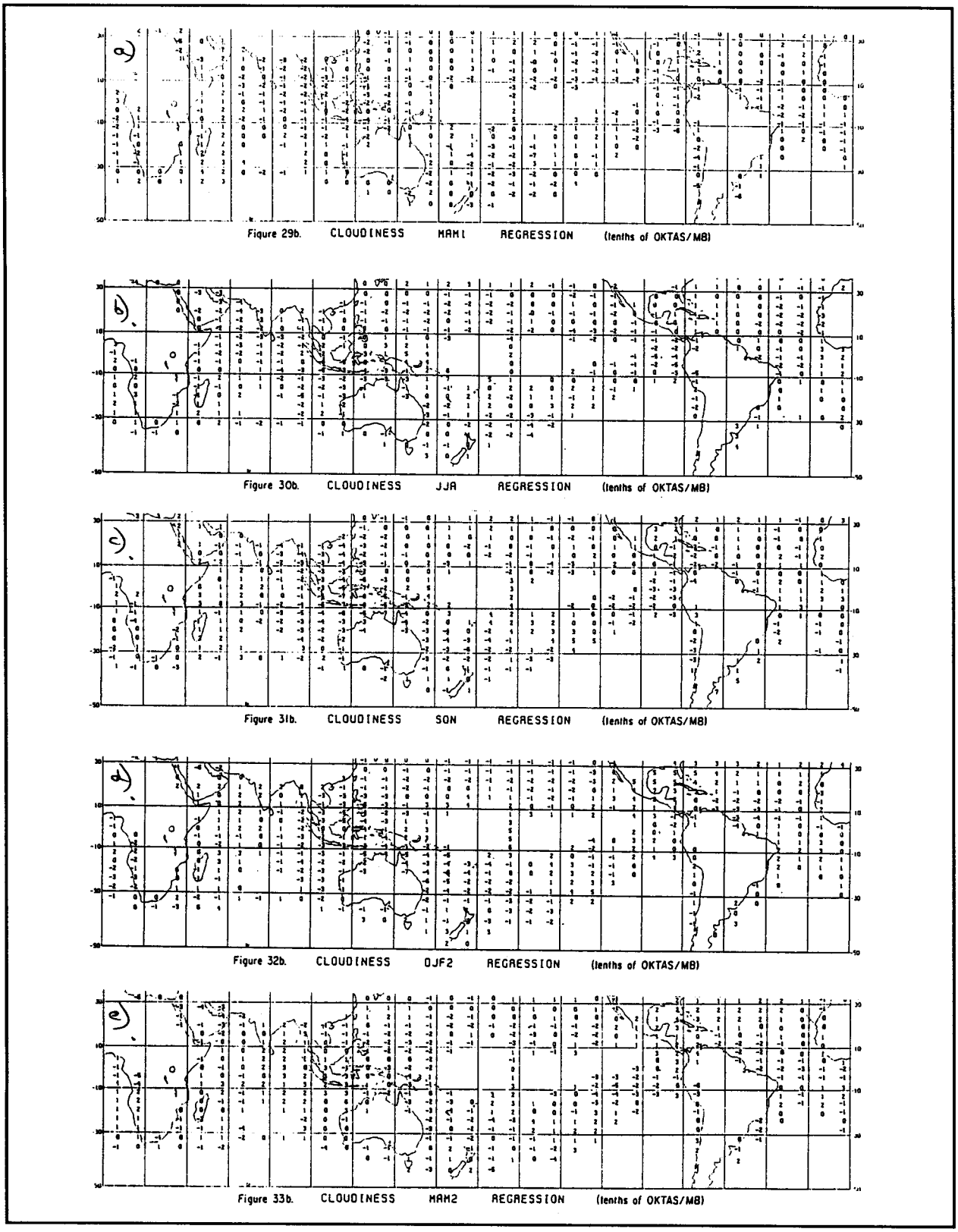

Figure 20. As in Figure 19 for COADS cloudiness anomalies in the Indian and Pacific Oceans. Adapted from Wright et al. (1985).

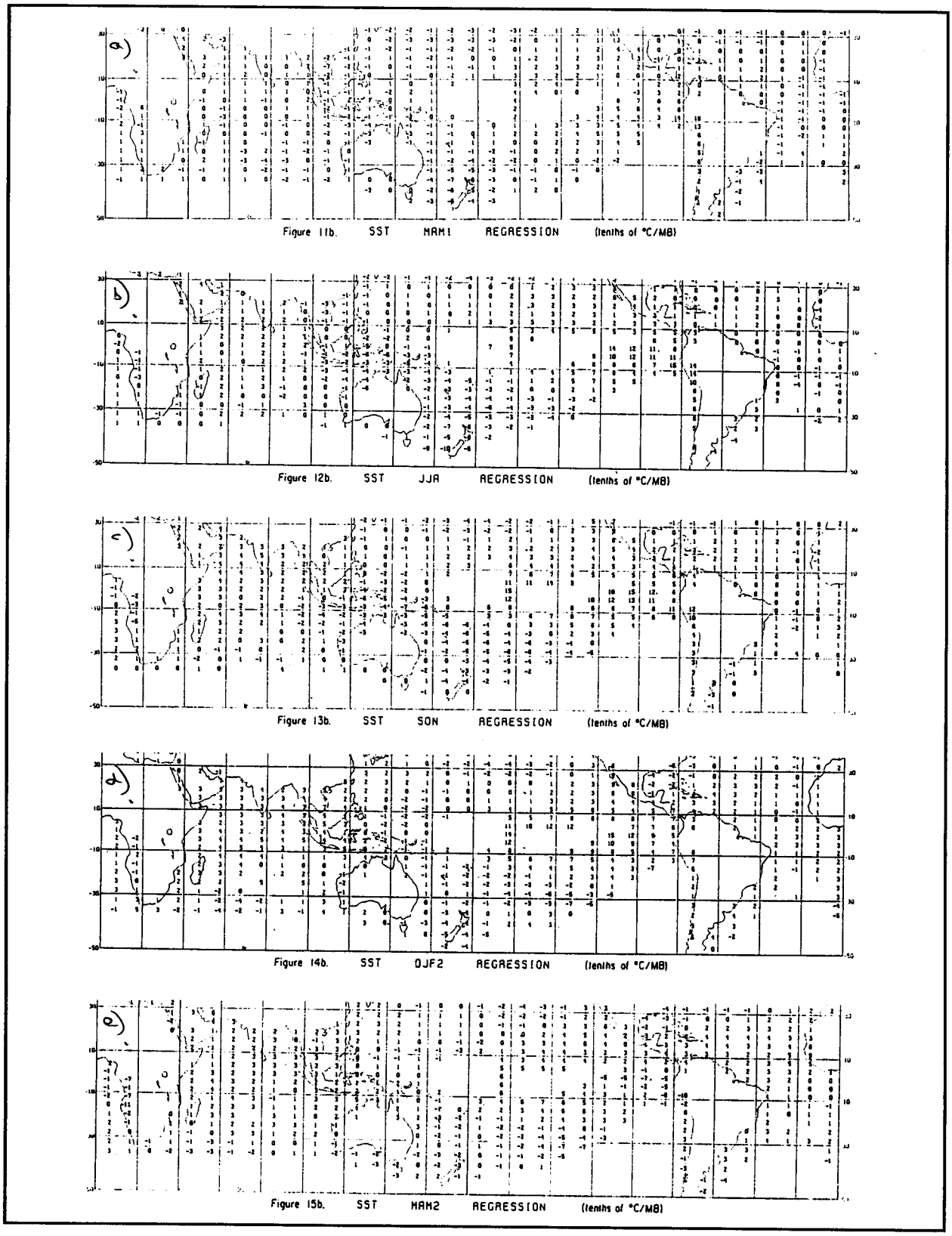

Figure 21. As in Figure 19 for COADS SST anomalies in the Indian and Pacific Oceans. Adapted from Wright et al. (1985).

Cloudiness decreases over most of the tropical Indian Ocean in March-May at the start of a Darwin pressure year (Figure 20a); this region strengthens and shifts towards Indonesia in June-August. The eastward shift continues, till by March-May at the end of the year (Figure 20e) the pattern is almost the negative of the pattern of the preceding March-May, at least in the tropical Indian and Pacific Oceans.

These patterns in winds and cloudiness may be helpful in understanding the variations in SST in the Indian Ocean through an ENSO event (Figure 21). SST anomalies start slightly cold in December-February preceding the "Darwin pressure year". They are slightly positive in the northern Indian Ocean in March-May preceding the monsoon (Figure 21a), but this part of the ocean warms steadily over the following 6 months (Figures 21b and 21c). The eastern tropical Indian Ocean remains cool till December-February at the end of the Darwin pressure year (Figure 21d).

As remarked earlier, the winds over the northern Indian Ocean do not change much during an ENSO event, so the temperature rises are probably not due to changes in upwelling, or in evaporation. Rather they may primarily be due to the increased insolation accompanying lower cloudiness (Figure 20). However, this cannot account for the pattern of SST change in the eastern Indian Ocean: SSTs remain low here till December-February, despite reduced cloud. Nor do the mean wind patterns help much: the total wind (seasonal climatology plus anomaly from Figure 19) is not clearly stronger, as one would expect if increased evaporation were holding SST down. However, the Indonesian region is marked by vigorous tidal mixing (Ffield and Gordon, 1992), and sea level (thermocline depth) is certainly reduced in this region during ENSO events. This would tend to generate reduced SST in this region during an ENSO event, since colder water would be brought closer to the surface where tidal mixing could act on it. The reduced sea level in this region during ENSO years can be seen, for example, in Wyrtki (1975) and Bye and Gordon (1982).

It may also be noted that the ENSO-related variations of mean sea level along the Western Australian coast are associated with reductions in the strength of the Leeuwin Current. The climatic significance of ENSO variations in the Leeuwin Current is unknown, but they provide a plausible explanation for an observed ENSO variability in the recruitment of western rock lobster larvae (Pearce and Phillips, 1988)

4.2. Non-ENSO Interannual Variations—the Quasi-Biennial Oscillation

Our present picture of the relationship between Indian Ocean SST and the Asian summer monsoon is somewhat contradictory. Indian Ocean SST is certainly not the only factor causing variability in Asian monsoon rain; SST in the Pacific Ocean and Asian snow cover preceding the monsoon are also strong influences. Since each of these is correlated with the others, it is difficult to disentangle cause-and-effect relationships.

The observations show clearly that northern Indian Ocean SST—at least, as sampled along the major shipping route from the Red Sea to Singapore—is *not* the major determinant of Indian summer rainfall (Shukla, 1987). Furthermore, some runs of an atmospheric General Circulation model over the monsoons of 1987 and 1988 (an ENSO and anti-ENSO year respectively) suggest

that the huge SST anomalies in the Pacific have substantially more effect on the global atmospheric circulation than the Indian Ocean SST anomalies (Palmer et al., 1992). On the other hand, Meehl (1987, 1993) and Yasunari (1990) suggest that the biennial oscillation of Indian monsoon rainfall—a fairly marked tendency towards year-to-year "sawtoothing" from one year to the next in total Indian rainfall quantity, Figure 22—may be associated with a large-scale air-sea interaction phenomenon, involving both the Indian and Pacific Oceans. According to these authors, a strong Asian monsoon tends to be followed by a strong Australasian monsoon, so a "monsoon year" should be defined to start in May (i.e., just before a complete Asian monsoon, and just after a complete Australasian monsoon) rather than January. (Note that Wright et al.'s (1985) annual mean SLP for Darwin was precisely over a "monsoon year".) Meehl analyzed composites of 29 such "strong monsoon years" and 30 "weak monsoon years", between 1900 and 1982. Rainfall in a "strong/weak monsoon" year was heavier/lighter than in both the preceding and following years. Strong monsoon years tend to be anti-ENSO years, but there are many more strong monsoon years than anti-ENSO years.

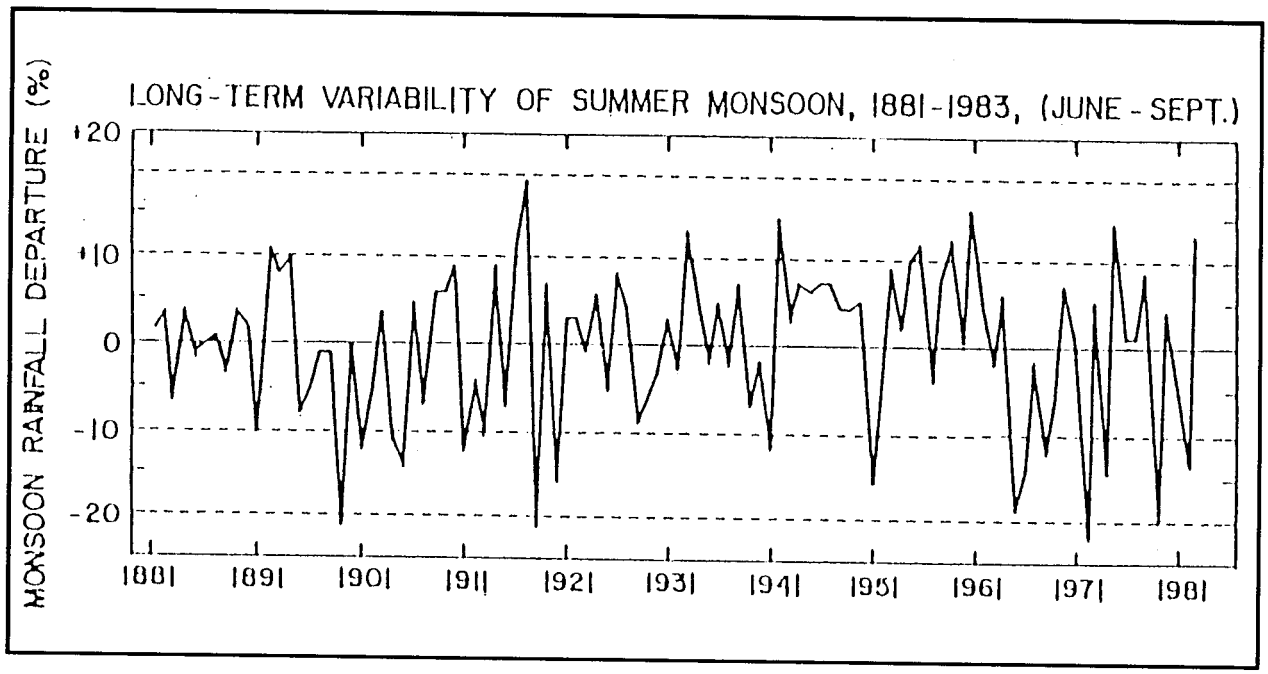

Figure 22. Indian monsoon rainfall 1881-1983 expressed as a percentage departure from the long-term mean. Values averaged over India for June-September are updated by Verma et al., 1984 (from Meehl, 1987).

While there are many similarities between the anomaly patterns associated with the QBO (quasi-biennial oscillation) and those of ENSO, there is one crucial difference. ENSO in the Indian Ocean appears to be a passive response to events in the Pacific Ocean, because Pacific Ocean winds lead Indian Ocean winds. By contrast, the lead-lag relationships between the two oceans are not nearly so clear in the QBO; both seem to be related to the monsoon system itself, and it is not clear that the ocean is playing a passive role in the development of the monsoons.

The composite SST differences between strong monsoon years and the preceding years are seen in Figure 23. The composite SST anomalies show a clear pattern, in the entire Indian Ocean as well as the Pacific. These patterns should be viewed in conjunction with the mean seasonal winds of Figure 16. In April just preceding the start of a strong monsoon year, the SST minus that of the previous year is essentially the negative of Figure 23d: i.e., the SST is slightly positive throughout the Indian Ocean—particularly in the southeast Indian Ocean. It is evident from Figure 16 that once the monsoon winds start, the air parcels will flow northwards over the Indian Ocean. It has been estimated that about 70% of the water vapor that crosses the coast of India is evaporated from the Southern Indian Ocean (Cadet and Reverdin, 1981). The positive SST anomalies in the southeast Indian Ocean before a strong monsoon may contribute significantly to the increase in evaporation, and hence possibly to Asian rainfall. North of the equator the SST anomaly in (the negative of) Figure 23d is only just positive, consistent with Shukla's (1987) result—and with Wright et al.'s (1985) result, for ENSO years.

By July (Figure 23a) the SST anomalies have fallen to near zero in the western and southern Indian Ocean, and by October they have reversed sign everywhere except in the eastern Indian Ocean. The magnitude of the SST anomaly change from April to October is about 0.6-0.8°C in the middle of the southern Indian Ocean, and 0.2-0.3°C in the northern Indian Ocean. Analysis of these changes using COADS data for the relevant strong monsoon years (Mansbridge and Godfrey, in preparation) shows that they are at least partly due to anomalous evaporative cooling, and to increased cloudiness; however, the differences in heat fluxes between strong and weak years are so small in magnitude (of order 5 watts/m^2) that noise in the data place a severe limitation on the results. For example, it is certainly not possible to exclude the possibility that ocean processes, such as anomalous heating/cooling associated with the tidal mixing in Indonesian waters or upwelling in the northern Indian Ocean, may make important—possibly even dominant—contributions. These conclusions are similar to those of Cadet (personal communication), who obtained a time series of heat flux anomalies into Eastern Arabian Sea (Figure 24a); these typically led SST by 10 months (Figure 24b), suggesting that SST anomalies were primarily caused by local heat flux anomalies—but that other processes could be important. However, Cadet also found that off the East African coast, his estimates of local heating rate did not correlate well with SST change, suggesting that oceanic processes such as upwelling were important there. McPhaden (1982) found that in the central equatorial Indian Ocean, surface heat fluxes accounted for over 80% of the variance of mixed layer temperature; horizontal advection was relatively unimportant, because even though zonal currents were strong, the horizontal temperature gradients were very weak.

Returning to the sequence of SST anomalies in Figure 23, the anomalies are still positive in the eastern Indian Ocean in October (Figure 23b). This situation changes after October, with the onset of the Australasian monsoon: the SST difference now changes sign in the eastern Indian Ocean as well (Figures 23b and 23c). Associated with this, Mansbridge and Godfrey find that cloudiness and wind speed both increase in the eastern Indian Ocean, partly explaining the anomalous cooling from October to January. The anomalies fade somewhat from January to April (Figures 23c and 23d), particularly in the northern hemisphere, no doubt partly because this is a period when winds are relatively light and net heat flux is *into* the ocean throughout the entire Indian Ocean (Figures 16 and 17): a thin mixed layer therefore forms over the older, cooled water. However, the SST

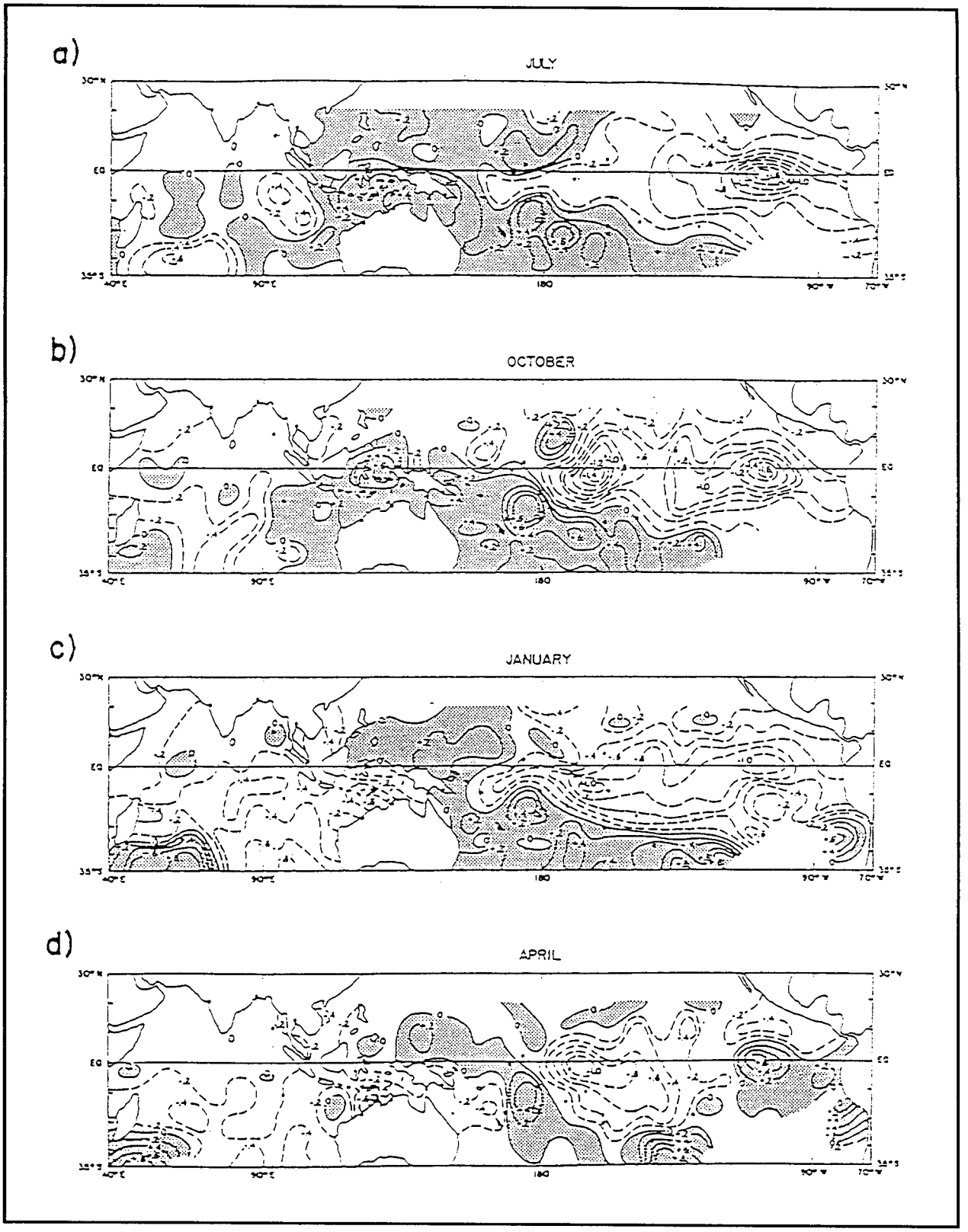

Figure 23. Composite differences in SST between 30 "strong" monsoon years (defined in text) and the preceding year as a function of season (from Meehl, 1987).

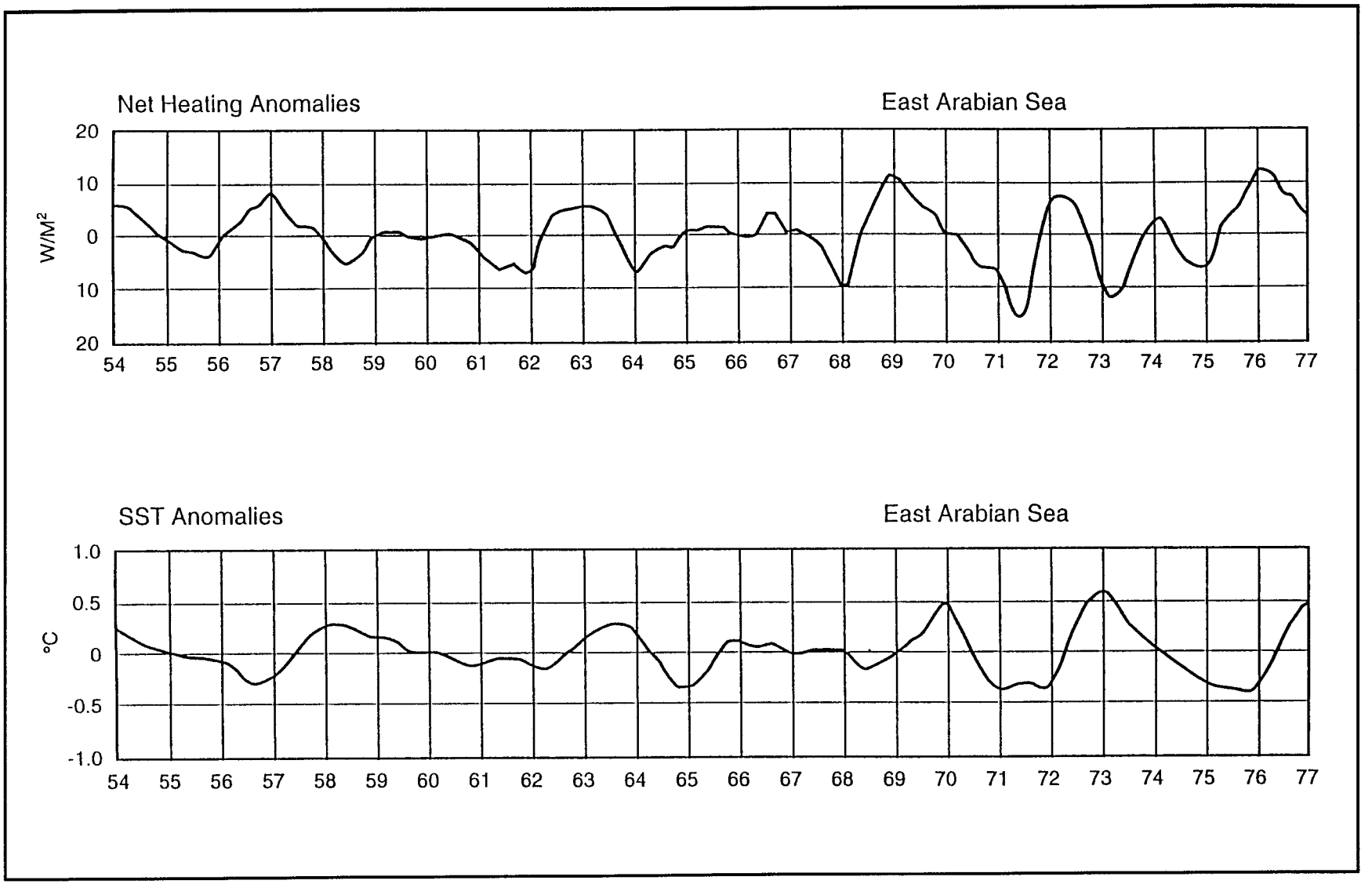

Figure 24. Band-pass filtered time series of monthly values of (a) net surface heat flux anomalies (watts/m^2) and (b) SST anomalies (°C). The cutoff periods (half response) of the filter are 20 months and 84 months (from Cadet, personal communication, 1988).

anomalies remain negative throughout the Indian Ocean from January to April. Furthermore, this older, anomalously cool water is presumably still present beneath the surface, where it will tend to generate anomalously cool SSTs through the early months of the following monsoon year. Thus the rather small SST anomalies seen in the reverse of Figure 23d just before the start of the Asian monsoon, particularly in the northern Indian Ocean (Shukla, 1987) may not be representative of the anomaly of heat content of the seasonal thermocline for the entire region of the Indian Ocean supplying moisture to the monsoon.

Note also, in Figure 23, that the SST difference is large and negative in the eastern Pacific throughout the strong monsoon year—until April, when the anomaly reverses. The result of Palmer et al. (1992) suggests that these east Pacific SST anomalies are probably more influential in causing the Asian (and Australasian) monsoons to be strong than the Indian Ocean SST anomalies discussed here.

Meehl (1993) showed that the SST anomalies of Figure 23 extend well below the surface mixed layer. Using hydrographic data, he obtained composite temperature profiles for strong and weak years in selected ocean regions (Figure 25a) and found clear differences—and these were not confined to the mixed layer (Figure 25b). In each case the SST anomaly in Figure 25b coincides in sign with the annual mean temperature anomaly for that region, from Figure 23. The solid lines in Figure 25b are for the composite differences between *all* strong and *all* weak monsoon years; in the dashed lines, all years that are also recognized as ENSO or anti-ENSO years (Warm Events (W.E.) and Cold Events (C.E.)) are excluded. ("Cold Events"/"Warm Events" tend to be particularly strong/weak monsoon years, though the correlation is not perfect). The dashed and solid lines in Figure 25b are qualitatively similar, i.e., the nature of the distinction between "strong monsoon" and "weak monsoon" years persists, even when the extremes of ENSO are excluded. Note in particular that in the western Indian Ocean, the anomalies extend to 125 m—almost certainly well below the level from which upwelling takes place. Thus in the year following a strong monsoon, it seems likely that the upwelled water will be anomalously cold, by perhaps as much as 1°C. The sensitivity of model results to such subsurface temperature changes has been demonstrated by Anderson et al. (1991).

This result suggests that ocean dynamics do play a significant part in determining SST anomalies. Dube et al. (1990) drove a model of the Arabian Sea with the time series of wind anomalies from Cadet and Diehl (1984), covering the period 1954-1976, and found that the upper warm water layer was thinner following weak monsoons, in agreement with Meehl's observations. Dube et al. also noted that the QBO signal tended to be present only during years of wet monsoons (e.g., the years 1954-1966).

4.3. Intraseasonal Oscillations

A problem with attempts to "explain" the interannual variability of the Asian monsoon is that they are subject to major intraseasonal variability. Monsoon rains will be strong for a few weeks, then stop, to start again a few weeks later. Perhaps for this reason, runs over a monsoon season with atmospheric General Circulation Models have been found to be particularly sensitive to the choice of initial conditions, for fixed SSTs (Palmer et al., 1992). These intraseasonal oscillations are not well-understood; and it is possible that the (rather strong) statistical link between ENSO and Asian

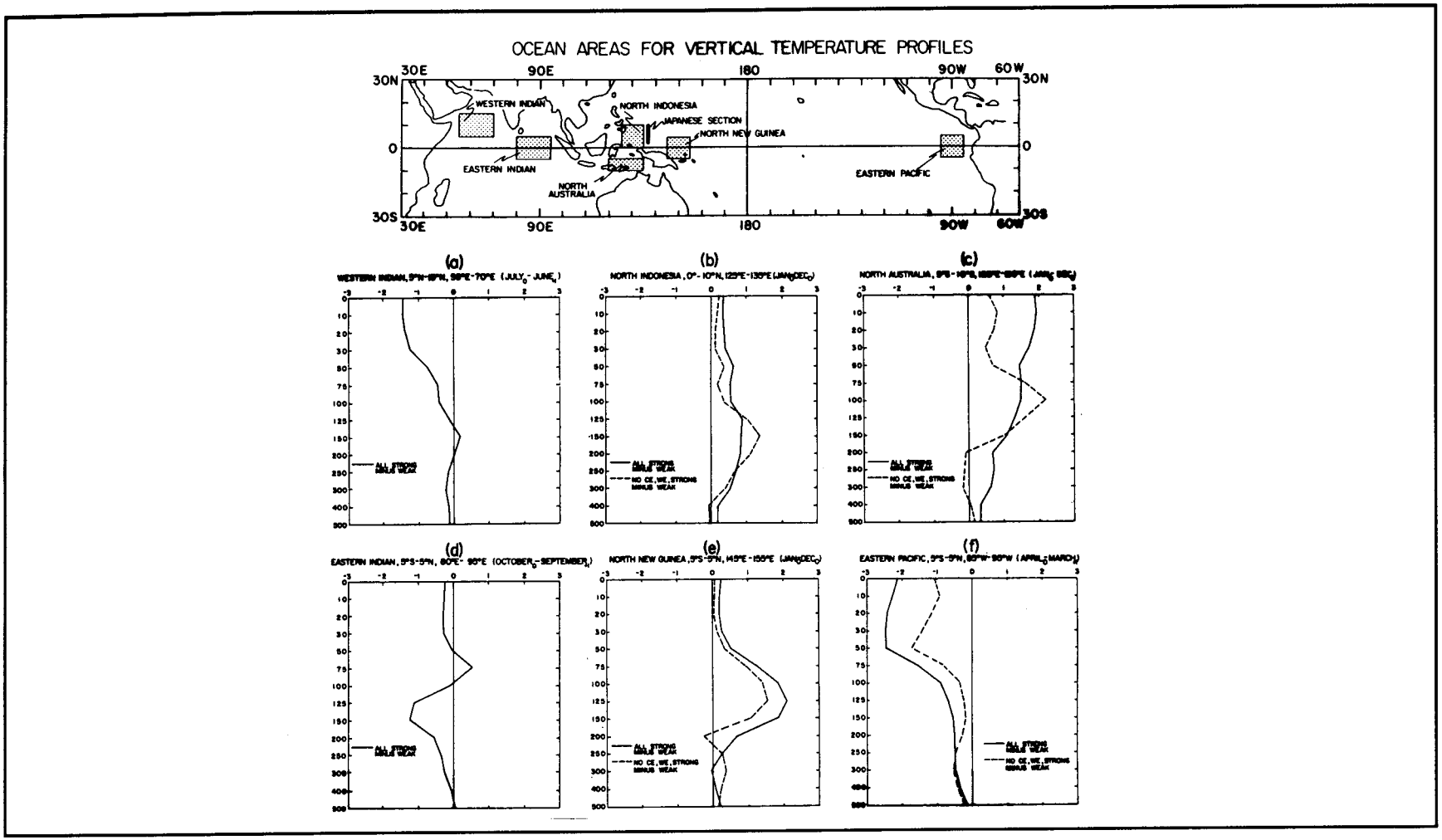

Figure 25. (above) Areas chosen for hydrographic station data composites (stippled areas). Japanese section along 137°E is also shown (from Meehl, 1993). (below) Strong minus weak composite ocean vertical temperature profiles for all strong minus weak years (solid lines) and strong minus weak years without cold or warm events (dashed lines) for areas shown in Figure 21a. (a) western Indian, (b) north Indonesia, (c) North Australia, (d) eastern Indian, (e) north New Guinea, and (f) eastern Pacific. Latitudinal and longitudinal extents of the areas, as well as the duration of the annual mean averaging intervals, are given at the top of each frame (from Meehl, 1993).

monsoon rainfall may be due to ENSO modulating the intraseasonal oscillations, rather than by a direct mechanism.

Sikka and Gadgil (1980) and Gadgil and Asha (1992) found that Indian summer rainfall seems to be mainly controlled by variability of rain bands that form over the eastern equatorial Indian Ocean. Each band typically migrates northwards to northern India, decays, and is replaced by a new rainfall band on the equator. This phenomenon, which mainly occurs on timescales of a few weeks is not yet well understood, though some theories have been developed for idealized geometries (Webster and Chou, 1980; Webster, 1987; Nanjundiah et al., 1992; Krishnan et al., 1992). Northward gradients of water vapor content play an important role in these theories. In the real world, where the Arabian Sea and the Bay of Bengal lie on either side of India, it seems quite likely that meridional gradients of both soil moisture variations and SST variations are involved in the mechanism of northward propagation, i.e. it is a true "land-sea-air" phenomenon.

Another type of Intraseasonal Oscillation involves disturbances that propagate eastward around the world, along the equator. They are most active in the East Indian and West Pacific regions, on timescales of 40-60 days (Madden and Julian, 1972). SST varies markedly in the Bay of Bengal and eastern equatorial Indian Ocean (and the western equatorial Pacific) on 40-60 day timescales (Figure 26, courtesy Dr. R. R. Rao; see also Krishnamurti et al., 1988), and it is possible that these variations play an active role in the mechanism, rather than being simply a passive response. However, the relationship between the Madden-Julian equatorial waves and the northward-going waves in the Indian Ocean is not clear.

Our lack of understanding of these phenomena may prove a stumbling block to further progress in predicting monsoon-related climate variability. In particular, the design of an the ocean observing system for climate might be different depending on whether SST plays an active role in such phenomena.

4.4. Indian Ocean Sea Surface Temperature Anomalies and the Monsoon Transitions

Around April and October—a month after the equinoxes—the tropical rain disturbances cross the equator, between the Asian and Australasian summer monsoons. Sumatra and equatorial East Africa have two rainfall maxima a year, at these times. In this section we consider the interannual variability of this equatorial rainfall pattern. It is of particular interest, since there might be analogies with the ENSO-related "competition" between rain centers over Indonesia and the central and east Pacific. This might lead to some weaker version of the ENSO phenomenon within the Indian Ocean. This possibility has been explored observationally by Reverdin et al. (1986) and Hastenrath et al. (1993), and in coupled models by Anderson and McCreary (1985).

The Sumatra rain maxima can be seen in the Outgoing Longwave Radiation (OLR) patterns of Fig 27 (from Meehl, 1987). OLR has been found to be a useful proxy for rainfall, because the high, cold cloud tops associated with deep convection emit weak thermal radiation. Figure 27 shows the mean OLR patterns for July, October, January, and April. The rainfall patterns are rather different in April and October: a clearly-defined OLR minimum centered on Sumatra occurs in October, while in April two weaker minima occur. This difference may be related to the so-called

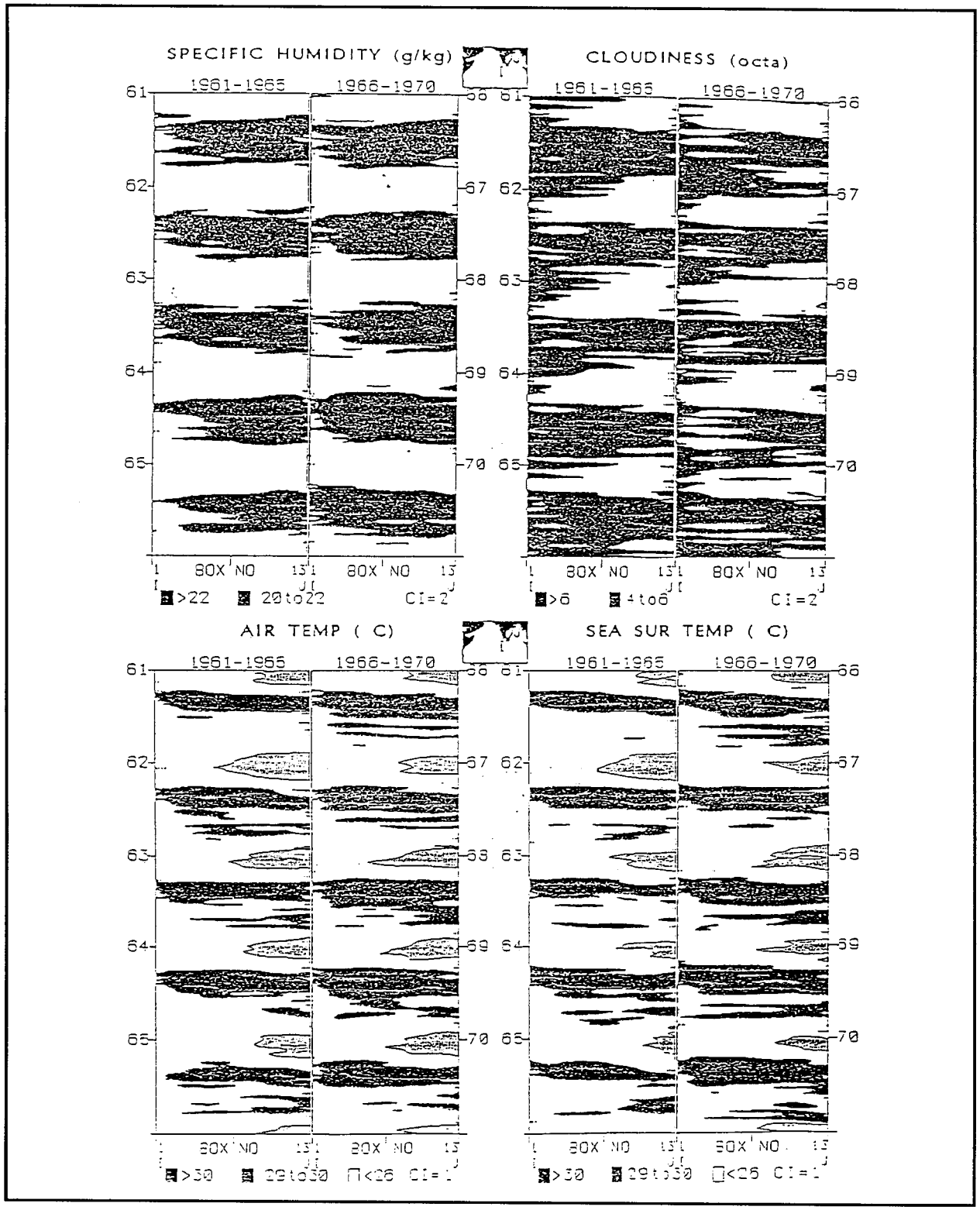

Figure 26. Ten-day mean merchant ship data along the Sri Lanka-Calcutta track (inset), for 1961 to 1970 (R. R. Rao, personal communication). The cloudiness data shows obvious intraseasonal oscillation activity. It is also apparent, though less marked, in sea surface temperature, air temperature, and specific humidity.

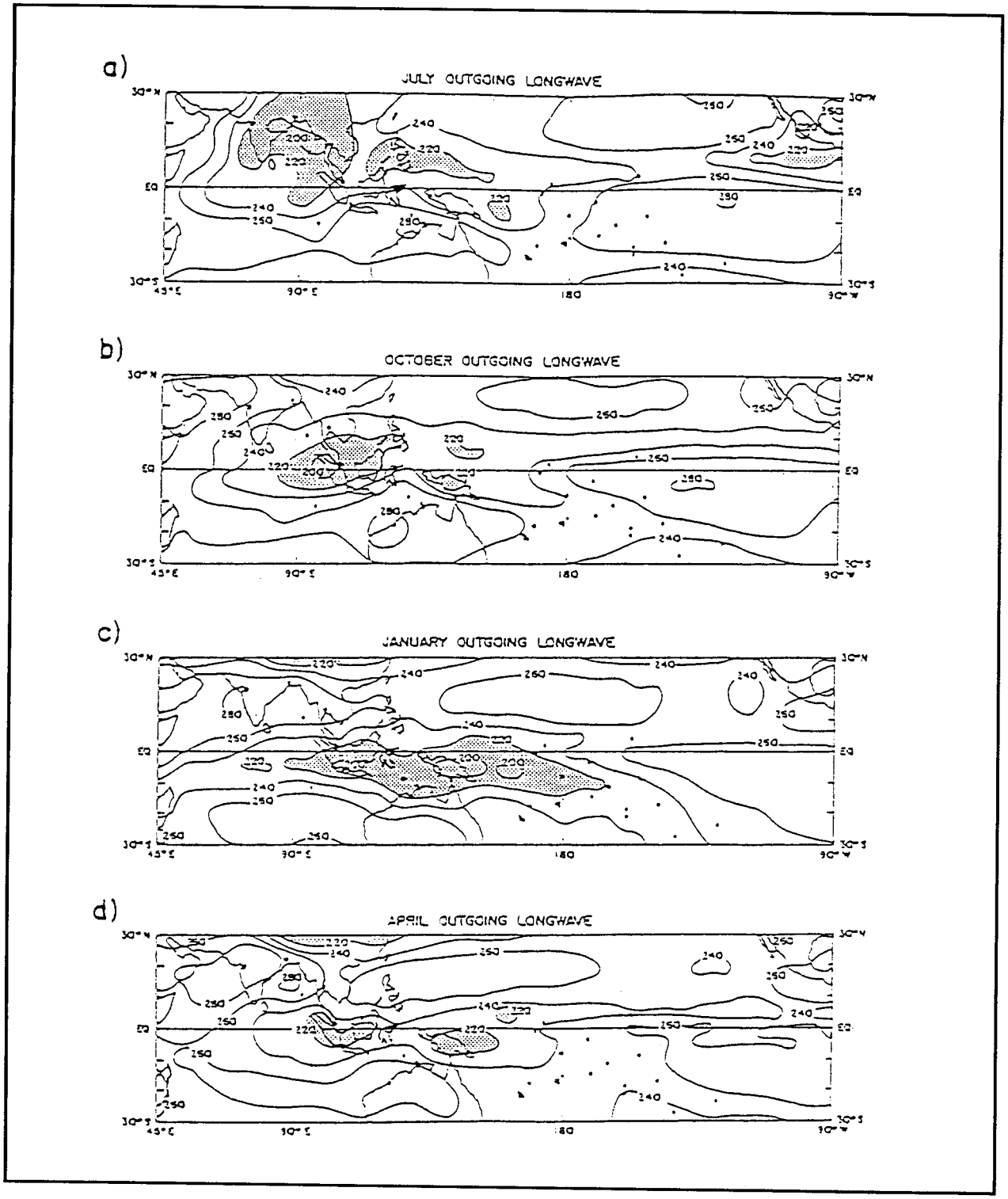

Figure 27. Long-term (eight-year) means of outgoing longwave radiation (watts/m^2) for the period covering June 1974-November 1983 for the Indian and Pacific sectors for (a) July, (b) October, (c) January, and (d) April (after Janowiak et al., 1985). Areas less than 220 watts/m^2 are stippled; they are regions of greatest tropical rainfall (from Meehl, 1987).

"predictability gap" that occur each April (e.g., Webster, 1994): experience with the Cane-Zebiak model and other ENSO prediction models suggests that predictive skill drops markedly around April. It seems the tropical atmosphere is weakly organized in April. Empirically, the Southern Oscillation Index (SOI; the anomalous sea level pressure difference between Darwin and Tahiti) is more likely to change sign at this time of year than any other. This is part of the reason why the "monsoon year" is a useful concept—the SOI tends to have one sign throughout each monsoon year.

The mean seasonal pattern of rain, winds, currents and SSTs in the equatorial Indian Ocean is partially consistent with the hypothesis that an independent ENSO-type competition between the Sumatran and east African rain centers is occurring—but one essential link is missing. The October/November equatorial westerlies in the central Indian Ocean are stronger than those of April/May (see Figure 34b), as would be expected from the stronger Sumatra rainfall in October (Figures 27b and 27d). Also consistent with the hypothesis, the May rains are stronger than those of October in East Africa. As noted earlier, the April/May and October/November westerlies generate eastward equatorial currents—the Wyrtki jets. Wyrtki (1973b) pointed out that this results in decreases in mixed layer depth near the East African coast, and increases near Sumatra, particularly in November; these effects can be seen in Figure 18. However, if the analogy were complete, one would expect the upwelling near East Africa to result in *minima* of SST in this region, near May and November. In fact, the behavior is nearly the opposite of this: SST near East Africa has clear *maxima* in April and November (Figure 28). This is probably because the cross-equatorial winds are weakest at these times so a shallow, warm surface mixed layer can briefly form near the East African coast. It seems that the semiannual upwellings near East Africa are too shortlived, and accompanied by winds that are too weak, to result in surface cooling by entrainment—despite the fact that MLD is shallowest at these times. This is consistent with the model result of Anderson and McCreary (1985): they found that when the major convection zone lay at the east of a model ocean basin (as in the Indian Ocean), rather than to its west (as in the Pacific), ENSO-like disturbances did not develop.

Hastenrath et al. (1993) have considered interannual variations in the equatorial Indian Ocean system, by correlating indices of rainfall over East Africa with the anomalies of winds, SSTs, cloud cover, sea level pressure (SLP) and surface currents, and with the Southern Oscillation Index (SOI). They first note that the April-May rainfall over East Africa (the stronger of the two peaks) has only slight correlation with the SOI (possibly because, as noted above, the SOI tends to change sign at that time). On the other hand, October-November rainfall has a tight *negative* correlation with the SOI.* This is consistent with the "competition" hypothesis: rainfall anomalies over Indonesia and Australia in October-November correlate positively with the SOI. The facts that SLP correlates negatively with SOI near Indonesia and positively near equatorial East Africa (Figure 29a) while cloudiness has the reverse pattern (Figure 29e) are also consistent with the hypothesis of "competition" between the Indonesian and East African rain centers: high pressure and low cloud amount are expected near the anomalously dry East Africa, while the reverse is true

* However, Reverdin et al. (1986), in a rather similar analysis based on a smaller data set, noted some striking cases where East African rain anomalies are *not* correlated with the SOI—for example, the strongest East African rains on record occurred in 1961, which was not an El Nino year.

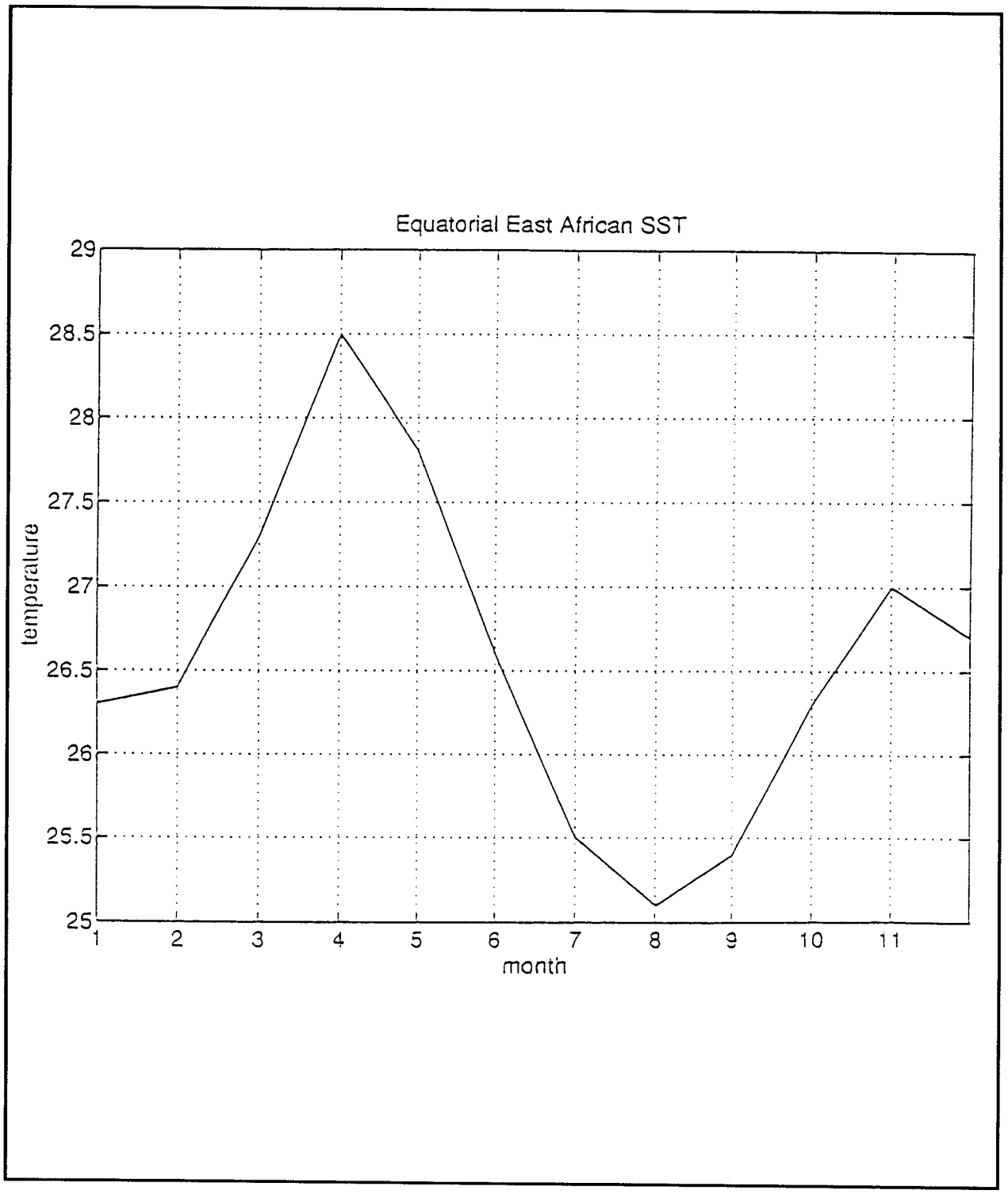

Figure 28. Mean seasonal sea surface temperature on the equator, near the east African coast (from the data of Sadler et al., 1987). Note that there are marked maxima in May and November despite the fact that divergence associated with the Wyrtki jets causes the mixed layer to be thinnest at that time. By contrast, in the equatorial east Pacific there is a tight relationship between SST and subsurface temperatures.

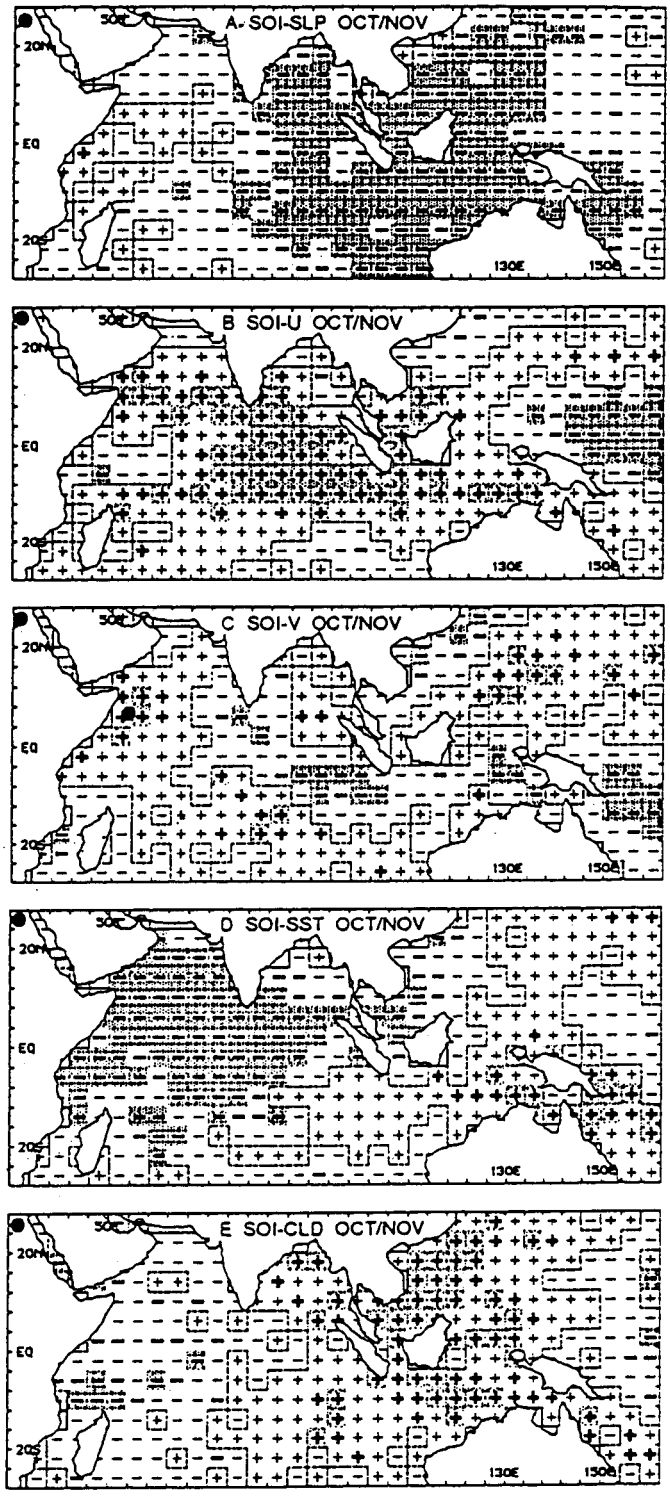

Figure 29. Patterns of correlations between the Southern Oscillation Index and (a) sea level pressure (SLP), (b) zonal wind (U), (c) meridional wind (V), (d) SST, and (e) cloud cover for October-November (from Hastenrath et al., 1993).

near the anomalously rainy Sumatra. Zonal winds are anomalously westerly when the SOI is high (Figure 29b), not merely close to the equator but over most of the tropical Indian Ocean, presumably to feed the stronger rains of the developing Australasian summer monsoon. Interestingly—despite the above remarks about the inability of SSTs to respond to the shallowing of the mixed layer near East Africa, associated with the Wyrtki jets—SSTs are lower in the western Indian Ocean when the SOI is high (Figure 29d). This suggests that the air masses converging on East Africa will be drier, again consistent with the reduced rainfall over East Africa. However, the region of reduced SST in Figure 29d is not confined to equatorial regions, but lies under the path of the Asian summer monsoon winds. This is consistent with the pattern pointed out by Meehl (1987), and discussed above: negative SOIs are correlated with strong monsoon years, and SST is markedly reduced in the western Indian Ocean following a strong Asian monsoon (Figure 23b).

Correlation patterns of winds, SSTs, cloud cover, and sea level pressure (SLP) with East African October/November rainfall, rather than with the SOI, are remarkably similar to Figure 29. Hastenrath et al. (1993) also found that (as expected) the November Wyrtki jet was anomalously strong when the SOI was high, though the effect of the SOI on equatorial mixed layer depth was not as expected, perhaps due to severe data limitations.

4.5. Indian Ocean Sea Surface Temperature Anomalies and Southern Hemisphere Climate

4.5.1. Southern Australian winter rain

Nicholls (1989) performed an EOF analysis on Australian rainfall data, and found that Australian winter rainfall had two leading EOFs: one (centered in eastern Australia) was correlated with the SOI, while the second (centered along the southern Australian coast, and in a band extending from northwest to southeast across central Australia) was essentially independent of the SOI. Correlation of the second time series with SST anomalies revealed a dipole pattern. Strong southern Australian winter rain was associated with warm SSTs in Indonesia, and cold SSTs in the central and eastern Indian Ocean south of 15°S, as in Figure 30c. Correlations with SST anomalies in the east Pacific were not significant.

A more sophisticated analysis, using rainfall anomalies throughout the year and some other technical refinements, revealed 3 EOF patterns with similar spatial and temporal structures (Fredericksen et al., 1990); all 3 patterns correlated with an Indian Ocean SST dipole, and not significantly with east Pacific SSTs. Figure 30 shows the time evolution of the SST differences, between a composite of the seven wettest years and of the seven driest years, in the area of the three EOF patterns. The dipole is present in May, and has reached full strength in July. Note that the central Indian "pole" of the dipole is elongated towards the northwest, into the Arabian Sea. A warm anomaly is also present in the Tasman Sea in May. Figure 31 shows the corresponding observed SLP and wind anomaly differences for the (seven wet year-seven dry year) composite. In May and June, SLP is low over Australia, resulting in anomalous southerlies along Australia's west coast; these augment the southerlies normally present in this region (or at least prolong them; in the mean they weaken almost to zero in July). Anomalous northwesterlies to the north of Australia tend to weaken the Trades that normally increase at this time; they also feed moist air towards the rain bands that extend along a NW-SE axis across Australia.

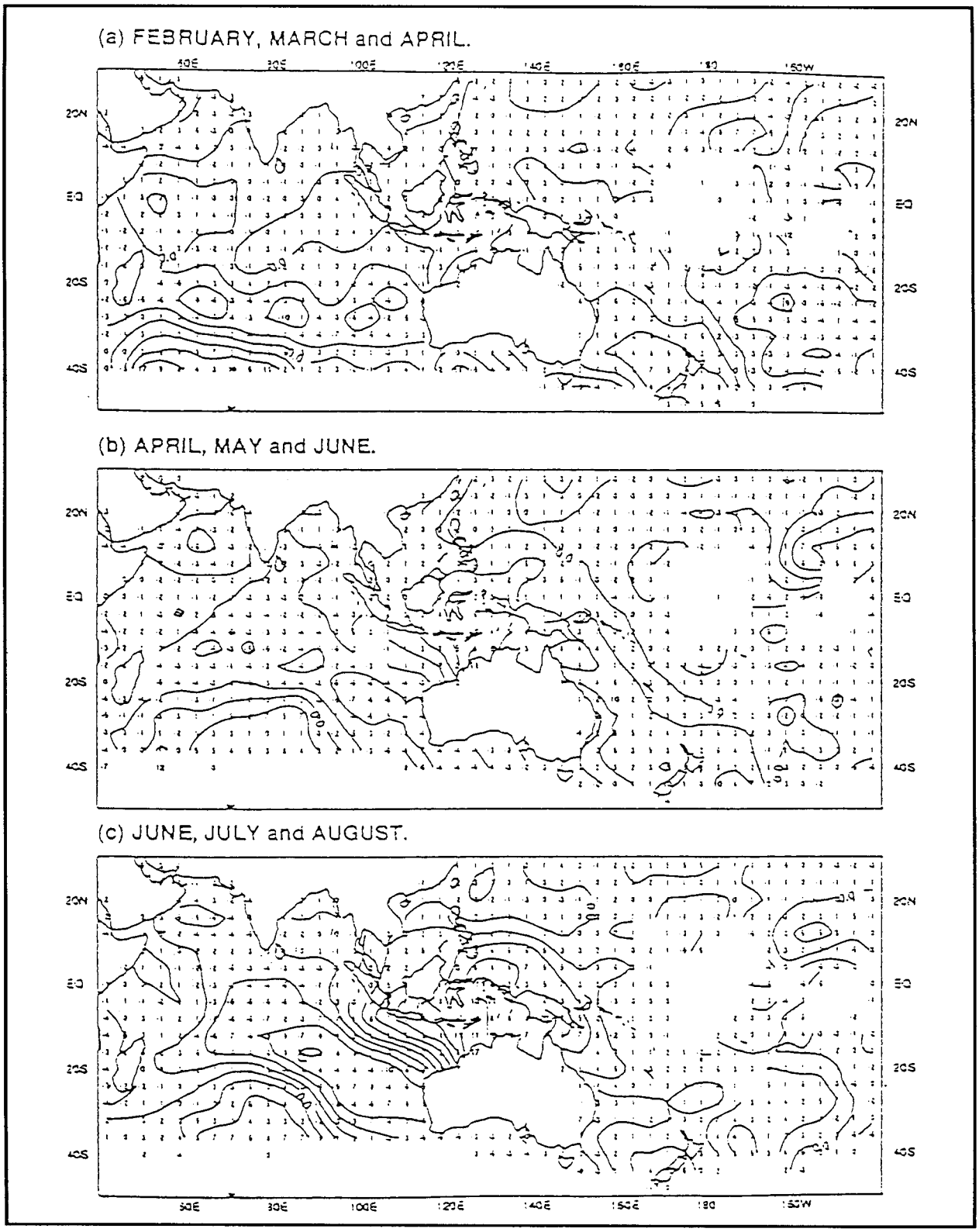

Figure 30. Sequence of SST differences between composites of the seven wettest and seven driest years in the region of the southern Australian rainfall anomaly pattern (see text). Contour interval 0.2°C (from Fredericksen et al., 1990).

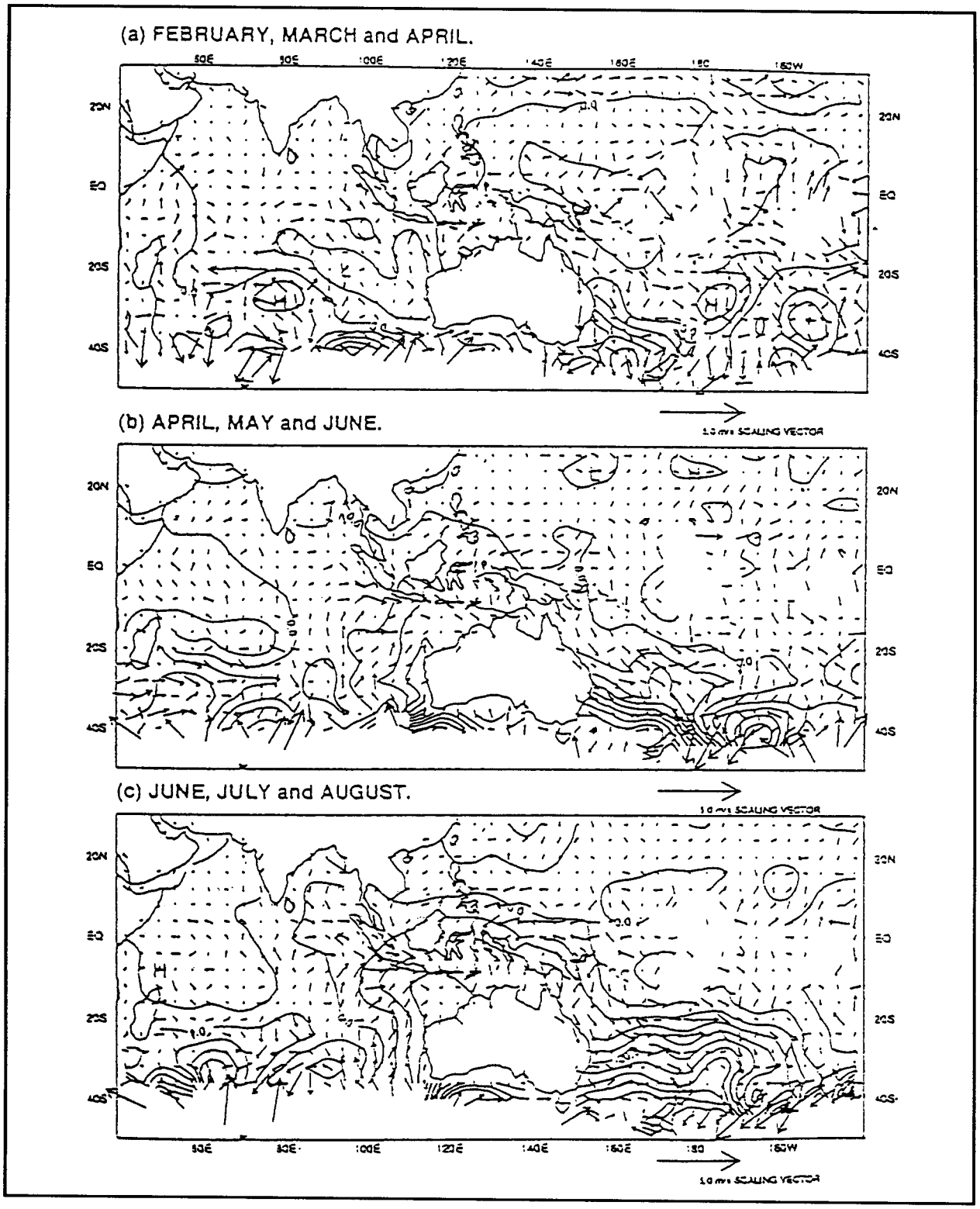

Figure 31. Sequences of SLP differences (contour interval 0.5 hPa) and surface wind differences (m/s) between composites of the seven wettest and seven driest years in the region of the southern Australian rainfall anomaly pattern (see text) (from Fredericksen et al., 1990).

Fredericksen et al. (1990) are quite successful in reproducing the main features of the observed SLP and winds of Figure 31 in an atmospheric GCM run, and also the observed rainfall patterns, provided they impose the full details of the SST anomalies of Figure 30 underneath their model. They also suggest a mechanism for the development of the Indian Ocean dipole. They argue that the anomalous southerly winds (which add to a background southerly wind) may tend to cool SSTs along the Western Australian coast, due to enhanced evaporation; while to the north of Australia, the reduced Trades result in reduced evaporative cooling, and an increase in SST anomaly. They also suggest that the anomalous winds may cause upwelling near Western Australia. In fact, upwelling never occurs along this coast, due to the presence of the Leeuwin Current; but the enhanced southerlies are likely to weaken the Leeuwin Current, and thus reduce its strong southward advection of heat (see Section 3.2).

However, this argument cannot explain the shape of the SST anomaly of Figures 30b and 30c, which lies northwest of the southern half of Western Australia. Other mechanisms may also be important. For example, the period from May to July is also a time when the mixed layer deepens considerably, throughout the domain of Figure 25. If the mixed layer formed at the end of the previous winter were anomalously cold, the normal winter cooling would cause these deeper waters to be entrained into the surface mixed layer by July, thus creating a cold SST anomaly. Similar mechanisms were proposed by Namias (1970) to explain broad-scale SST anomalies in the North Pacific. The large annual Rossby waves referred in Section 3.2 , and the Leeuwin Current Extension—itself a strong function of the Indonesian Throughflow—are both candidates for affecting SST in this region. These possibilities are being explored, using XBT data.

4.5.2. Trends in southwest Australian rainfall and in Indian Ocean SST

Rainfall over southwestern Australia has been decreasing rather steadily since the 1920s and particularly since 1960; this has major economic consequences for the region . Unfortunately the causes of such long-term trends are rather hard to diagnose, partly because we only have one case and so the "composite" technique described in Sections 4.1a and 4.3a cannot be used. Also, changes in instrumental techniques can introduce a "noise" on a rather small signal. Nevertheless, Allen and Haylock (1993) were able to show that the rainfall trend in SW Australia was associated with an opposing long-term trend in sea level pressure in southern Australia. An SLP trend of opposite sign to southern Australia occurred in New Zealand. Over the same period, SST showed a rather well-defined pattern of long-term trend (Figure 32; from Allan and Haylock, 1993). Comparison of this pattern with Figure 13 (noting that in the Hirst-Godfrey model, SST anomalies are strictly proportional to heat flux anomalies) shows fairly strong similarities. In both patterns, the dominant feature is a band of large positive SST trend near 40°S. SST trends are also strongly positive in both pictures off the Western Australian coast. Weaker bands of high SST difference occur in Figure 13 off Arabia and southern India, probably associated with the fact in the model, the water upwelled in these regions is warmer when the Indonesian Throughflow is present. Rather similar bands are seen in Figure 32, though their magnitude is relatively greater. It was noted previously that the band of mean heat gain near 5°S in the western Indian Ocean in the models is not observed; it is therefore not surprising that the band of weak heat gain in the same location (in Figure 13) has no analogue in Figure 32.

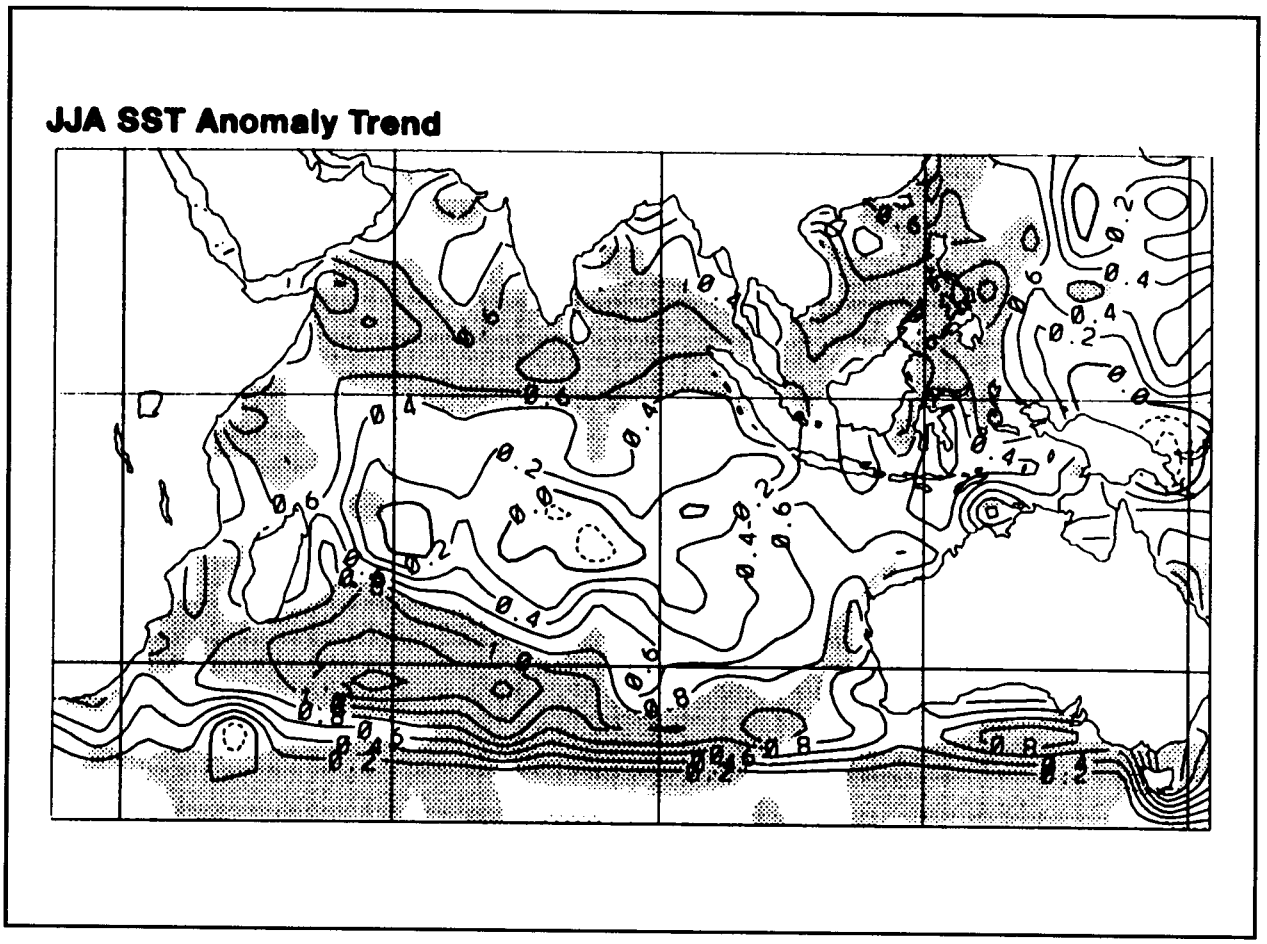

Figure 32. Trend in June-July-August sea surface temperature, 1911-1989 (from Allan and Haylock, 1994).

These remarks suggest that an increase in the Indonesian Throughflow over the last several decades may be responsible for many of the features of SST trend seen in Figure 32. Consistent with this hypothesis, westerly geostrophic winds in the South Pacific near 44°S (the latitude of Australasia's southern tip) have clearly increased over the same period, at least in the western Pacific (see figure 11a of Allan and Haylock, 1993). According to Godfrey (1989) and Wajsowicz (1993), these enhanced westerlies will tend to increase the magnitude of the Indonesian Throughflow. Numerical experiments are under way to explore these hypotheses further (Reason, personal communication)

5. Interannual Variability of Other Variables in the Indian Ocean

In the previous section we have emphasized studies of the interannual variability of SST, since it is through the SST that the ocean affects the atmosphere. However, if we are to diagnose the causes of these SST variations, information is needed regarding the variability of a number of other fields—winds, cloudiness, subsurface temperature, salinity and currents. In this section the presently-available sources of information on these other quantities is briefly outlined.

5.1. Surface Meteorological Data

The most comprehensive of these sources is the COADS (Woodruff et al., 1987), which provides monthly data in 2° x 2° squares for the world ocean, from a major fraction of all merchant ship's reports from about 1900 to the most recent update. Variables covered include wind speed and direction, cloud cover, air temperature and humidity, sea surface temperature and sea level pressure (the standard variables reported by Volunteer Observing Ships). The data have been quality controlled by various means (e.g., the trimming of data points lying more than a few standard deviations away from the mean). While COADS represents a major new tool for studies of interannual variability, the data suffer inevitably from the fact that they are sparse outside the usual shipping lanes. An earlier, more intensive study of the northern Indian Ocean was prepared by Cadet and Diehl (1984) probably received more detailed quality control than COADS.

Legler et al. (1989) have used a variational principle to obtain a "best-guess" at the Indian Ocean wind field on a 1°x1° grid (the Florida State University winds), described further below. Stricherz et al. (1993) have used the results of this to provide an atlas of FSU winds for the Indian Ocean, 1970-1985. Breidenbach's (1990) EOF analysis of these winds shows that interannual variations of Indian Ocean winds are not very large: the first EOF to have a large interannual component accounts for only 3.2% of the variance. A newly analyzed set of Indian Ocean monthly mean, 2°-resolution surface fields of winds, temperatures (both SST, and air temperature), humidity, as well as wind stress, sensible and latent heat fluxes was recently completed at Florida State University (Jones et al., 1995), for the period of 1960-1989 using a newly developed variational technique. These objectively analyzed fields are based on COADS. EOF analyses of the wind stress fields from this analysis shows strong biennial variability, but little interannual variability. In contrast, a similar EOF analysis of the latent heat flux fields shows very little annual or biennial variability, and instead indicates significant interannual variability.

The major operational weather forecasting centers also provide wind stress estimates for the global oceans, as a byproduct of their work. The ECMWF product has been used particularly: Trenberth et al. (1990) provide a climatology of wind stress based on ECMWF data, and Halpern et al. (1991) provide a global atlas of ECMWF wind components for 1988.

Since 1991, estimates of wind vectors have come available through the ERS-1 scatterometer. Validations of these against "ground truth" are encouraging, with daily mean RMS differences between ERS-1 winds and moored buoy winds estimated to be 2-3 m/s, and monthly mean RMS differences calculated to be 1-1.5 m/s (Halpern et al., 1992) Comparing ERS-1 monthly mean wind fields over the Indian and Pacific Oceans to the FSU winds indicates that the spatial sampling of the ERS-1 scatterometer introduces aliasing errors into the ERS-1 winds (Legler and O'Brien, 1993).

Comparable efforts to create an improved product for sea surface temperature have also been made by Reynolds and coworkers. The "blended SST analysis" uses merchant ship SSTs to provide calibration points for SST anomalies from satellite data. (Reynolds, 1988; Reynolds and Smith, 1994).

5.2. Expendable Bathythermographs and Sea Level

As part of the TOGA program, a major effort has been undertaken to obtain improved data on the interannual variability of the tropical oceans during the TOGA Decade (1985-1995). Figure 33a shows the distribution of expendable bathythermographs during 1987 (from Meyers et al., 1991). Analysis of this data set is continuing; among other things, it shows substantial interannual variability in the Indonesian Throughflow, as discussed earlier.

Sea levels have been measured at a few Indian Ocean sites for several decades, particularly along the coasts of the northern Indian Ocean and of western Australia. The western and south Australian sea levels correlate well among themselves, and there is a strong anticorrelation between south Australian and Californian sea levels, probably because both are closely related to the ENSO phenomenon (Bye and Gordon, 1982). Northern Indian sea levels also correlate quite well among one another, with an rms amplitude of a few centimeters; western Australian and north Indian sea levels show a weak but statistically significant correlation (Clarke and Liu, 1994). More recently, the University of Hawaii extended their Pacific sea level network into the Indian Ocean, greatly increasing the coverage of sea level stations. (e.g., CCCO Indian Ocean Climate Studies Panel, 1990).

Satellite altimeters are providing a new source of sea level data for the world ocean; interannual sea level variability data from GEOSAT are available from 1985. Perigaud and Delecluse (1989, 1992) have demonstrated the value of these observations. More recently, the TOPEX-POSEIDON altimeter appears to improve on the accuracy of GEOSAT.

5.3. Surface Currents

The XBT and sea level data discussed above provide information on geostrophic surface currents; however, substantial data are available through reported drifts of merchant ships. The United Kingdom Meteorological Office has an archive of ship drift data from 1854 through 1974. A climatology of surface currents from this source is given in Rao et al., 1989. A rather extensive program of drifting buoy releases was undertaken in the 1979-1981 (e.g., Reverdin and Luyten, 1986; Molinari et al., 1990); these showed—among other things—the 26-28-day equatorial waves discussed in Section 2.1.

6. Error Sources with Indian Ocean Data

In all of the foregoing, we have largely ignored the fact that measurements of all relevant quantities that affect SSTs—the SSTs themselves, winds, air temperatures and humidities, cloud cover, deeper ocean thermohaline structure and currents—are subject to major errors. This problem is the subject of OOSDP Background Report 3 (Weller and Taylor, 1993), so it will not be treated in great detail here. It is worth noting, however, that the problem is quite acute in the Indian Ocean, primarily for two reasons. First is the obvious one, that shipping routes are relatively sparse so the data base is comparatively weak. The second is that the signals being sought are generally smaller; for example, there is no analogue to the huge interannual variations in SST that occur in the eastern Pacific Ocean. The two together imply that the signal-to-noise ratio for anomaly measurement in the Indian Ocean is generally much lower than in the Pacific Ocean.

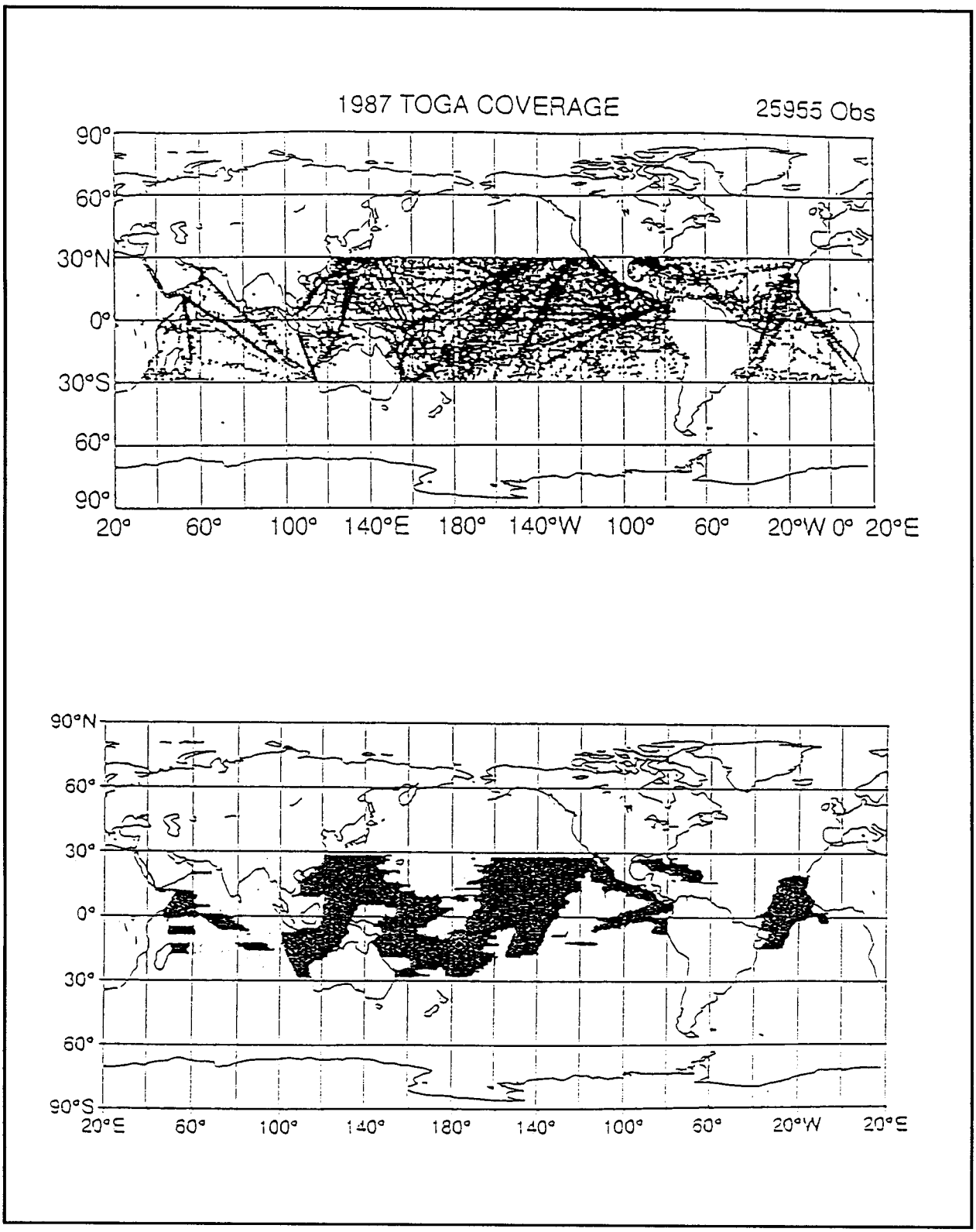

Figure 33. (above) Positions of all XBT launches during 1987 between 30°N and 30°S for the TOGA program. (below) Areas where two samples per decorrelation scale was achieved 75% of the time during 1987 are shaded. (Both from Meyers et al., 1991.)

Two examples of the relative magnitude of data problems in the Indian Ocean will be discussed. First, XBT drops in 1987 for the TOGA program are shown in Figure 33a, from Meyers et al., 1991. A "decorrelation scale"—basically, the range (in space or time) over which the data may be regarded as providing useful information regarding temperature anomalies—can be estimated from these data; Figure 33b shows the regions where better than 2 samples per decorrelation scale was achieved 75% of the time. Evidently, the tropical Indian Ocean is particularly poorly sampled in this regard, compared especially with the Pacific Ocean. Recently, it has been demonstrated that the subsurface temperature data now available in the Pacific (including both XBTs and TAO) have resulted in a marked improvement in the skill of coupled models of the ENSO phenomenon. We cannot expect similar performance from data-assimilating models of the Indian Ocean, with the present data supply.

The second example relates to climatologies of wind stress. It has been noted earlier that the mean patterns of Indian Ocean circulation and heat transport—and presumably also their anomalies—appear in models to be crucially dependent on certain aspects of the wind stress field; yet there are major uncertainties in published climatologies. For example, Figure 34 (from Anderson and Carrington, 1993) shows the mean seasonal values of zonal wind stress at two points in the equatorial Indian Ocean: 0°, 55°E and 0°, 73°E, from two climatologies. One (Hellerman and Rosenstein, 1983) is based directly on ship-borne observations: wind stresses were obtained for each individual ship report, and the result averaged to obtain monthly means. The second (the United Kingdom Meteorological Office (UKMO) product) comes from averages of the output of the UKMO operational numerical weather forecasting model, over the four years 1987-1990. Evidently, the two products are extremely different. They are not even qualitatively similar at 55°E, where Hellerman and Rosenstein (HR) basically show a single annual peak and trough in zonal wind stress, while the UKMO product shows two strong semiannual peaks. At 73°E, the HR wind stresses are at least a factor of 2 larger in magnitude than the UKMO stresses. These differences are much larger than the interannual variability (shown by the spread of individual points in Figure 34). Interestingly, Anderson and Carrington find that when each of these products is used to drive an ocean model, the UKMO product results in more realistic surface currents in the equatorial Indian Ocean, compared to the result from the product derived directly from observation. On the other hand, Kent et al. (1991) found that the UKMO model (in its 1989 version) uniformly underestimated the observed wind speed by about 2-3 knots (1-1.5 m/s). Such differences are of the right sign to account for some of the differences in Figure 34, though in themselves they are not large enough in magnitude. Also, climatic conditions in the Indian Ocean are sufficiently different from the North Atlantic that a similar analysis might give different results.

To examine this problem further, we have formed plots of the southward Ekman transport as a function of latitude and season, for 4 readily-available wind stress climatologies (Figure 35). As discussed earlier, model results suggest that the net heat flux into the tropical Indian Ocean is closely proportional to the product of southward Ekman transport with the transport-averaged temperature difference between the Ekman transport and the compensating deep inflow. Thus the Ekman transport is an important quantity for estimating the net heat flux into the Indian Ocean. It is rather reassuring to find that (as seen in Figure 35) three available products (Figures 35a, 35b, and 35d) provide estimates of Ekman transport that agree within 5 Sverdrups over most seasons and latitudes (though it should be noted that care must be taken to have the borders of the "Indian

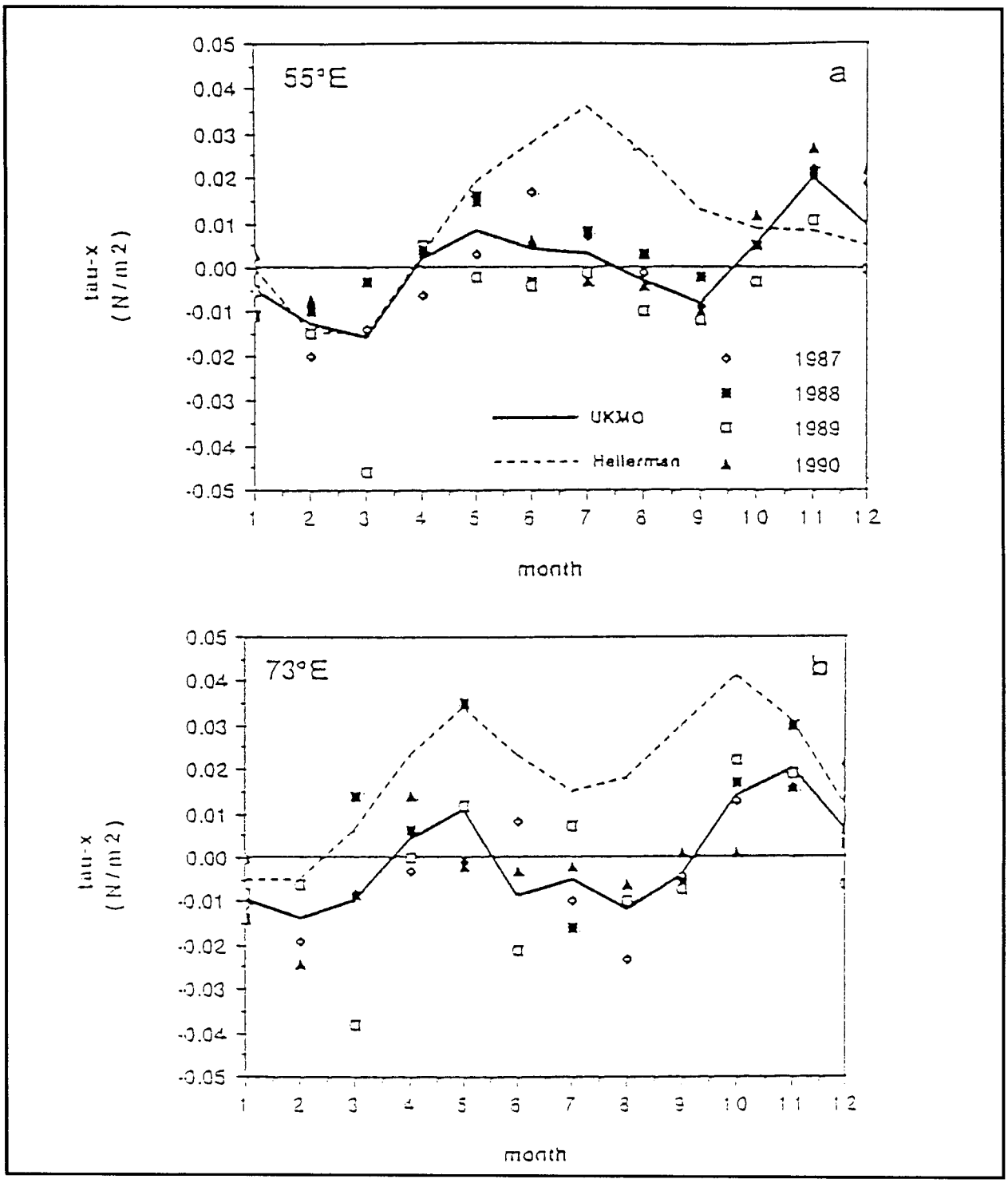

Figure 34. Seasonal cycle of zonal wind stress from the UK Meteorological Office analyses (solid line) averaged over the four years 1987-1990 for (a) 55°E and (b) 73°E. For comparison, the seasonal cycle from Hellerman and Rosenstein (1983) is shown (dashed line). UK Meteorological Office values for individual years are shown to indicate the magnitude of interannual variability. (From Anderson and Carrington, 1993.)

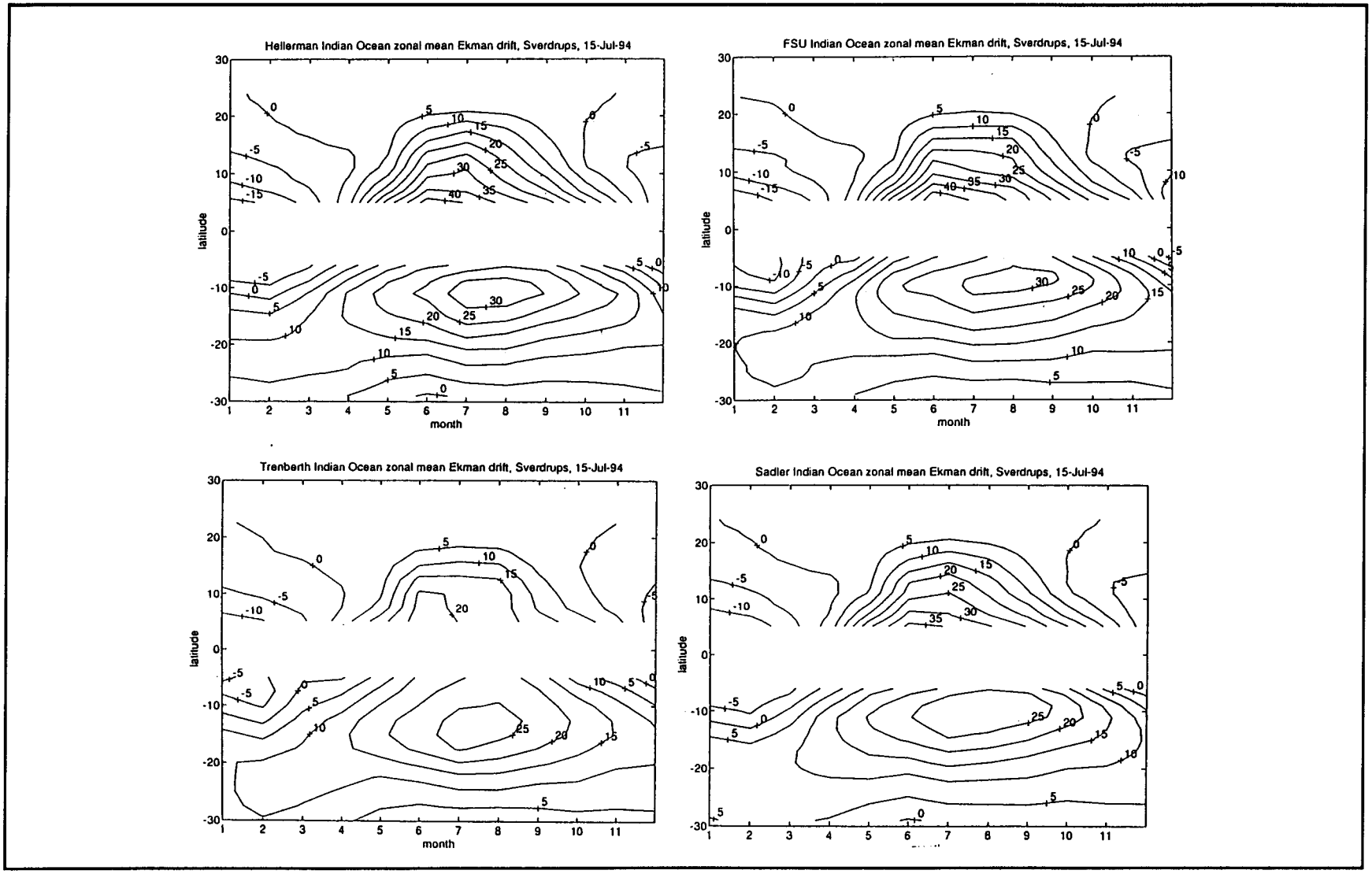

Figure 35. Southward Ekman transport integrated across the Indian Ocean basin as a function of latitude and season for four wind products: (a) Hellerman and Rosenstein (1983); (b) Florida State University winds; (c) Trenberth et al. (1990) winds; and (d) Sadler et al. (1987) winds.

Ocean" be the same in these products, which have different grid intervals). Figure 35c is an outlier; this is thought to be due to the fact that it was based on an analysis of the ECMWF model in a version that did not contain recent improvements (see below). The methods used to obtain these products are quite different; below, we describe further these products.

(i) Hellerman and Rosenstein (1983) wind stresses. These were obtained by estimating stresses from over 35 million individual ship's reports between 1870-1976, with Bunker's (1976) drag coefficient. Interpolation from nearby 2° x 2° squares was used for squares with less than 4 observations in a box, in a given calendar month.

(ii) Florida State University wind "pseudostresses". "Pseudostresses" are calculated by (in effect) taking the drag coefficient to be unity; users can then supply their own. The monthly mean FSU pseudostresses are obtained from ship reports between 1970-1985, (Legler et al., 1989; Stricherz et al., 1993), using a variational technique. This variational method includes constraints on proximity to input (ship) data, smoothness, and kinematic properties of divergence and curl. A wind stress climatology was generated from FSU pseudo-stress using a constant bulk transfer coefficient of 0.0015.

(iii) Trenberth et al. (1990) wind stresses. These were obtained by using the winds at 1000 mb, from twice-daily analyses of the ECMWF operational model between 1980-1986. This removes the (severe) problem for the other climatologies that the wind variability is not sampled frequently enough to yield reliable stress estimates. However, (to quote Trenberth et al.) "the disadvantage is that results depend entirely on the veracity of the analysis system in reproducing the true wind fields". While this has been quite well demonstrated at (57°N, 20°W) (Bottger, 1982), it apparently has not been demonstrated in the tropical Indian Ocean.

(iv) University of Hawaii pseudostresses (Sadler et al., 1987). These were obtained by subjective analysis of the available data between 1900 and 1979, taking into account the mean sea level pressure field and other relevant variables. In Figure 35d, a constant bulk transfer coefficient of 0.0015 was used.

Consistently with Figure 34, the HR Ekman transports (Figure 35a) are larger than those from the ECMWF-based Trenberth et al. winds (Figure 35c) by as much as a factor of 2—though Figure 30 shows integrals across an ocean basin, rather than just point values.. This difference arises partly from a different choice of bulk transfer coefficients: the HR coefficients were larger by about 30% at typical wind speeds encountered in the tropical Indian Ocean (see Trenberth et al., 1990, Figure 2). The FSU and University of Hawaii products give smaller Ekman transports than HR even though the bulk transfer coefficient of 0.0015 used in Figures 35b and 35d is generally larger than would be obtained by HR for typical wind speeds. This suggests that the winds obtained by Sadler et al. and Legler et al. must have been somewhat slower than those found by Hellerman and Rosenstein. It is interesting that these discrepancies are just as marked near 7°N as at other latitudes; here the data from the Singapore-Red Sea line are plentiful, so it seems unlikely that the discrepancies are due to inadequate quantities of data.

The causes of these discrepancies are hard to understand. It is possible (e.g., Trenberth, 1989) that the differences represent genuine interdecadal climate variations; their data are from 7 recent years,

while the other three products are weighted averages over as much as 100 years. Trenberth et al. also note that storms are not adequately captured in coarse-grid models like ECMWF, so stresses may be systematically underestimated. The observations could be subject to a measurement drift—however, they are nearly all made by subjective inspection of the sea state around the ship, using the Beaufort scale. This at least should not be subject to too much drift, apart from that associated with the increasing size of the ships used.

Since one major aim of the ocean observing system for climate is to document objectively any "climate change" it is evidently essential that the causes of discrepancies such as those of Figure 35 need to be identified, so that a quantitatively reliable time series of wind stresses for the Indian Ocean can be assembled over coming decades.

7. Summary, Scientific Questions, and Recommendations

7.1. Summary

Briefly, one can conclude that we are now fairly close to having a first-order understanding of how the Indian Ocean works as a component of the global climate system, on seasonal mean. Vertical overturning plays a major role in the heat budget at all latitudes, and probably dominates in the tropics. However, knowledge of the shape of the zonally-integrated meridional flow in the tropical Indian Ocean remains qualitative at best, based on tracer arguments and limited current meter data. The qualitative picture is as follows.

One major component of the overturning cell in the Indian Ocean occurs in the top few hundred meters, and involves wind-driven upwelling. In contrast to the Atlantic and Pacific Oceans, equatorial upwelling is weak in the Indian Ocean. Instead, upwelling occurs in the northern ocean, primarily along the coasts of Somalia, Arabia and near the tip of India; these locations are set by details of the wind field. Both models and tracer data (oxygen and freon) indicate that the main source of the upwelled water is the subtropical southern Indian Ocean (with possible contributions from the Indonesian Throughflow and the deeper ocean). The subtropical Indian Ocean water subducts, and then moves northward at relatively shallow depths (<500 m) within the Indian Ocean Tropical Gyre. It crosses the equator, either in a western boundary current or in the ocean interior. It is not clear just where this happens. Eventually it flows to the upwelling regions, and returns south in the top few tens of meters.

It seems probable that the near-surface meridional flow (and hence, through mass continuity, its subsurface replacement) is primarily due to Ekman transports, both seasonally and on annual mean. These have the right sign and magnitude on each side of the equator, throughout most of the year. However, this certainly cannot be true near the equator; and geostrophic flows (particularly in the western boundary) may be important off the equator. The inflow upwells and returns southwards possibly 10-15°C warmer than when it entered. One model result also suggests that a near-surface "roll" develops across the equator to connect the Ekman flows of the northern and southern hemispheres, though this has not been confirmed observationally. The same model results suggest, in agreement with very limited current meter data, that seasonally-reversing abyssal flows are also important for the seasonal heat budget. The semiannual equatorial current system (the "Wyrtki jets") is an important part of the seasonal cycle, and away from the western

boundaries the various near-equatorial waves explain much of the observed seasonal variations in currents in the tropical Indian Ocean.

A second large component of the annual mean heat flux is associated with inflow below 2000 m, with a typical temperature of perhaps 2°C. In the tropics, this is thought to return south below the thermocline at temperatures of order 7°C. Numerical model results are generally consistent with the (sparse) available current meter data within the thermocline, but at least on annual mean they are inconsistent with observations below the thermocline. The deep cell is thought to be driven by thermohaline circulation. The unusual strength of this cell in the Indian Ocean must be due to particularly strong vertical mixing, whose physical cause is not yet known. The seasonal variation of heat transport is quite complex; in one model, abyssal currents play a role as well as surface currents. Model results also suggest that variations in the Indonesian Throughflow can alter the surface heat flux and SST pattern at a number of locations in the Indian Ocean.

Consistent with the WCRP Indian Ocean Panel's aims, the emphasis in this document is on understanding SST anomalies *within* the Indian Ocean, on timescales of up to a few years. The deep cell is certainly a major source of heat for the Antarctic region; however, it probably has little influence on SSTs or SST anomalies within the Indian Ocean, at least on timescales of a few years. A major program—the WOCE Indian Ocean campaign of 1994-1996—is in any case very likely to change our ideas about the deep cell. Hence we emphasize the upper ocean in this document. It was noted that several fairly well-defined patterns of SST anomaly have been identified in the Indian Ocean, associated with particular types of interannual variability of climate. Six of these patterns are discussed in this text. The first is associated with ENSO, and the second with the tropospheric Quasi-Biennial Oscillation. A third is associated with the northern Indian Ocean intraseasonal oscillations; a fourth with east African rainfall anomalies; a fifth with southern Australian rain (the "Nicholls dipole"); and the sixth is the spatial pattern of the long-term trend of SST over 80 years. These SST anomaly patterns have been discussed, and a tentative attempt made to identify the physical reasons why they occur. In particular: Do interannual variations in the strengths of the upwelling, or of the Indonesian Throughflow, play a role in forming these SST anomaly patterns? Or are they formed locally, though processes within the surface mixed layer? In either case, how predictable are they, and what data would be needed to predict them? Such questions are crucial to the design of an the ocean observing system for climate in the Indian ocean.

One common feature emerges from these studies. The divergence of heat flux needed to generate the observed anomalies within the surface mixed layer are typically of order 5 w/m^2 or less. There is a major noise problem in these circumstances, since—in absolute terms—errors in climatological heat fluxes can be several tens of w/m^2 (though errors in flux anomalies may not be quite so serious). Available data do suggest that anomalies in net surface heat flux correlate with the rate of change of SST, even in the Arabian Sea (Figure 24), where upwelling might be expected to be a particularly strong contributor to interannual SST variations. Patterns of cloudiness anomaly associated with ENSO disturbances (Wright et al., 1985) suggest that variations in shortwave radiation are important for these anomalies over much of the Indian Ocean. Unfortunately, it is particularly hard to extrapolate the cloudiness data measured on shipping lanes to other locations, so the noise problem in existing surface heat flux estimates—particularly in the solar radiation—may seriously limit our attempts to understand the causes of Indian Ocean SST anomalies. **It is therefore essential to have good data on the shortwave radiation flux, if we are to**

diagnose causes of SST change in the Indian Ocean (it is probably important also in the other oceans).

On the positive side, numerical models have shown their strength as a tool for unraveling the complexities of Indian Ocean flows above the thermocline. They can suggest physically reasonable mechanisms, consistent with the observations, for understanding how the mean seasonal cycle of heating takes place in the Indian Ocean (Sections 2 and 3). It is therefore reasonable to hope that progress may be made in understanding Indian Ocean SST anomalies, despite the noise problems just mentioned, using numerical models. However, it may also turn out that improvements in the quality and quantity of surface flux information are needed in the Indian Ocean, before we can understand the SST anomaly patterns that occur there—let alone predict them.

Another aspect of the observed patterns of SST anomalies is the use of atmospheric general circulation models to test how such anomaly patterns affect the atmospheric circulation. We have referred to such studies where they are available, but it is beyond the framework of this document to discuss this task in any detail. However, we do recommend that atmospheric modelers expand their studies of this topic.

7.2 Scientific Questions

In the previous section we outlined the facts that we were reasonably confident of, as a group. The following is a list of questions that we need answers to, to continue progress in understanding the role of the upper Indian Ocean in the global climate system.

Basic Question: To what extent are ocean thermodynamics and dynamics actively involved in determining climate variability in the IO region? What oceanic processes generate and maintain SST anomalies?

7.2.1. Questions regarding the seasonal mean climate (cf. Sections 2, 3)

a. Cross-equatorial cell

What is the long-term mean shape of the meridional overturning pattern in the northern Indian Ocean? In particular, what are the relative strengths of the upper (thermocline) and deep cells?

What processes determine the temperature of the upwelled water?

Do remote processes play a role, as well as the local strength of Ekman divergence?

Is it true, as suggested by available model results, that the large lateral variations in meridional flows in the tropical Indian Ocean have such small lateral temperature contrasts that they play little role in transporting heat?

Is the cross-equatorial "roll", that occurs in the top few tens of meters in at least one model, supported by observations? If not, how do the meridional Ekman flows of the two hemispheres really communicate across the equator?

b. 28-day waves

28–day waves are observed in SSTs and in current meter data. They appear to be generated in models whenever the winds drive the Somali Current across the equator.

How important are these waves in the dynamics of the cross-equatorial transport? That is, are they crucial for allowing the potential vorticity (f/h) of the fluid to change sign?

Do they play a role in carrying the Ekman transports across the equator?

c. Equatorial currents

Do the strong semiannual variations of zonal current along the equator influence SST—either directly, or by exciting Rossby waves at the eastern boundary?

Does the region north of the throughflow form a separate dynamical regime? That is, are Kelvin and Rossby waves "stopped" by the Indonesian passages?

d. Indo-Pacific throughflow

Vertical mixing in the Indonesian Seas, probably tidally-induced, appears to change water mass structure markedly, as water flows from the Pacific to the Indian Ocean.

Is it responsible also for absorbing the large (O (40-60 watts/m^2)) surface heat flux found in this region, in most climatologies?

Do near-coastal effects, and salinity effects, seriously bias available measurements of the Throughflow strength?

How valid are the model results (Figure 13) on the way a change in the Indonesian Throughflow changes the SST and heat flux pattern in the Indian Ocean?

e. Mixed layer physics

In some locations in the Indian Ocean, very thin surface mixed layer are observed—near 10°S, 60°E throughout the year; and near the western end of the equator, in May and November. However, SSTs do not seem to decrease in these places (e.g., Figure 28) and heat fluxes into the ocean do not increase.

Why do thin mixed layers imply SST reduction and heat gain in some places, and not in others?

In some locations at least, salinity effects certainly modify SSTs; for example, rainfall and runoff in the northern Bay of Bengal appears to reduce the cooling associated with upwelling. How widespread are these effects? Are they important in the Indonesian region?

7.2.2. Questions regarding specific SST anomalies

a. ENSO

Indian Ocean SST anomalies lag behind the Southern Oscillation Index, i.e., they appear to be a passive response to ENSO. Nevertheless, since these are the best-defined SST anomaly pattern in the Indian Ocean, it is interesting to ask the basic question above, of Indian Ocean ENSO anomalies. I.e., To what extent are ocean thermodynamics and dynamics actively involved in determining ENSO SST variability in the IO region? What oceanic processes generate and maintain ENSO SST anomalies?

b. QBO

How are its dynamics different from those of ENSO? Does seasonal mixed layer deepening play a role in the longevity of QBO SST anomalies, by "hiding" anomalies from one southern winter until the following southern winter (Figure 23)?

c. Intraseasonal oscillations

Are intraseasonal oscillations the cause of the lack of predictability of monsoon rainfall in atmospheric GCMs?

SST anomalies are observed on these timescales. What is their phase relationship with ISO rain—do they lead it, or lag it? In particular, do they play an active role in the mechanism of ISOs, or are they a purely passive response to them?

e. Nicholl's dipole

Does seasonal mixed layer deepening (and resurfacing of the previous winter's anomalies) play a role in the rather sudden appearance of the dipole in Southern Hemisphere winter (Figure 30)?

Do Ekman currents, Rossby waves or the Indonesian Throughflow play a role in the formation of the dipole?

f. Interdecadal variability

Is there any independent evidence to test the hypothesis that the observed spatial pattern of SST trends over the last 80 years is due to a strengthening of the Indonesian Throughflow over this period (Figure 32)?

7.3 Recommendations

It is evident from the foregoing list of questions that, in the view of the Panel, much basic work remains to be done before it will be appropriate to plan the permanent Indian Ocean component of the ocean observing system for climate in any detail. The recommendations below are divided into three categories:

1) Analyses of existing data or of presently-planned research (including the analysis of WOCE results, after the Indian Ocean campaign is complete);
2) Development and analysis of numerical models; and
3) "Exploratory monitoring".

7.3.1. Data analyses

Recommendation 1: Continue the analysis of the existing TOGA XBT time series of thermal structure, along shipping routes in the Indian Ocean.

Recommendation 2: Explore methods of using satellite altimeter data for inferring changes in thermal structure outside shipping routes.

Recommendation 3: In the Arabian Sea, the net surface heat flux seems to be a major contributor to SST change (Figure 24)—and anomalies of shortwave radiation (associated with cloudiness) are probably the strongest contributor to net surface flux anomalies. In the Indian Ocean, with its light shipping traffic, a satellite product on shortwave radiation must be developed, if the potential of numerical models for interpreting SST anomalies is to be realized. The potential uses of the International Satellite Cloud Climatology Project (ISCCP) data for this purpose should be explored.

Recommendation 4: Figure 35 shows that there are large differences between the seasonal cycles of zonally-integrated meridional Ekman transports, from different data sources. Interannual differences are small by comparison in the Indian Ocean. It would therefore be useful to compare interannual anomalies in available wind stress products (e.g., zonally-integrated meridional Ekman transports), to see how well-defined the anomalies are, and hopefully identify sources of differences. Intercomparison with satellite wind products, e.g., ERS-1 winds, should be continued.

Recommendation 5: Similar remarks apply to surface fluxes of latent (and sensible) heat.

Recommendation 6: If results from implementing recommendations 3-5 were sufficiently encouraging, it would be useful to develop an interannual version of Figure 15, as a quality control tool. Available XBTs, supplemented by satellite altimeter data, could be used for estimating the rate of change of heat content. From comparing Figure 15 with Figure 35, one might expect that interannual anomalies of zonally-integrated meridional Ekman transport should roughly match anomalies of the estimated zonally-integrated meridional heat transport

Recommendation 7: The data from drifting buoys, and of ALACE floats, deployed during the WOCE Indian Ocean campaign (U.S. WOCE, 1993) should be used for validating the performance of numerical models of the Indian Ocean's upper layer.

7.3.2. Modeling

Recommendation 1: The efforts by atmospheric modeling groups to explore the impact of various Indian Ocean SST anomaly patterns on their AGCMs are welcomed. They are encouraged

to continue these efforts, and to explore the effects of other patterns of SST anomaly—such as those discussed in this document—on their AGCMs.

Recommendation 2: On the ocean side, it would be useful to intercompare the Indian Ocean mean seasonal cycle, as simulated by various thermodynamic ocean models, with some specified driving—perhaps similar to those undertaken by TOGA-NEG for Pacific models (Stockdale et al., 1993). An intercomparison could be used to identify the causes of differences in Indian Ocean model performance.

Recommendation 3: Several questions concerning model SST and surface heat fluxes may relate to mixed layer physics. The community of Indian Ocean modelers should explore the effect of different mixed-layer model parameterizations on their model performance. Similarly, the effects of salinity on mixed-layer thickness, SST, and ocean circulation should be explored.

7.3.3. Exploratory Monitoring

Recommendation 1: The 10-year time series of XBTs, though limited in scope by the paucity of shipping lanes, has proved extremely valuable for documenting interannual variability in the Indian Ocean. It is essential that this time series be continued at its present density or greater, for the foreseeable future.

Recommendation 2: A few years' data from one or two TAO moorings in the eastern Pacific Ocean, in the early to mid 1980s, was an essential step towards the present basin-wide TAO mooring array. Present logistic difficulties make it uncertain that a similar trial deployment can be achieved in the next few years, in the Indian Ocean. However, ways (possibly involving new technology) should be explored to develop and maintain one or more moorings in the equatorial Indian Ocean, as a similar pilot deployment.

Recommendation 3: The Japanese initiative in planning the deployment of moorings in the eastern Indian Ocean towards the end of this century is warmly welcomed.

Recommendation 4: A process study in the Indian Ocean, towards the end of this century, might be used as an opportunity for deploying more extensive TAO moorings for a limited period. At a brief joint meeting between some meteorologists (Webster, Yasunari, and Palmer) attending the Trieste Monsoon Conference and the WCRP Indian Ocean Panel, it was agreed that a process study of the Intraseasonal Oscillations in the Bay of Bengal was an attractive and feasible objective. If this is to be undertaken, it should be planned before the end of the TRMM mission in the year 2000, to take advantage of TRMMs detailed coverage of the rain events in the area which would be the focus of attention in the study of Intraseasonal Oscillations.

Acknowledgments

This document has been some years in preparation. We are indebted to several people for their comments on this and earlier drafts of this document: Fritz Schott, Jim O'Brien, Bob Molinari, Bruce Warren, and Worth Nowlin. Jim Mansbridge worked hard on preparation of Figure 35. We thank Professor Sulochana Gadgil for hosting the August 1992 Indian Ocean Panel meeting in

Bangalore, and Drs. Tim Palmer and Roger Newson for their help in organizing the May 1994 Panel meeting in Trieste. The careful proofreading of Ms. Susan Martin is much appreciated.

References

Allan, R. J. and M. R. Haylock. 1993. Circulation features associated with the winter rainfall decrease in Southwestern Australia. *J. Climate*, 6: 1356-1367.

Anderson, D. L. T. and D. J. Carrington. 1993. Modeling interannual variability in the Indian Ocean using momentum fluxes from the operational weather analyses for the United Kingdom Meteorological Office and European Centre for Medium Range Weather Forecasts. *J. Geophys. Res.*, 98: 12,483-12,499.

Anderson, D. L. T. and J. P. McCreary. 1985. Slowly propagating disturbances in a coupled ocean-atmosphere model. *J. Atmos. Sci.*, 42: 615-629.

Anderson, D. L. T., D. J. Carrington, R. Corry, and C. Gordon. 1991. Modeling the variability of the Somali Current. *J. Mar. Res.*, 49: 659-696.

Batteen, M. and M. Rutherford. 1990. Modeling of eddies in the Leeuwin Current: The role of thermal forcing. *J. Phys. Oceanog.*, 20: 1484-1520.

Bauer, S., G. L. Hitchcock, and D. B. Olson. 1991. Influence of monsoonally-forced Ekman dynamics upon mixed layer depth and plankton biomass distribution in the Arabian Sea. *Deep-Sea Res.*, 38: 531-554.

Bottger, H. 1982. Local weather element guidance from the ECMWF forecasting system in the medium range. A verification study. Seminar/Workshop 1982 Interpretation of numerical weather products. *ECMWF*: 417-441.

Breidenbach, J. 1990. EOFs of pseudo-stress over the Indian Ocean. *Bull. Am. Met. Soc.*, 71: 1448-1454.

Bunker, A. F. 1976. Computations of surface energy flux and annual air-sea interaction cycles in the North Atlantic Ocean. *Mon. Wea. Rev.*, 104: 1122-1140.

Bye, J. A. T. and A. H. Gordon. 1982. Speculated cause of interhemispheric oceanic oscillation. *Nature*, 296: 52-54.

Cadet, D. L. 1985. The Southern Oscillation over the Indian Ocean. *J. Climatology*, 5: 189-212.

Cadet, D. L. and B. C. Diehl. 1984. Interannual variability of surface fields over the Indian Ocean during recent decades. *Mon. Wea. Rev.*, 112: 1921-1935.

Cadet, D. L. and G. Reverdin. 1981. Water vapour transport over the Indian Ocean during summer 1975. *Tellus*, 33: 476-487.

Cane, M. 1992. Tropical Pacific ENSO models: ENSO as a mode of the coupled system. In: Climate System Modeling. Ed. K. E. Trenberth. Cambridge University Press.

CCCO Indian Ocean Climate Studies Panel. 1990. Report of the 6th Session of the CCCO Indian Ocean Climate Studies Panel, SCOR-IOC/CCCO-IND-VI/3.

Clarke, A. J. and X. Liu. 1994. Interannual sea level in the northern and eastern Indian Ocean. *J. Phys. Oceanogr.*, 24: 1224-1235.

Cresswell, G. R. and T. J. Golding. 1980. Observations of a south-flowing current in the southeastern Indian Ocean. *Deep-Sea Res.*, 27A: 449-466.

Donguy, J.-R. and B. Piton. 1991. The Mozambique Channel revisited. *Oceanologica Acta*, 14(6): 1-9.

Dube, S. K., M. E. Luther, and J. J. O'Brien. 1990. Relationships between interannual variability in the Arabian Sea and Indian Summer Rainfall. *Meteorol. Atmos. Phys.*, 44: 153-165.

Ffield, A. and A. L. Gordon. 1992. Vertical mixing in the Indonesian thermocline. *J. Phys. Oceanogr.*, 22: 184-195.

Fieux, M., C. Andrie, P. Delecluse, A. G. Ilahude, A. Kartavseff, F. Mantisi, R. Molcard, and J. C. Swallow. 1994. Measurements within the Pacific-Indian oceans throughflow region. *Deep-Sea Res.*, 41: 1091-1130.

Fletcher, J. O., R. J. Slutz, and S. D. Woodruff. 1983. Towards a comprehensive ocean-atmospheric data set. *Tropical Ocean-Atmosphere Newsletter*, 20: 13-14.

Fredericksen, C. S., W. Drosdowsky, R. C. Balgovind, and N. Nicholls. 1990. Indian Ocean Sea Surface Temperature features and Australian rainfall. Paper presented at TOGA Scientific Conference, Hawaii, Honolulu, July 1990.

Fu, L.-L. 1986. Mass, heat and freshwater fluxes in the South Indian Ocean. *J. Phys. Oceanogr.*, 16: 1683-1693.

Gadgil, S. and G. Asha. 1992. Intraseasonal variation of the summer monsoon. I: Observational aspects. *J. Met. Soc. Japan*, 70: 517-527.

Godfrey J. S. and A. J. Weaver. 1991. Is the Leeuwin Current driven by Pacific heating and winds? *Progr. Oceanog.*, 27: 225-272.

Godfrey, J. S. 1989. A Sverdrup model of the depth-integrated flow for the World Ocean, allowing for island circulations. *Geophys. Astrophys. Fluid Dynamics*, 45: 89-112.

Godfrey, J. S. and K. R. Ridgway. 1985. The large-scale environment of the poleward-flowing Leeuwin Current, Western Australia: longshore steric height gradients, wind stresses and geostrophic flow. *J. Phys. Oceanogr.*, 15: 481-494.

Godfrey, J. S., A. C. Hirst, and J. Wilkin. 1993. Why does the Indonesian Throughflow appear to originate from the North Pacific? *J. Phys. Oceanog.*, 23: 1088-1098.

Gordon, A. L. 1986. Interocean exchange of thermocline water. *J. Geophys. Res.*, 91: 5037-5046.

Gordon, A. L., R. F. Weiss, W. M. Smethie, Jr., and M. J. Warner. 1992. Thermocline and intermediate water communication between the South Atlantic and Indian Oceans. *J. Geophys. Res.*, 97: 7233-7240.

Gregg, M. C. 1987. Diapycnal mixing in the thermocline - a review. *J. Geophys. Res.*, 92: 5249-5286.

Halpern, D., M. H. Freilich, and R. S. Dunbar. 1992. Evaluation of two January-June 1992 ERS-1 AMI wind vector data sets. Papers from First ERS-1 Symposium, Cannes, France, ESA. pp. 135-139.

Halpern, D., V. Zlotnicki, J. Newman, O. Brown, and F. Wentz. 1991. An atlas of the monthly mean distributions of GEOSAT sea surface height, SSMI surface wind speed, AVHRR/2 Sea Surface Temperature, and ECMWF surface wind components during 1988. NASA JPL Publication 91-8.

Hastenrath, S. and L. L. Greischar. 1989. Climatic Atlas of the Indian Ocean, Part III: Upper-ocean structure. The University of Wisconsin Press.

Hastenrath, S. and L. L. Greischar. 1993. Monsoonal heat budget of the hydrosphere-atmosphere system in the Indian Ocean sector. *J. Geophys. Res.*, 98: 6869-6881.

Hastenrath, S. and P. J. Lamb. 1979a. Climatic Atlas of the Indian Ocean, Part I: Surface climate and atmospheric circulation. The University of Wisconsin Press.

Hastenrath, S. and P. J. Lamb. 1979b. Climatic Atlas of the Indian Ocean, Part II: The oceanic heat budget. The University of Wisconsin Press.

Hastenrath, S. and P. J. Lamb. 1980. On the heat budget of hydrosphere and atmosphere in the Indian Ocean. *J. Phys. Oceanog.*, 10: 694-708.

Hastenrath, S., A. Nicklis, and L. Greischar. 1993. Atmospheric-hydrospheric mechanisms of climate anomalies in the western equatorial Indian Ocean. *J. Geophys. Res.*, 98: 20,219-20,236.

Hellerman, S. and M. Rosenstein. 1983. Normal monthly wind stress over the World Ocean with error estimates. *J. Phys. Oceanog.*, 13: 1093-1104.

Hirst, A. C. and J. S. Godfrey. 1993. The role of the Indonesian Throughflow in a global ocean GCM. *J. Phys. Oceanog.*, 23: 1057-1086.

Hirst, A. C. and J. S. Godfrey. 1995. The response to a sudden change in the Indonesian Throughflow in a global ocean GCM. *J. Phys. Oceanog.*, in press.

Hsiung, J. 1985. Estimates of global oceanic meridional heat transport. *J. Phys. Oceanog.*, 15: 1405-1413.

Hsiung, J., R. E. Newell, and T. Houghtby. 1989. The annual cycle of oceanic heat storage and oceanic meridional heat transport. *Quart. J. Roy. Met. Soc.*, 115: 1-28.

Hughes, T. M. C., A. J. Weaver, and J. S. Godfrey. 1992. Thermohaline forcing of the Indian Ocean by the Pacific Ocean. *Deep-Sea Res.*, 39: 965-995.

Isemer, H. J., J. Willebrand, and L. Hasse. 1989. Fine adjustment of large-scale air-sea energy flux paramerizations by direct estimates of ocean heat transport. *J. Climate*, 2: 1173-1184.

Janowiak, J. E., A. F. Krueger, P. A. Arkin, and A. Gruber. 1985. Atlas of outgoing longwave radiation derived from NOAA satelite data, NOAA Atlas No. 6, U.S. Dept of Commerce, Silver Spring, MD. 44 pp.

Johnson, E. S. and B. A.Warren. 1979. Density-diffusive model of the NinetyEast Ridge current. *J. Phys. Oceanogr.*, 9: 1288-1293.

Jones, C. S., D. M. Legler, and J. J. O'Brien. 1995. Variability of surface fluxes over the Indian Ocean, 1960-1989. *The Global Atmosphere-Ocean System*, in press.

Kent, E. C., B. S. Truscott, P. K. Taylor, and J. S. Hopkins. 1991. The accuracy of ship's meteorological observations. Marine Meteorology and Related Oceanographic Activities: Report No. 26. WMO/TD- No. 455.

Kindle, J. C. and J. D. Thompson. 1989. A numerical model of the Somali Current. *J. Phys. Oceanogr.*, 6: 646-664.

Knox, R. A. 1987. The Indian Ocean: Interaction with the Monsoon. In: "Monsoons", J. S. Fein and P. L. Stephens, eds. John Wiley and Sons. 632 pp.

Kraus, E. B. and J. S. Turner. 1967. A one-dimensional model of the seasonal thermocline. II. The general theory and its consequences. *Tellus*, 19: 89-105.

Krishnamurti, T. N., D. K. Oosterhof, and A. V. Mehta. 1988. Air-sea interaction on the time scale of 30-50 days. *J. Atmos. Sci.*, 45: 1304-1322

Krishnan, R., S. V. Kasture, and R. N. Keshavamurty. 1992. Northward movement of the 30-50 day mode in an axisymmetric global spectral model. *Current Science*, 62: 732-735.

Legler, D. M. and J. J. O'Brien. 1993. Comparison of ERS-1 scatterometer and Florida State UIniversity Tropical Winds. Papers from Second ERS-1 Symposium, Hamburg, Germany, ESA, pp. 1123-1126.

Legler, D. M., I. M. Navon, and J. J. O'Brien. 1989. Objective analysis of pseudo-stress over the Indian Ocean using a direct-minimization approach. *Mon. Wea. Rev.*, 117: 709-720.

Levitus, S. 1982. Climatological atlas of the World Ocean. NOAA Professional Paper 13. U.S. Department of Commerce.

Levitus, S. 1987. Meridional Ekman heat fluxes for the World Ocean and individual ocean basins. *J. Phys. Oceanogr.*, 17: 1484-1492.

Luther, M. E. and J. J. O'Brien. 1989. Modelling the Variability in the Somali Current. from: "Mesoscale/Synoptic Structures" in Geophysical Turbulence, J. C. J. Nihoul and B. M Jamart, eds., Elsevier Science Publishers.

Luyten, J. R. and D. H. Roemmich. 1982. Equatorial currents at semi-annual period in the Indian Ocean. *J. Phys. Oceanogr.*, 12: 406-413.

Madden, R. A. and P. R. Julian. 1972. Description of global scale circulation cells in the tropics with a 40-50 day period. *J. Atmos. Sci.*, 29: 1109-1123.

Manabe, S. and R. J. Stouffer. 1988. Two stabel equilibria of a coupled Ocean-atmosphere model. *J. Climate*, 1: 841-866.

McCartney, M. S. 1977. SubAntarctic Mode Water. A Voyage of Discovery, M.V. Angel, ed., *Deep-Sea Res.*, 24(Suppl): 103-119.

McCreary, J. P. and P. K. Kundu. 1986. Thermohaline forcing of eastern boundary currents: with application to the circulation off the west coast of Australia. *J. Mar. Res.*, 44: 71-92.

McCreary, J. P. and P. K. Kundu. 1988. A numerical investigation of the Somali Current during the Southwest Monsoon. *J. Mar. Res.*, 46: 25-38.

McCreary, J. P., P. K. Kundu, and R. L. Molinari. 1993. A numerical investigation of dynamics, thermodynamics and mixed-layer processses in the Indian Ocean. *Prog. Oceanogr.*, 31: 181-244.

McCreary, J. P., Y. Fukamachi, and P. Lu. 1992. A nonlinear mechanism for maintaining coastally-trapped eastern boundary currents. *J. Geophys. Res.*, 97: 5677-5692.

McPhaden, M. J. 1982. Variability in the central equatorial Indian Ocean, Part II: Oceanic heat and turbulent energy balances. *J. Mar. Res.*, 40: 403-419.

Meehl, G. A. 1987. The annual cycle and interannual variability of the tropical Pacific and Indian Ocean regions. *Mon. Wea. Rev.*, 115: 17-50.

Meehl, G. A. 1993. A coupled air-sea biennial mechanism in the tropical Indian and Pacific Oceans: role of the ocean. *J. Climate*, 6: 31-41.
Meyers, G., H. Phillips, N. Smith, and J. Sprintall. 1991. Space and time scales for optimal interpolation of temperature—tropical Pacific Ocean. *Prog. Oceanog.*, 28: 189-218.
Molinari, R. L., D. Olson, and G. Reverdin. 1990. Surface current distributions in the tropical Indian Ocean derived from compilations of surface buoy trajectories, *J. Geophys. Res.*, 95: 7217-7238.
Namias, J. 1970. Macroscale variations in sea surface temperatures in the North Pacific. *J. Geophys. Res.*, 75: 565-582.
Nanjundiah, R. S., J. Srinavasan, and S. Gadgil. 1992. Intraseasonal variation of the Indian summer monsoon II: Theoretical aspects. *J. Met. Soc. Japan*, 70: 529-549.
Nicholls, N. 1989. Sea surface temperatures and Australian winter rainfall. *J. Climate*, 2: 965-973
O'Neill, K. 1984. Equatorial velocity profiles: I. Meridional component. *J. Phys. Oceanogr.*, 14: 1829-1841.
Oberhuber, J. M. 1988. An atlas based on the "COADS" data set: the budgets of heat, buoyancy and turbulent kinetic energy at the surface of the global ocean. Max-Planck-Institut für Meteorologie, Report No. 15.
Olson, D. B., G. L. Hitchcock, R. A. Fine, and B. A. Warren. 1993. Maintenance of the low-oxygen layer in the central Arabian Sea. *Deep-Sea Res.*, 40: 673-685.
Olson, D. B., R. A. Fine, and A. L. Gordon. 1988. Convective modification of water masses in the Agulhas. *Deep-Sea Res.*, 39(Suppl. 1): S163-S181.
Ou, H. W. and W. P. M. de Ruijter. 1986. Separation of an inertial boundary current from a curved coastline. *J. Phys. Oceanogr.*, 16: 280-289.
Palmer, T. N., C. Brankovic, P. Viterbo, and M. J. Miller. 1992. Modelling interannual variations of summer monsoons. *J. Climate*, 5: 399-417.
Pariwono, J. I., J. A. T. Bye, and G. W. Lennon. 1986. Long-period variations of sea-level in Australasia. *Proc. Roy. Astronom. Soc.*, 87(1): 43-54
Pearce, A. F. and B. F. Phillips. 1988. ENSO events, the Leeuwin Current and larval recruitment of the western rock lobster. *J. Cons. Int. Explor. Mer.*, 45: 13-21.
Perigaud, C. and P. Delecluse. 1989. Simulation of dynamic topography in the northwestern Indian Ocean with input of SEASAT altimeter and scatterometer data. *Ocean-Air Interactions*, 1: 289-309.
Perigaud, C. and P. Delecluse. 1992. Annual sea level variations in the southern Indian Ocean from Geosat and shallow-water simulations. *J. Geophys. Res.*, 97: 20,169-20,178.
Philander, S. G. H. 1990. El Niño, La Nina, and the Southern Oscillation. Academic Press, Inc. 293 pp.
Polzin, K. L., J. M. Toole, and R. W. Schmitt. 1995. Finescale parameterizations of turbulent dissipation. *J. Phys. Oceanogr.*, in press.
Potemra, J. T., M. E. Luther, and J. J. O'Brien. 1991. The seasonal circulation of the upper layers of the Bay of Bengal. *J. Geophys. Res.*, 96: 12,667-12,683.
Qu, T., G. Meyers, and J. S. Godfrey. 1995. Ocean dynamics in the region between Australia and Indonesia and its influence on the variation of sea surface temperature in a global GCM. *J. Geophys. Res.*, in press.
Rao, R. R. 1986. Cooling and deepening of the mixed layer in the central Arabian Sea during MONSOON-77: observations and simulations. *Deep-Sea Res.*, 33: 1413-1424.
Rao, R. R. and B. Mathew. 1990. A case study on the mixed layer variability in the south central Arabian Sea during the onset phase of MONEX-79. *Deep-Sea Res.*, 37: 227-243.
Rao, R. R., R. L. Molinari, and J. Festa. 1989. Evolution of the climatological near surface thermal structure of the tropical Indian Ocean. Part I: Description of mean monthly mixed layer depth and sea surface temperature, surface current and surface meteorological fields. *J. Geophys. Res.*, 94: 10,801-10,815.
Rao, R. R., R. L. Molinari, and J. Festa. 1991. Surface Meteorological and Near Surface Oceanographic Atlas of the Tropical Indian Ocean. NOAA Technical Memorandum, ERL AOML-69.

Rasmusson, E. M. and T. H. Carpenter. 1982. Variations in tropical sea surface temperature and surface wind fields associated with the Southern Oscillation/El Niño. *Mon. Wea. Rev.*, 110: 354-384.
Reverdin, G. and J. Luyten. 1986. Near-surface meanders in the equatorial Indian Ocean. *J. Phys. Oceanogr.*, 16: 1088-1100.
Reverdin, G., D. L. Cadet, and D. Gutzler. 1986. Interannual displacements of convection and surface circulation over the equatorial Indian Ocean. *Quart. J. Roy. Met Soc.*, 112: 43-67
Reynolds, R. W. 1988. A real-time global sea-surface temperature analysis. *J. Climate*, 1: 75-86.
Reynolds, R. W. and T. S. Smith. 1994. Improved global sea surface temperature analyses. *J. Climate*, 7: 929-948.
Rintoul, S. R. 1991. South Atlantic interbasin exchange. *J. Geophys. Res.*, 96: 2675-2692.
Sadler, J. C., M. A. Lander, A. M. Hori, and L. K. Oda. 1987. Tropical Marine Climatic Atlas, Volume I: Indian Ocean and Atlantic Ocean. University of Hawaii Report UHMET 87-01.
Sandwell, D. T. and B. Zhang. 1989. Global mesoscale variability from the Geosat exact repeat mission: Correlation with ocean depth. *J. Geophys. Res.*, 94: 17,971-17,984.
Schmitz, W. J., Jr. On the global thermohaline circulation. Manuscript in preparation.
Schott, F., M. Fieux, J. Kindle, J. Swallow, and R. Zantopp. 1988. The boundary currents east and north of Madagascar 2. Direct measurements and model comparisons. *J. Geophys. Res.*, 93: 4963-4974.
Schott, F., J. C. Swallow, and M. Fieux. 1989. Deep currents underneath the equatorial Somali Current. *Deep-Sea Res.*, 36: 1191-1199.
Schott, F., J. C. Swallow, and M. Fieux. 1990. The Somali Current at the equator: annual cycle of currents and transports in the upper 1000 m and connection to neighbouring latitudes. *Deep-Sea Res.*, 37: 1825-1848.
Seager, R., S. E. Zebiak, and M. A. Cane. 1988. A model for the tropical Pacific sea surface temperature climatology. *J. Geophys. Res.*, 93: 1265-1280.
Semtner, A. J. and R. M Chervin. 1992. Ocean general circulation from a global eddy-resolving model. *J. Geophys. Res.*, 97: 5493-5550.
Shetye, S. R., A. D. Gouveia, S. S. C. Shenoi, G. S. Michael, D. Sundar, A. M. Almeida, and K. Santanam. 1991a. The coastal current off western India during the northeast monsoon. *Deep-Sea Res.*, 38: 1517-1529.
Shetye, S. R., S. S. C. Shenoi, A. D. Gouveia, G. S. Michael, D. Sundar, and G. Nampoothiri. 1991b. Wind-driven coastal upwelling along the western boundary of the Bay of Bengal during the southwest monsoon. *Continental Shelf Res.*, 11: 1397-1408.
Shukla, J. 1987. Interannual variability of monsoons. In: "Monsoons", J. S. Fein and P. L. Stephens, eds. John Wiley and Sons. 632 pp.
Sikka, D. R. and S. Gadgil. 1980. On the maximum cloud zone and the ITCZ over India longitude during the southwest monsoon. *Mon. Wea. Rev.*, 108: 1840-1853.
Sjoberg, B. and A. Stigebrandt. 1992. Computations of the geographical distribution of the energy flux to mixing processes via internal tides and the associated vertical circulation in the ocean. *Deep-Sea Res.*, 39: 269-291.
Smith, N. 1991. The Role of Models in an Ocean Observing System. CCCO-JSC Ocean Observing System Development Panel, Texas A&M University, College Station, TX 77843-3146. 85 pp.
Smith, R. L., A. Huyer, J. S. Godfrey, and J. A. Church. 1991. The Leeuwin Current off Western Australia, 1986-1987. *J. Phys. Oceanogr.*, 21: 323-345.
Sprintall J. and M. Tomczak. 1992. Evidence of the barrier layer in the surface layer of the tropics. *J. Geophys. Res.*, 97(C5): 7305-7316.
Stockdale, T., D. Anderson, M. Davey, P. Delecluse, A. Kattenberg, Y. Kitamura, M. Latif, and T. Yamagata. 1993. TOGA Numerical Experimentation Group: Intercomparison of Tropical Ocean GCMs. World Climate Research Report WCRP-79; WMO/TD- No. 545.
Stommel, H. and A. B. Arons. 1960. On the abyssal circulation of the world ocean - I. Statinary planetary flow patterns on a sphere. *Deep-Sea Res.*, 6: 140-154.
Stramma, L. 1992. The South Indian Ocean Current. *J. Phys. Oceanogr.*, 22: 421-430.

Stricherz, J., D. M. Legler, and J. J. O'Brien. 1993. Atlas of Florida State University Indian Ocean winds for TOGA 1970-1985. Florida State University, Tallahassee, FL. 216 pp.
Sverdrup, H. U. 1947. Wind driven currents in a baroclinic ocean with applications to the equatorial currents in the eastern Pacific. *Proc. Natl. Acad. Sci. U.S.A.*, 33: 318-336.
Swallow, J. C. 1984. Some aspects of the physical oceanography of the Indian Ocean. *Deep-Sea Res.*, 31: 639-650.
Swallow, J., M. Fieux, and F. Schott. 1988. The boundary currents east and north of Madagascar 1. Geostrophic currents and transports. *J. Geophys. Res.*, 93: 4951-4962.
Tomczak, M. and J. S. Godfrey. 1994. Regional Oceanography: An Introduction. Pergamon Press. 422 pp.
Toole, J. M. and B. A. Warren. 1993. A hydrographic section across the subtropical South Indian Ocean. *Deep-Sea Res.*, 40: 1973-2019.
Toole, J. M., K. L. Polzin, and R. W. Schmitt. 1994a. Estimates of diapycnal mixing in the abyssal ocean. *Science*, 264: 1120-1123.
Toole, J. M., E. Kunze, K. L. Polzin, and R. W. Schmitt. 1994b. Finestructure and microstructure observations about a subtropical latitude seamount. AGU-ASLO Ocean Sciences Meeting. *EOS*, 75 suppl.: 164.
Trenberth, K. E. 1989. Surface Wind Stress from Global Atmospheric Analyses. In: Oceans '89, an international conference addressing methods of understanding the Global Ocean. Vol. 1. IEEE Publication Number 89CH2780-5.
Trenberth, K. E., W. G. Large, and J. G. Olson. 1990. The mean annual cycle in global wind stress *J. Phys. Oceanogr.*, 20: 1742-1760.
Tsai, P. T. H., J. J. O'Brien, and M. E. Luther. 1992. The 26-day oscillation observed in the satellite sea surface temperature measurements in the equatorial Indian Ocean. *J. Geophys. Res.*, 97: 9605-9618.
U.S. WOCE. 1993. U.S. Contribution to WOCE Core Project 1 The Program Design for the Indian Ocean. U.S. WOCE Office, College Station, Texas. 80 pp.
Verma, R. K., K. Subramamaniam, and S. S. Dugam. 1984. Long-term variability of summer monsoon and climatic change. Contributions from the Indian Institute of Tropical Meteorology, Sci. Rep. R-041, Ramdury House, Pune. 41 pp.
Wacongne, S. and R. C. Pacanowski. 1994. Seasonal heat transport in the tropical Indian Ocean. Submitted.
Wajsowicz, R. C. 1993. The circulation of the depth-integrated flow around an island with application to the Indonesian Throughflow. *J. Phys. Oceanogr.*, 23: 1470-1484.
Warren, B. A. 1981. Transindian hydrographic section at 18°S: property distributions and circulation in the south Indian Ocean. *Deep-Sea Res.*, 28: 759-788.
Warren, B. A. 1994. Driving the meridional overturning in the Indian Ocean. *Deep-Sea Res.*, 41: 1349-1360.
Warren, B. A., H. Stommel, and J. C. Swallow. 1966. Water masses and patterns of flow in the Somali Basin during the Southwaest Monsoon of 1964. *Deep-Sea Res.*, 13: 825-860.
Weaver, A. J. and J. H. Middleton. 1989. On the dynamics of the Leeuwin Current. *J. Phys. Oceanogr.*, 19: 626-647.
Webster, P. J. 1987. The variable and interactive monsoon. In: "Monsoons", J. S. Fein and P. L. Stephens, eds. John Wiley and Sons. 632 pp.
Webster, P. J. 1994. The annual cycle and the predictability of the tropical coupled ocean-atmosphere system. *Meteorology and Atmospheric Physics*, in press.
Webster, P. J. and L. C. Chou. 1980. Low-frequency transitions of a simple monsoon system. *J. Atmos. Sci.*, 37: 368-382.
Weller, R. A. and P. K. Taylor. 1993. Surface conditions and air-sea fluxes. CCCO-JSC Ocean Observing System Development Panel, Texas A&M University, College Station, TX 77843-3146. 131 pp.
WOCE. 1992. TOGA/WOCE XBT/XCTD Programme Planning Committee: report of the first meeting. WOCE Report No. 85/92.

Woodberry, K. E., M. E. Luther, and J. J. O'Brien. 1989. The wind-driven seasonal circulation in the southern tropical Indian Ocean. *J. Geophys. Res.*, 94: 17,985-18,002.
Woodruff, S. D., R. J. Slutz, R. L. Jenne, and P. M. Steurer. 1987. A Comprehensive Ocean-Atmosphere Data Set. *Bull. Am. Met. Soc.*, 68: 1239-1250.
Wright, P. B., T. P. Mitchell, and J. M. Wallace. 1985. Relationships between surface observations over the global oceans and the Southern Oscillation. NOAA Data Report ERL PMEL-12.
Wyrtki, K. 1971. Oceanographic Atlas of the International Indian Ocean Expedition. National Science Foundation.
Wyrtki, K. 1973a. Physical Oceanography of the Indian Ocean. In: The Biology of the Indian Ocean, B. Zeitzschel and B. A. Gerlach, eds. Springer-Verlag.
Wyrtki, K. 1973b. An equatorial jet in the Indian Ocean. *Science*, 181: 262-264.
Wyrtki, K. 1975. El Niño—the dynamic response of the equatorial Pacific Ocean to atmospheric forcing. *J. Phys. Oceanogr.*, 5: 572-584.
Yasunari, T. 1990. Impact of Indian Monsoon on the coupled atmosphere/ocean system in the tropical Pacific. *J. Meteor. Atmos. Phys.*, 44: 29-41.
Zebiak, S. and M. A. Cane. 1987. A model ENSO. *Mon. Wea. Rev.*, 115: 2262-2278.

Appendix 1: WCRP Indian Ocean Panel and Authorship List

Dr. J. Stuart Godfrey, Chair
CSIRO Division of Oceanography
GPO Box 1538
Hobart, Tasmania 7001
AUSTRALIA
Fax: 002-24-1710
e-mail: godfrey@aqueous.ml.csiro.au

Dr. Art Alexiou
IOC/UNESCO
7 Place de Fontenoy
75700 PARIS
FRANCE
fax : 0015-33-1-43061122
e-mail: a.alexiou@unesco.org

Dr. Abdul Gani Ilahude
Pusat Penelitian dan Pengembangan Oseanologi-LIPI
Jl. Pasir Putih No. 1, Ancol Timur
Jakarta Utara
INDONESIA
Fax: 62-21-681948

Dr. David Legler
Mesoscale Air-Sea Interaction Group
Florida State University
Room 020 Love Building
Tallahassee, FL 32306-3041
USA
Fax: 904-644-4841
e-mail: legler@masig.fsu.edu

Dr. Mark E. Luther
USF Dept of Marine Science
140 Seventh Ave South
St. Petersburg, FL 33701
USA
Fax: 813-893-9189
email: luther@kelvin.marine.usf.edu

Dr. Julian P. McCreary, Jr.
Nova University Oceanographic Center,
8000 North Ocean Drive,
Dania, Florida 33004
USA
Fax: 305-947-8559
email: jay@ocean.nova.edu

Dr. Gary Meyers
CSIRO Division of Oceanography
GPO Box 1538
Hobart, Tasmania 7001
AUSTRALIA
Fax: 002-24-1710
e-mail: meyers@aqueous.ml.csiro.au

Dr. Keisuke Mizuno
National Research Institute of Far Seas Fisheries
5-7-1, Orito
Shimizu-shi
Shizuoka-ken 424, JAPAN
Fax: 81-543-359642
email: kmizuno@ss.enyo.affrc.go.jp

Dr. R. R. Rao
Scientist, Physical Oceanography Division
NPOL
BMC Post Office
Cochin 682021
INDIA
Fax: 91-0484-532178

Dr. S. R. Shetye
Physical Oceanography Division
National Institute of Oceanography
Dona Paula, Goa 403004
INDIA
Fax: 91-832-223340 or 832-221360

Dr. J. M. Toole
Woods Hole Oceanographic Institute
Woods Hole, MA 02543
USA
e-mail: ctdjmt@bonzo.whoi.edu

Dr. Sophie Wacongne
Laboratoire de Physique des Oceans
UBO/ Faculte des Sciences et Techniques
6 Avenue Le Gorgeu
29287 BREST CEDEX
FRANCE
Fax: 33-98-31-64-68
e-mail: wacongne@brest.ifremer.fr